Growth and characterization of dilute bismide GaAs based alloys for high efficiency infra red laser diodes

Dissertation

zur
Erlangung des Doktorgrades
der Naturwissenschaften
(Dr. rer. nat.)

dem

Fachbereich Physik
der Philipps-Universität Marburg

vorgelegt von

Peter Ludewig, M. Sc.

aus

Wiesbaden

Marburg/Lahn, 2014

Vom Fachbereich Physik der Philipps-Universität Marburg
als Dissertation angenommen am: 17.06.2014
Erstgutachter: Prof. Dr. Kerstin Volz
Zweitgutachter: PD Dr. Sangam Chatterjee
Tag der mündlichen Prüfung: 23.06.2014
Hochschulkennziffer: 1180

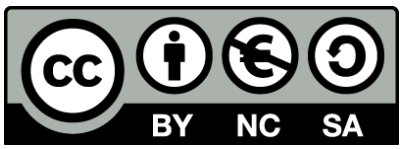

Contents

CHAPTER 1

Introduction

Life without internet is hardly imaginable today and its usage is still increasing rapidly. In times of multimedia streaming, social networks and cloud storage, aside from huge storage capacities, high speed data transfer is essential. For long distances the transfer runs optically via fiber networks that will get more and more extended towards fiber-to-the-home (FTTH) systems in future. Since fiber optics show an absorption minimum at a wavelength of 1.55 µm (0.8 eV) all involved optoelectronic devices, such as laser (Light Amplification by Stimulated Emission of Radiation) diodes and electro-absorption modulators need to operate at this wavelength. Conventional devices consist of well established gallium indium arsenide phosphide ((GaIn)(AsP)) based structures that are deposited on InP substrates. However, there are two intrinsic drawbacks that considerably affect their efficiency. First, the spin-orbit splitting in the valance band (VB) is smaller than the bandgap (E_g), which enables loss mechanisms such as Auger recombination and inter band absorption involving inter valance band transitions that lead to increasing threshold currents in laser diodes and heating of the devices[1–3]. Second, the bandgap itself is very sensitive to the temperature and therefore thermo-electric coolers and an air-conditioned environment are necessary to keep the wavelength of all involved optoelectronic devices constant. The efficiency of a laser diode in optical networks is only approximately 20%[2,4], not yet taken the power into account that is needed for temperature management and thought to further reduce the total efficiency by an order of magnitude. This shows that there is a huge potential for power saving, especially given the rapidly growing nature of the telecommunication network.

One approach to address this potential is the use of the dilute bismuth (Bi) containing Ga(AsBi) material system that can be deposited on GaAs substrates. For the alloy where roughly 10% As is replaced by Bi the required emission wavelength of 1.55 µm could be reached and the before mentioned loss mechanisms be suppressed, leading to more efficient devices and less heating[5,6]. Furthermore, it was found that the temperature sensitivity of the emission wavelength of this compound is much lower than that of (GaIn)(AsP)[7–10], which would enable a wider range of operation temperatures and further reduce the need

for cooling. Beyond pure Ga(AsBi), the addition of nitrogen (N) in the quaternary dilute bismide and nitride Ga(NAsBi) is also of interest for near- and mid infrared (IR) laser devices[5]. N and Bi have opposite impacts on the strain of the alloy but both decrease the bandgap of GaAs, hence, a wide range of different bandgap materials grown on GaAs are conceivable. The potential not only for high efficiency infrared light sources but also other applications, such as solar cells[5,11,12] and photo detectors[5,13], has attracted a lot of attention to the dilute bismides recently. However, the development of the rather new material using metal organic vapor phase epitaxy (MOVPE)[7,8,14–18] and molecular beam epitaxy (MBE)[19–26] only proceeded since the noughties and the deposition of high quality Ga(AsBi) with sufficient Bi fractions is still very challenging and the object of current research.

In the present work the growth of Ga(AsBi) and Ga(NAsBi) on GaAs substrates using MOVPE was studied systematically. A growth model including Bi segregation was developed and the influence of several growth parameters analyzed, which enabled the successful deposition of Ga(AsBi) layers with up to 7% Bi. Furthermore, the first Ga(AsBi) containing electrically pumped laser was demonstrated, providing a proof of principle for dilute bismide lasers.

The research was part of the BIANCHO (BIsmide And Nitride Components for High temperature Operation) project founded by the European Union within the 7th Research Framework.

This thesis is written in cumulative form and is structured as follows: Chapter 2 will introduce the investigated alloys Ga(AsBi) and Ga(NAsBi) and the experimental techniques applied in this work. The research results are briefly presented in Chapter 3 and summarized in Chapter 4 as they are discussed in detail in the following publications that were published in course of this work and are printed in full length in Chapter 5:

List of publications:

- P. Ludewig, N. Knaub, W. Stolz, K. Volz, *MOVPE growth of Ga(AsBi)/GaAs multi quantum well structures*, Journal of Crystal Growth **370**, 186 (2013). DOI: 10.1016/j.jcrysgro.2012.07.002. (Ref. 27, Section 5.1)

- P. Ludewig, N. Knaub, N. Hossain, S. Reinhard, L. Nattermann, I. P. Marko, S.R. Jin, K. Hild, S. Chatterjee, W. Stolz, S.J. Sweeney, K. Volz, *Electrical injection Ga(AsBi)/(AlGa)As single quantum well laser*, Applied Physics Letters **102**, 242115 (2013). DOI: 10.1063/1.4811736. (Ref. 28, Section 5.2)

- P. Ludewig, Z. L. Bushell, L. Nattermann, N. Knaub, W. Stolz, K. Volz, *Growth of Ga(AsBi) on GaAs by continuous flow MOVPE*, Journal of Crystal Growth **396**, 95 (2014). DOI: 10.1016/j.jcrysgro.2014.03.041. (Ref. 29, Section 5.3)

- Z. L. Bushell, P. Ludewig, N. Knaub, Z. Batool, K. Hild, W. Stolz, S. J. Sweeney, K. Volz, *Growth and characterisation of GaNAsBi alloy by metal organic vapour phase epitaxy*, Journal of Crystal Growth **396**, 79 (2014). DOI: 10.1016/j.jcrysgro.2014.03.038. (Ref. 30, Section 5.4)

- B. Breddermann, A. Bäumner, S. W. Koch, P. Ludewig, W. Stolz, K. Volz, J. Hader, J. V. Moloney, C.A. Broderick, E.P. O'Reilly, *Luminescence properties of dilute bismide systems*, Journal of Luminescence **154**, 95 (2014). DOI: 10.1016/j.jlumin.2014.04.012 (Ref. 31, Section 5.5)

- E. Sterzer, N. Knaub, P. Ludewig, R. Straubinger, A. Beyer, K. Volz, *Investigation of the microstructure of metallic droplets on Ga(AsBi)/GaAs*, Journal of Crystal Growth **408**, 71 (2014). DOI: 10.1016/j.jcrysgro.2014.09.006 (Ref. 32, Section 5.6)

- I. P. Marko, P. Ludewig, Z. L. Bushell, S. R. Jin, K. Hild, Z. Batool, S. Reinhard, L. Nattermann, W. Stolz, K. Volz and S. J. Sweeney, *Physical properties and optimization of GaBiAs/(Al)GaAs based near-infrared laser diodes grown by MOVPE with up to 4.4% Bi*, Journal of Physics D: Applied Physics **47**, 345103 (2014). DOI: 10.1088/0022-3727/47/34/345103. (Ref. 33, Section 5.7)

- M. K. Shakfa, M. Wiemer, P. Ludewig, K. Jandieri, K. Volz, W. Stolz, S. D. Baranovskii, M. Koch, *Thermal quenching of photoluminescence in Ga(AsBi)*, Journal of Applied Physics **117**, 025709 (2015). DOI: 10.1063/1.4905687 (Ref. 34, Section 5.8)

CHAPTER 2

Investigated materials and methods

2.1 Investigated materials

This chapter covers the theoretical background and state of development of Ga(AsBi) and Ga(NAsBi). For better understanding a short overview of the GaAs host material is given first.

2.1.1 GaAs

GaAs is a very well known and often used semiconductor. Because of its direct bandgap (E_g) of 1.42 eV at room temperature, which corresponds to a wavelength of 873 nm, it is a suitable material for photonic applications in the near infrared. The first laser diodes made out of GaAs were already developed in 1962 [35]. As for most III-V semiconductors, GaAs crystallizes in the zinc blende (ZB) structure, which consists of two face centered cubic (fcc) sublattices that are shifted by a quarter of the space diagonal of the unit cell with respect to each other. Each kind of atom thereby occupies one of the fcc sublattices (Figure 2.1 (a)). The lattice parameter, which is the length of the cubic unit cell, is a_{GaAs}=5.65 Å. Crystal planes are described by the Miller indices (hkl) that are given by the inverse of the intercepts of the considered plane with each of the three lattice vectors (0, if there is no intercept) (Figure 2.1 (b)). High purity GaAs single crystalline wafers are produced on industrial scale and hence can be used as substrates for the deposition of Ga(AsBi) and Ga(NAsBi). In the present work GaAs wafers of 2" diameter with (001) surface orientation were used. Furthermore, depending on the experiment, GaAs barrier and cap layers were deposited epitaxially for the carrier confinement, since the GaAs bandgap is larger than the one of Ga(AsBi) and Ga(NAsBi). Additionally, the (AlGa)As alloy was used in cases where larger electronic or optical confinements were required. The intermixture of Al (aluminum) into GaAs increases the bandgap (it becomes indirect at about 40% Al) but only slightly increases the lattice constant, which allows the growth of the whole composition range of (AlGa)As on GaAs. (AlGa)As itself and its growth are well known, so it will not be discussed in more detail here.

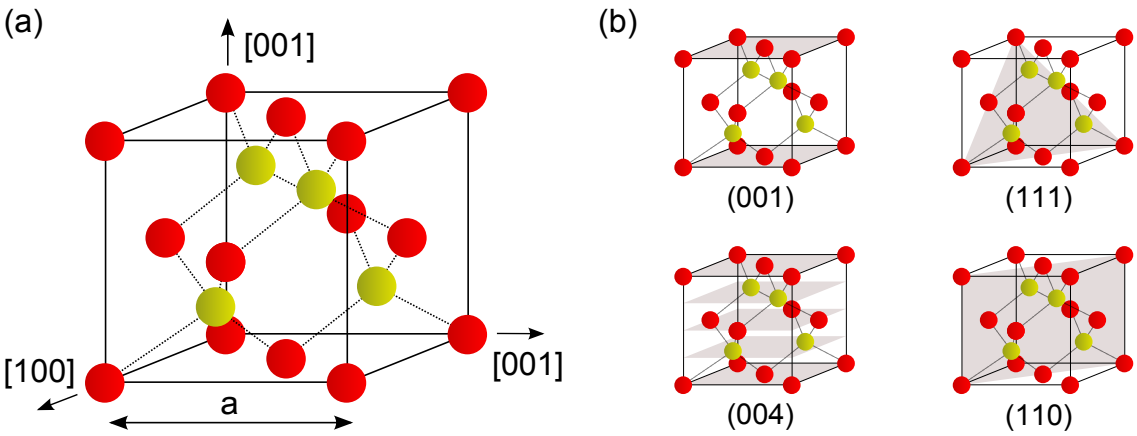

Figure 2.1: (a) Unit cell of the zinc blende crystalline structure with lattice constant a. Group-V (red) and group-III (yellow) elements occupy fcc sublattices that are shifted by a quarter of the space diagonal of the unit cell with respect to each other. Crystalline directions are noted in squared brackets (a) and lattice planes in round brackets (b).

2.1.2 Ga(AsBi)

The binary crystalline compound GaBi does not exist since Ga and Bi phase separate as soon as Bi solidifies from liquid[36] and hence there is no experimental knowledge on this material. Nevertheless many parameters of GaBi in zinc blende configuration have been calculated predicting it to be metallic with a lattice constant of about 6.3 Å (all important parameters of the GaBi material are summarized in Table 2.1). The rather new dilute bismide Ga(AsBi) compound can, however, be synthesized and has attracted increasing attention in recent years because of its interesting electronic properties. Experiments showed that the intermixture of Bi into GaAs causes a very large bandgap reduction of about 80 to 90 meV per % of Bi[20,37–40], which is the largest value of all ternary GaAs alloys with respect to strain and provides the possibility of depositing mid infrared photonic devices on GaAs. Since the strong bandgap reduction is far beyond virtual crystal approximation (VCA) and implies a large bowing parameter, theoretical studies on the description of the Ga(AsBi) band structure have been carried out. Alberi et al. showed that the experimental observations can be explained with a valance band anti crossing (VBAC) model[41,42], similar to the conduction band (CB) anti crossing (CBAC) model that was established for the dilute nitride (GaIn)(NAs)[43]. In the VBAC model, which is only valid for small Bi fractions, the Bi is considered as an isoelectric impurity in the GaAs host as it has a much larger covalent radius and smaller electronegativity than As (see Table 2.1). The Bi atoms form states below the valance band edge (VBE), which couple to the bands of the GaAs host resulting in energetically higher E_+ and lower E_- bands. The presence of a band anti crossing in Ga(AsBi) was confirmed by tight-binding supercell calculations that also showed that, in contrast to the first studies[41,42], only the heavy hole (HH) and light hole (LH) bands are significantly involved in the anti crossing and only the E_+ bands can be observed[44]. Based on the results of the tight binding calculations a $\mathbf{k}\cdot\mathbf{p}$

model including VBAC was developed, which provides simple and accurate description of the band structure of the dilute bismide Ga(AsBi)[45]. The valance band edge in the band anti crossing model can be calculated by:

$$E_{+}^{HH}(x) = \frac{E_{HH} + E_{Bi}}{2} + \sqrt{\left(\frac{E_{HH} + E_{Bi}}{2}\right)^2 + V_{Bi}^2(x)} \tag{2.1}$$

where E_{Bi} is the energy of the Bi induced state in relation to the GaAs valance band edge, $V_{Bi}(x) = \beta\sqrt{x}$ with the coupling parameter β and the Bi fraction x and E_{HH} is the HH band edge energy from VCA:

$$E_{CB}(x) = E_{CB}(GaAs) - \alpha_{Bi}x + \delta E_{CB}^{hy} \tag{2.2}$$
$$E_{HH}(x) = E_{HH}(GaAs) + \kappa_{Bi}x + \delta E_{VB}^{hy} + \delta E_{VB}^{ax} \tag{2.3}$$
$$E_{LH}(x) = E_{LH}(GaAs) + \kappa_{Bi}x + \delta E_{VB}^{hy} - \delta E_{VB}^{ax} \tag{2.4}$$
$$E_{SO}(x) = E_{SO}(GaAs) - \gamma_{Bi}x + \delta E_{VB}^{hy} \tag{2.5}$$

α_{Bi}, κ_{Bi} and γ_{Bi} are the VCA contributions of Bi and $E_{CB/VB}^{hy/ax}$ are the hydrostatic and axial components of the strain that are described in more detail in Ref. 45 and Ref. 46. The values for β, E_{Bi} and the virtual crystal contributions are summarized in Table 2.1. The spin-orbit-splitting (Δ_{SO}), which is the separation of the HH and LH bands to the spin-orbit split off band (SO), is increasing with the atomic number Z of the group-V element in III-V semiconductors[47]. Therefore it is expected that Δ_{SO} strongly increases if As is replaced by Bi in GaAs which can experimentally be observed by photo reflectance (PR) spectroscopy in good agreement with theoretical considerations[39,41,44,45,48]. Studies predict that the bandgap of the Ga(AsBi) compound with Bi fractions of approximately 10% is

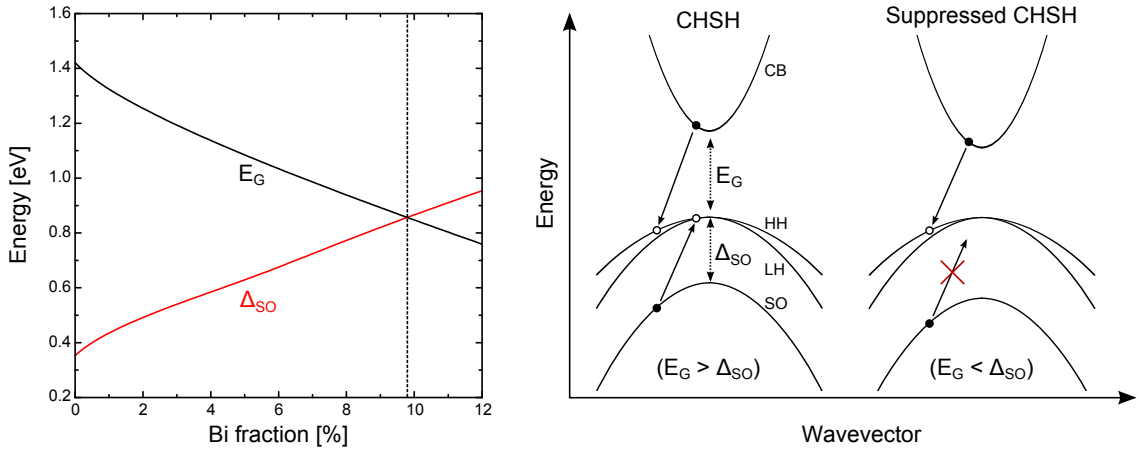

Figure 2.2: Bandgap E_G and spin-orbit-splitting Δ_{SO} energy of strained Ga(AsBi) on GaAs as function of the Bi content[45]. For Bi fractions higher than 10% Δ_{SO} becomes grater than E_G and hence loss mechanisms such as the CHSH Auger recombination that occurs in conventional 1.55 µm laser devices are suppressed (adapted from Ref. 6).

smaller than Δ_{SO} with an emission wavelength of 1.55 µm[5,6,44,48]. Thus, in Ga(AsBi$_{\approx 10\%}$) laser diodes, inter valance band absorption and CHSH Auger recombination (recombination from CB to HH and subsequent excitation from SO to HH), which are the dominant loss mechanisms in present 1.55 µm devices[1–3], would be suppressed leading to higher efficiencies and less heating. The reduced temperature sensitivity of the Ga(AsBi) band gap that was demonstrated by photoluminescence studies[7,8] and optical pumped lasing[10] would be of additional benefit in such laser devices.
However, the growth of Ga(AsBi) alloys is very challenging since it is highly metastable and therefore phase separations of solid GaAs, liquid Bi and liquid Ga may occur during growth. Another problem about the fabrication is that Bi, in contrast to the lighter group-V elements, does not desorb that easily from the surface because of its low vapor pressure. Hence, Bi droplets can form during deposition, making the sharp hetero interfaces required in optoelectronic devices difficult to achieve. The first experiments on the epitaxial growth of Ga(AsBi) on GaAs were carried out by Oe et al. in 1998 using MOVPE[7,8,14]. It was found that due to the metastability very low growth temperatures (<400 °C) were required in order to incorporate a significant amount of Bi (up to 2%) into GaAs. Other groups later also reported about the growth via MOVPE with Bi contents up to 4% but, especially at higher Bi fractions, metallic droplets accumulate[15–18]. In 2003 the first successful deposition of Ga(AsBi) using MBE with Bi fractions around 3% was presented by Tixier et al.[20]. Comparison of Rutherford backscattering and x-ray diffraction measurements enabled the experimental determination of the hypothetical GaBi zinc blende lattice constant a_{GaBi} of about 6.33 Å, which is in good agreement with calculations[11,47,49]. This value is still most often used in literature and the lattice parameter $a_{Ga(AsBi)}$ of the Ga(AsBi) alloy with the Bi fraction x can then simply be calculated using Vegard's law:

$$a_{Ga(AsBi)} = x \cdot a_{GaBi} + (1 - x) \cdot a_{GaAs} \tag{2.6}$$

Since in MBE, in contrast to MOVPE, no decomposition of precursors is needed, growth temperatures below 300 °C can be applied which enabled the deposition of Ga(AsBi) layers with Bi fraction above 10%[21]. The drawback of these low growth temperatures is that the surface mobility during growth is very low and more crystal defects occur, which can make the material useless for photonic devices. For this reason only MBE grown LED structures with less than 2% Bi[50,51] and optically pumped lasers with maximum Bi fractions of 5.9%[10,52] were presented until now. Similarly to the MOVPE growth, avoiding the formation of metallic droplets is also a big challenge using MBE.

2.1.3 Ga(NAsBi)

Dilute nitride compounds as Ga(NAs) and (GaIn)(NAs) have already been investigated for long time since N also strongly reduces the bandgap of the host material by about 130 to

Zinc blende properties (300K)	**GaN**	**GaAs**	**GaBi**
Bandgap (E_g/eV) [49,53]	3.30	1.42	0 (-1.45)
Spin-orbit-splitting (Δ_{SO}/eV) [53,54]	0.017	0.341	2.2
Lattice constant (a/Å) [20,53]	4.5	5.65	6.33
Elastic constants (C_{11},C_{12}/GPa) [53,55]	293, 159	1221, 566	73, 32.7
Group-V Element properties	**N**	**As**	**Bi**
Atomic number (Z)	7	33	83
Covalent radius (r_c/Å)	0.7	1.18	1.45
Electronegativity (χ) [56]	3.04	2.18	2.02
BAC and VCA parameters in GaAs	**N**	**As**	**Bi**
Impurity state energy ($E_{N,Bi}$/eV) [45,57]	1.706	-	-0.183
Coupling parameter (β/eV) [45,57]	2.0	-	1.13
VCA contributions in GaAs	**N**	**As**	**Bi**
Conduction band (α/eV) [45]	-1.51	-	2.82
Valance band (HH/LH) (κ/eV) [45]	1.36	-	1.01
Spin-split-off band (γ/eV) [45]	-1.53	-	0.55

Table 2.1: The Table summarizes the most important parameters of the binary zinc blende alloys GaN, GaAs and GaBi, their group-V elements and the BAC in GaAs for this work. The values for GaN and GaBi are either calculated or extrapolated from diluted alloys, GaBi as semi-metal would have a band gap of zero, however the negative value of -1.45 eV given in brackets is calculated from $\Gamma_{6c} - \Gamma_{8v}$ and hence more meaningful for comparison with the bandgap of GaAs and GaN. The impurity state energy $E_{N,Bi}$ is given with respect to the GaAs valance band edge.

150 meV per % N [43,58]. The electronic structure of the dilute nitrides can be described by the CBAC model where N, as the smallest group-V element with a large electronegativity compared to As (Table 2.1), is considered as an isoelectric impurity that induces resonant states in the conduction band of the GaAs host. Equivalent to (2.1), the conduction band edge is calculated by:

$$E_- = \frac{E_{CB} + E_N}{2} - \sqrt{\left(\frac{E_{CB} + E_N}{2}\right)^2 + V_N^2(y)} \tag{2.7}$$

where E_{CB} is the CBE energy from VCA, E_N the energy of the N induced state in relation to the GaAs VBE and the potential again $V_{Bi}(y) = \beta\sqrt{y}$ with the coupling parameter β and the N fraction y. The values for β and E_N as well as the virtual crystal contribution are summarized in table 2.1. It is also assumed that the N induced states are only slightly sensitive to temperature and hence the temperature sensitivity of the E_- band as mixture of E_{CB} and E_N is lower than the one of conventional III-V semiconductors, which is

experimentally confirmed[59]. However, not only is the epitaxial growth of Ga(AsBi) very challenging but so too is the growth of Ga(NAs). Due to the desorption of N from the growth surface, high N overpressures and growth temperatures of 500 to 600 °C are usually applied[60–62]. The crystalline quality of dilute nitride crystals suffers from N induced defects, such as N clusters, and hence in most cases a post growth annealing is necessary in order to improve the photoluminescence (PL) signal[63,64].

The advantage of the quaternary Ga(NAsBi) alloy is that the strain induced by N and Bi is contrary while both reduce the bandgap in GaAs due to BAC interactions. The impact of Bi on the VBE and N on the CBE can be treated independently[45] as in (2.1) and (2.7) with the VCA equivalent to (2.2) - (2.5):

$$E_{CB}(x) = E_{CB}(GaAs) - \alpha_{Bi}x - \alpha_N y + \delta E_{CB}^{hy} \tag{2.8}$$

$$E_{HH}(x) = E_{HH}(GaAs) + \kappa_{Bi}x + \kappa_N y + \delta E_{VB}^{hy} + \delta E_{VB}^{ax} \tag{2.9}$$

$$E_{LH}(x) = E_{LH}(GaAs) + \kappa_{Bi}x + \kappa_N y + \delta E_{VB}^{hy} - \delta E_{VB}^{ax} \tag{2.10}$$

$$E_{SO}(x) = E_{SO}(GaAs) - \gamma_{Bi}x - \gamma_N y + \delta E_{VB}^{hy} \tag{2.11}$$

Thus, lattice matched Ga(NAsBi) could theoretically be deposited on GaAs covering the whole bandgap range from 1.42 eV down to zero, with the use in temperature stable photonic devices at 1.55 µm wavelength of particular interest[5,6]. Though only a few studies on its growth have been carried out so far and only by MBE, the investigations on those structures support the hypothesis that Bi and N act independently and show that the temperature sensitivity of the bandgap is strongly reduced[9,38,65,66].

2.2 Methods

2.2.1 Metal organic vapor phase epitaxy (MOVPE)

Metal organic vapor phase epitaxy is a standard technique for the deposition of III-V semiconductor thin films on a given substrate. Since it operates at non-equilibrium conditions it is suitable for the production of metastable materials such as Ga(AsBi) and Ga(NAsBi). Metal organic molecules are brought to the surface of a mono crystalline wafer that is heated to a certain temperature. Due to the high substrate temperature the molecules decompose at the surface and, in the ideal case, only the metal is left behind and incorporates into the crystal whereas the organic group goes to the exhaust system (Figure 2.3). For the Ga(AsBi) and Ga(NAsBi) growth the all liquid precursors triethylgallium (TEGa), tertiarybutylarsine (TBAs), trimethylbismuth (TMBi) and unsymmetric dimethylhydrazine (UDMHy) were chosen. Additionally, trimethyaluminum (TMAl), diethyltellurium (DETe) and diethylzinc (DEZn) were used for Al containing layers and the n- and p-type doping, respectively. An important property of the precursors used in MOVPE is their decomposition characteristics since they need to be stable enough not to dissociate in storage but decompose sufficiently at the applied substrate temperature. This is especially crucial in this work as low growth temperatures (<450 °C) are required at which the used metal organics do no longer fully dissociate[67–69].
In contrast to the MBE technique that is also often used for the fabrication of III-V semiconductors, no ultra high vacuum (UHV) is needed for MOVPE and up-scaling to larger substrates is more straightforward. However, as decomposition characteristics need to be taken into account, the understanding and control of the growth process is more complex. For deeper understanding of the MOVPE growth of III-V semiconductors and the decompositions characteristics of the precursors Ref. 68 is advisable.
For the growth of the Ga(AsBi) and Ga(NAsBi) structures on GaAs an AIX 200 GFR

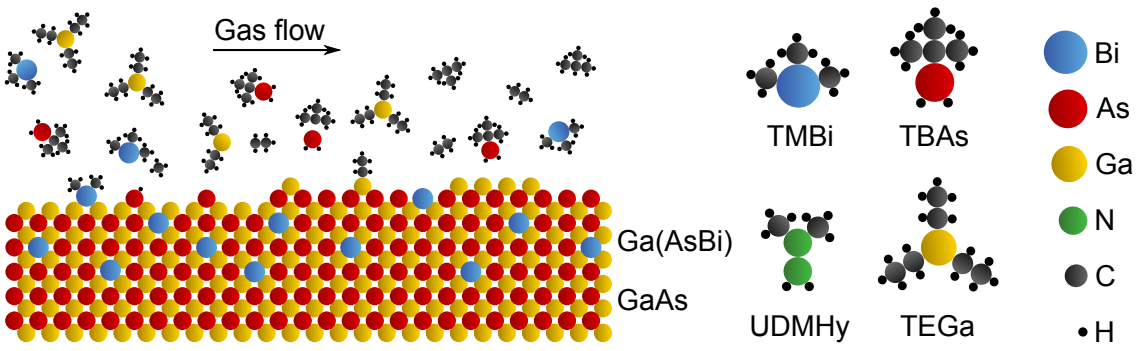

Figure 2.3: Schematic view of the MOVPE growth in a horizontal reactor system. The metal organic precursors approach the heated substrate surface, decompose and the group-III and group-V elements incorporate into the crystal while the organic groups go into the exhaust. The precursors used for the growth of Ga(AsBi) and Ga(NAsBi) are shown on the right hand side.

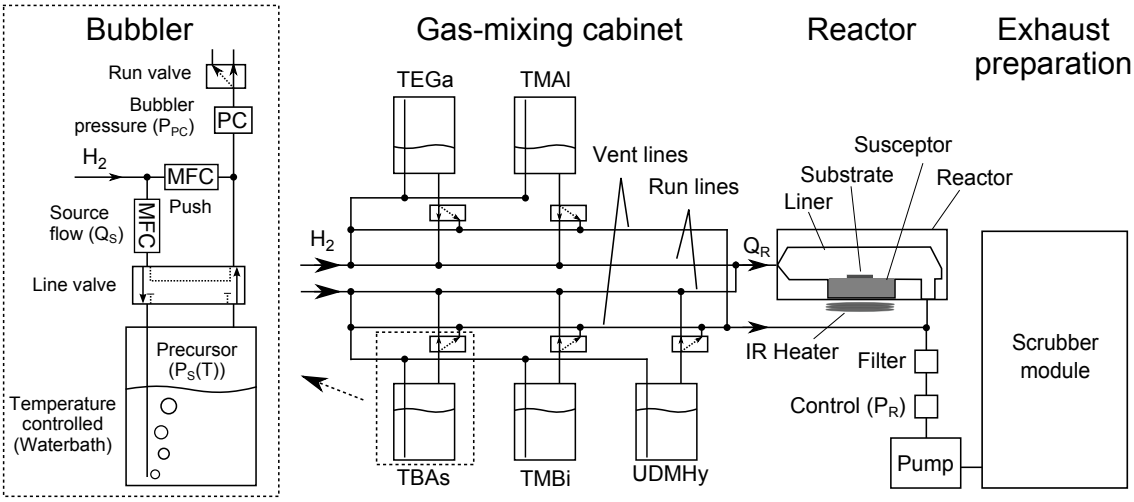

Figure 2.4: Sketch of a horizontal reactor MOVPE system. In the gas-mixing cabinet the amount of the precursors that get transported to the reactor by the H_2 carrier gas is controlled. The growth takes places in the reactor that includes the susceptor at which the substrate is located. Since the used chemicals are partially toxic the exhaust is cleaned by a scrubber module.

(gas flow rotation) system with a 2" horizontal reactor system was used. A scheme of the system shown in Figure 2.4, it can be divided into three parts: the gas-mixing cabinet, the reactor and the exhaust preparation.

In the gas-mixing cabinet the metal organic precursors are stored in closed stainless steel containers (bubblers), through which there may be a flow of Pd-purified hydrogen carrier gas. The carrier gas transports the saturated gas phase of the liquid precursor via a stainless steel pipe system to the reactor. The amount of material that is transported to the reactor depends on the source gas flow through the bubbler (Q_S), the pressure in the bubbler (P_{PC}) and the vapor pressure of the precursor (P_S) which varies with the temperature in the bubbler. Q_S and P_{PC} can be adjusted by a mass flow controller (MFC) and pressure controller (PC), respectively, whilst P_S is held constant by storing the bubbler in a temperature controlled water bath. The amounts of the metal organics within the reactor are discussed in terms of their partial pressure (P_P), which is calculated as follows:

$$P_P = \frac{Q_S}{Q_R} \cdot \frac{P_S}{P_{PC} - P_S} \cdot P_R \tag{2.12}$$

where Q_R is the total gas flow through the reactor and P_R is the reactor pressure, which are both held constant during growth at 6800 sccm and 50 mbar, respectively. In order to allow fast on- and off-switching of the precursors each source has a run-valve which can either lead the molecules to the reactor (run line) or directly into the exhaust (vent line). All parameters and valves, except the water bath temperature, are controlled by a computer which can run a prepared program with all important orders for the deposition process.

The substrate is placed inside the quartz glass reactor on a graphite plate that is embedded in a graphite block (susceptor) and can be rotated via gas flow below it. The temperature is adjusted with infrared lamps that are placed below and a temperature sensor inside the susceptor, which is calibrated to the substrate surface temperature by the use of an Al/Si eutectic. A special quartz glass box (liner) encloses the susceptor to ensure a laminar gas flow above the substrate. For the control of the reactor pressure a pump and a butterfly valve (control) are placed between the reactor and the scrubber module for exhaust preparation.

2.2.2 High resolution x-ray diffraction (HR-XRD)

High resolution x-ray diffraction is a non-destructive method to analyze crystalline structures. In this work a *Panalytical X'Pert Pro* system was used applying ω-2θ scans, which enable the determination of the thicknesses and compositions of individual layers of hetero structures. In XRD monochromatic x-rays get scattered at the lattice planes of the investigated crystal and constructive interference in reflection can be detected in case the Bragg condition

$$n \cdot \lambda = 2 \cdot d_{hkl} \cdot sin(\theta_B) \tag{2.13}$$

is fulfilled. In this formula n is the order of diffraction, λ the wavelength of the monochromatic x-ray beam, d_{hkl} the distance of the investigated lattice planes and θ_B the angle between the reflected beam and the lattice planes. In an ω-2θ scan the beam hits the sample at the angle ω and reflection is detected at the angle 2θ, which in the chosen geometry equals 2ω (Figure 2.5 (a)). The investigated (004) reflection corresponds in the zinc blende crystal to the distance between the lattice planes in growth direction.
In the case where a layer with larger lattice constant than the one of the substrate is

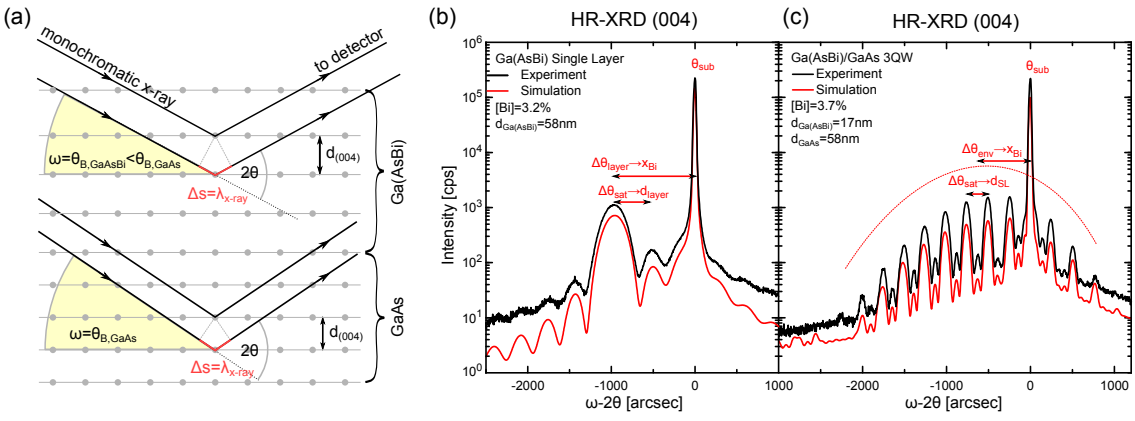

Figure 2.5: (a) Principle of the HR-XRD (004) ω-2θ scan: the x-rays hit the sample at the angle ω and in the case the Bragg condition is fulfilled constructive interference is detected in 2θ=2ω. An example of such a scan of a Ga(AsBi) single layer and a Ga(AsBi)/GaAs 3QW on GaAs is shown in (b) and (c), respectively. The dynamical simulation enables the determination of the layer thicknesses and composition of the deposited layers.

deposited and the difference is not too large, compressive strain in plane occurs since the layer will adopt the lattice constant of the substrate (pseudomorphic growth). Hence, in order to reduce the overall strain, the lattice distance in growth direction increases. In the ω-2θ scan this will lead to an additional peak in the profile with $\theta_{layer}<\theta_{sub}$ (2.13). For small $\Delta\theta = \theta_{layer} - \theta_{sub}$ it is possible to calculate the lattice distance ($a^{\perp}_{layer}$) using the kinematic theory of diffraction, which among others neglects multiple scattering:

$$\frac{a^{\perp}_{layer} - a_{sub}}{a_{sub}} = -\Delta\theta \cdot cot(\theta_{sub}) \tag{2.14}$$

where a_{sub} is the known lattice constant of the substrate. Taking the elastic constants C_{11} and C_{12} of the material into account allows the determination of the lattice constant a_{layer} of the relaxed crystal:

$$\frac{a_{layer} - a_{sub}}{a_{sub}} = \frac{C_{11}}{C_{11} + 2C_{12}} \cdot \frac{\Delta a^{\perp}}{a_{sub}} \tag{2.15}$$

For a ternary material system, such as Ga(AsBi), the knowledge of the relaxed lattice constant directly gives the composition using Vegards Law (2.6). However, in the case of a quaternary alloy such as Ga(NAsBi) additional information as e.g. from secondary ion mass spectroscopy (SIMS) is needed since one degree of freedom is left in Vegards Law.
Besides the constructive interference caused by the (004) lattice planes further peaks, so called satellite or thickness fringes, appear in the XRD pattern since the epilayer itself can be considered as a lattice. The separation is of course much larger than that of the crystal planes and therefore the separation of the maximums $\Delta\theta_{sat}$ is much smaller. $\Delta\theta_{sat}$ is linked to the layer thickness d_{layer} by Bragg's law:

$$d_{layer} = \frac{\lambda}{2cos(\theta_{sub})\Delta\theta_{sat}} \tag{2.16}$$

An example of the (004) reflection pattern of a Ga(AsBi) single layer on GaAs is given in Figure 2.5 (b). The most pronounced peak aside from the GaAs substrate peak refers to the d_{004} planes of the compressive strained Ga(AsBi) layer and is modulated by the thickness fringes.
In the more complex profile of a multi quantum well (MQW) structure with n quantum wells the $\Delta\theta_{sat}$ corresponds to the superlattice (SL) thickness ($D_{SL} = d_{QW} + d_{barrier}$). Furthermore $n-2$ smaller fringes appear in between that come from constructive interference of e.g. the first and third layers in a 3QW, the second one will then be destructive which leads to lower intensities. Figure 2.5 (c) shows the profile of a Ga(AsBi)/GaAs 3QW, the thin Ga(AsBi) QW lattice leads to a broadened envelope on the compressive side which gives the QW composition. The position of fringes with respect to the substrate peak depends on the thickness ratio of QW and barrier in the SL and hence makes it possible to determine the thicknesses of the QW and the barrier separately.

Since the kinematic theory of diffraction is only a good approximation for small angles it is more accurate to use dynamical simulations and compare those to the experimental data as shown in Figure 2.5 (b) and (c). The simulations were all done using the *Panalytical X'Pert epitaxy* software with the material parameters given in Table 2.1.

2.2.3 Atomic force microscopy (AFM)

Atomic force microscopy was used to investigate the surface morphologies of the fabricated structures. The principle of this method is based on short distance interactions such as van-der-Waals and electrostatic forces occurring between an ideally monoatomic tip, which is fixed on a cantilever, and the surface of the sample. All measurements in this work were done using a *Digital Instruments MultiMode SPM* applying the tapping mode at constant height. In tapping mode the cantilever oscillates with its eigenfrequency which is monitored using a laser beam that is reflected from the cantilever onto a horizontally divided photo diode. When the tip approaches the surface the oscillation gets quenched due to the interactions. Hence, a change in the oscillation amplitude can be related to a change of the distance between tip and sample. In the applied constant height mode such modulations are corrected by lifting or lowering the probe using a piezo crystal. A second piezo crystal moves the sample in x-y-direction by scanning the surface line by line to obtain the height profile. Since the piezo crystal is a tube scanner this movement is spherical and hence the images were corrected by the computer programs *Gwyddion* and *NanoScope (Digital Instruments)* after recording. AFM measurements can be performed under atmosphere and enable atomic resolution in z-direction. The resolution in x-y-direction is limited to a few nanometers due to the finite width of the tip.

2.2.4 Transmission electron microscopy (TEM)

Transmission electron microscopy enables the investigation of samples down to atomic scale. For this method the specimen needs to be electron transparent which is realized by extensive preparation including mechanical thinning and precision ion polishing. All crystals regarded in this work were prepared in cross section either in [010] or [-110] direction. Parts of the measurements were carried out using a *JEOL 3010* TEM in dark field mode (DF) and parts using a *JEOL 2200FS* scanning transmission electron microscope (STEM) in high angle annular dark field (HAADF) mode.

Dark field (002) mode

In conventional TEM mode a cathode in combination with a Wehnelt cylinder and a magnetic condenser lens system generates a parallel electron beam that irradiates the sample. The beam is transmitted through the crystal and the objective lens creates a virtual image in the image plane. This image is then magnified by the use of an intermediate

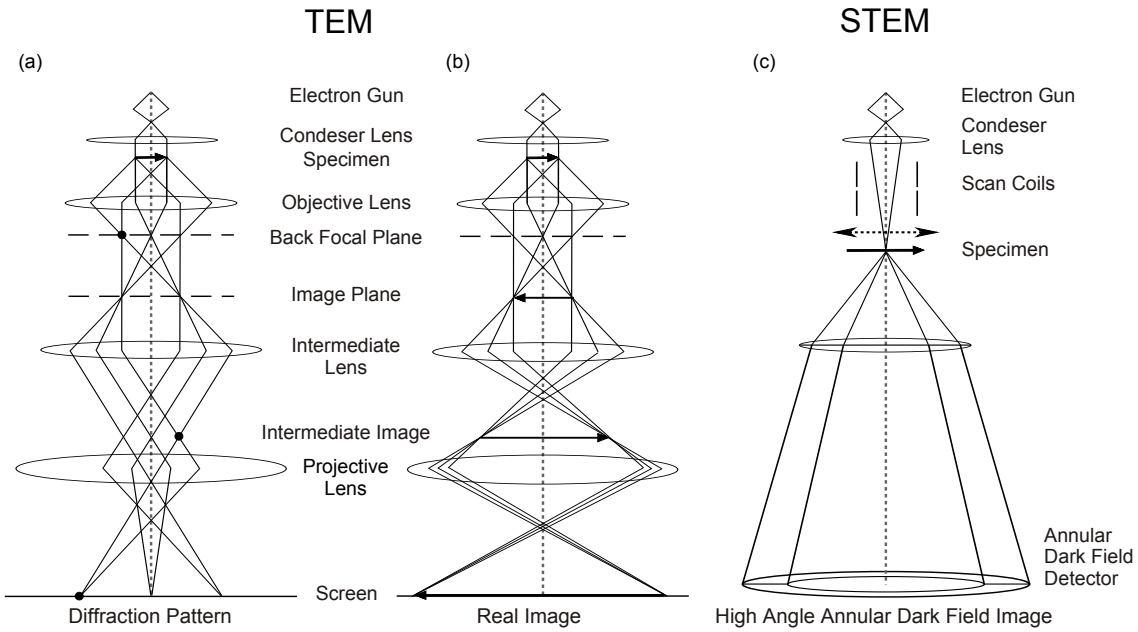

Figure 2.6: Sketch of the beam path in TEM and STEM. In TEM the contrast of the image is generated by diffraction of the parallel electron beam at the crystal lattice and either the diffraction (a) or the real image (b) can be viewed. In HAADF STEM a focused beam scans across the specimen and an annular detector collects electrons that are scattered into high angles (c).

and a projective lens system onto a screen or CCD-chip. The intermediate lens system can be tuned either to image the diffraction pattern (Figure 2.6 (a)) or the real image (Figure 2.6 (b)) of the investigated crystal.
Constructive interference in the diffraction pattern is observed if the Bragg condition is fulfilled (2.13) that is most often described by the equivalent Laue condition in TEM,

$$\vec{k} - \vec{k}' = \vec{G} \tag{2.17}$$

where $\vec{k}$ is the wave vector of the impinging wave, $\vec{k}'$ the wave vector of the diffracted wave and $\vec{G}$ a vector of the reciprocal lattice. This condition is illustrated by the Ewald's sphere where $\vec{k}$ ends at a reciprocal lattice point and hence all lattice points that are lying on the sphere with center at the origin of $\vec{k}$ and radius $|\vec{k}|$ result in a diffraction reflex. In non primitive lattices such as the zinc blende structure not all reflexes exist since there can be destructive interference of the sublattices. The amplitude of the (hkl) reflex is described by the structure factor:

$$F_{hkl} = \sum_{j=1}^{n} f_j e^{2\pi i \vec{r}_j \vec{G}} = \sum_{j=1}^{n} f_j e^{2\pi i (x_j h + y_j k + z_j l)} \tag{2.18}$$

In this case f_j is the atomic form factor of the atom j and is related to the atomic number Z. $\vec{r}_j$ is the translation vector of the sublattices and x_j, y_j and z_j the position of their

atoms. In the present work the real image of the (002) reflex of samples prepared in (010) direction was investigated which can be displayed by selecting the (002) spot in diffraction mode using an aperture. The structure factor of the ternary $Ga(As_{1-x}Bi_x)$ in this case is given by:

$$F_{002} = 4(f_{Ga} - f_{As_{1-x}Bi_x}) = 4(f_{Ga} - (1-x)f_{As} - xf_{Bi}) \tag{2.19}$$

This obviously results in a contrast in the image if the chemical composition is changing locally. The higher the Bi fraction in Ga(AsBi) is, the brighter the (002) reflex becomes. To keep the intensity high and aberration low the sample is usually tilted in a way that the diffracted beam is on the optical axis.
The wavelength of the electrons for the JEOL 3010 TEM with an acceleration voltage of 300 kV is only about a few picometer. However, due to aberration of the magnetic lenses the resolution of such microscopes without aberration correction is limited to about 2 Å.

High angle annular dark field scanning transmission electron microscopy

In contrast to the conventional TEM, in STEM a highly focused electron beam is used provided by a field emission gun and a condenser lens. Additionally, scan coils are positioned straight above the sample to scan the beam line by line across the sample (Figure 2.6 (c)). At each atomic column of the crystal the beam is scattered, mainly by Rutherford scattering. Hence, the higher the atomic number Z of the elements within one column and the higher the number of atoms, thus the thickness, the larger the intensity of electrons scattered into high angles becomes. These electrons are collected by the use of an annular detector in the high angle annular dark field (HAADF) mode. The inner angle of this detector can be adjusted by a system of projector lenses that are placed behind the sample. Since mainly Rutherford scattering takes place the brightness is roughly proportional to Z^2 for constant thickness and therefore the more Bi a column contains the brighter it appears in the image. The resolution of the used *JEOL 2200FS* microscope with 200 kV acceleration voltage and aberration correction is below 100 pm.

2.2.5 Photoluminescence spectroscopy (PL)

Photoluminescence spectroscopy gives information about the semiconductors electronic properties such as the band gap and position and density of defect levels. The sample gets excited by a focused laser beam with photon energy larger than the band gap. The photons interact with the electrons in the valance band of the semiconductor and lift them into the conduction band. After relaxation of the electrons and holes to the band extrema they can recombine and emit a photon which with approximately the energy of the band gap. Aside from the band edge PL signal, defect levels within the band gap can be detected as well, depending on the investigated energy range. Furthermore the comparison of the integrated PL signal of similar samples gives a clue about the density of

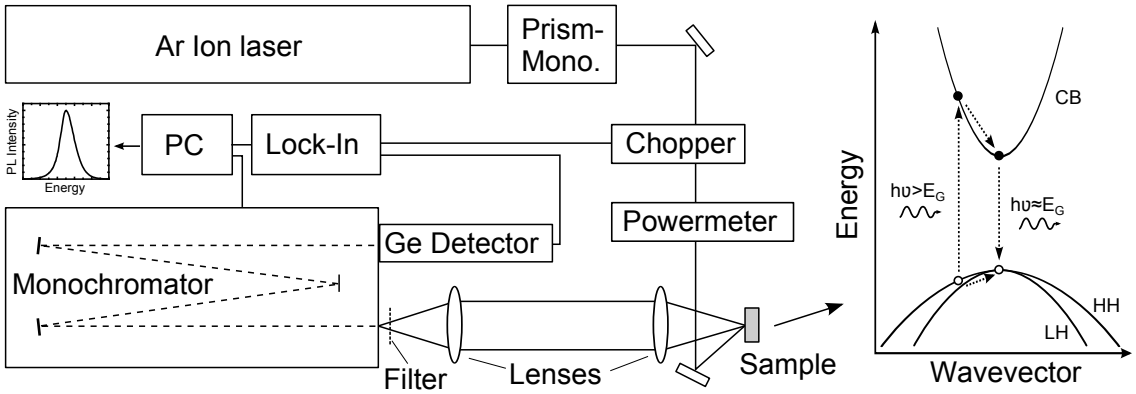

Figure 2.7: Photoluminescence spectroscopy set-up: The sample gets excited using an argon ion laser. Lenses feed photoluminescence signal into the monochromator with Ge detector for spectral analysis. Lock-in technique is used for an increased signal to noise ratio.

deep level defects that act as non-radiative recombination centers.

For excitation an argon ion laser was used, with its most pronounced wavelength of 514 nm selected by a prism monochromator and focused onto the sample by a system of mirrors and lenses (Figure 2.7). Excitation powers of 20 to 100 mW were applied at a spot size of approximately 160 µm. Two collecting lenses feed the emitted light into a 1 m grating monochromator (*THR 1000, Jobin-Yvon*) for spectral analysis. A *RG550-filter* is used to remove the reflected laser light. At the outlet of the monochromator a liquid nitrogen cooled Ge detector collects the photons. A lock-in amplifier (*SR510, Stanford Research Systems*) and a chopper in the optical path of the excitation laser beam are used to increase the signal to noise ratio. The lock-in amplifier is connected to a computer that also controls the monochromator and, hence, can record the PL intensity versus the energy. Since the sensitivity of the Ge detector also depends on the energy of the photons, the spectra need to be corrected afterward by using a calibration spectrum.

CHAPTER 3

Results

In the following all important research results on the MOVPE growth of Ga(AsBi) and Ga(NAsBi) and their characterization will be presented. At first metallic droplets are treated that can form at the surface during the growth (Section 3.1). The main part (Section 3.2) includes the growth of Ga(AsBi)/GaAs QW and bulk-like structures, providing a growth model that is influenced by several factors. Furthermore, the effect of the chosen growth conditions on the structure and electronic properties is covered in this part. The results on the first electrically pumped Ga(AsBi) containing laser diodes are presented in Section 3.3 and the chapter completes with the growth of quaternary Ga(NAsBi) structures (Section 2.1.3).

3.1 Metallic droplets and related structures

One of the main challenges occurring during the growth of Ga(AsBi) alloys is the formation of metallic droplets at the surface. In order to gain a better understanding of these droplets and thereby help to avoid their formation, they were investigated structurally. The results of these studies were published in *"Growth of Ga(AsBi) on GaAs by continuous flow MOVPE"*[29] (Section 5.3) and *"Investigation of the microstructure of metallic droplets on Ga(AsBi)/GaAs"*[32] (Section 5.6). Analyzing the surfaces of nominally Bi containing bulk structures that were grown in the temperature regime of 350 °C to 450 °C, it was found that depending on the growth conditions three types of droplets arise. They may consist either of crystalline Bi, liquid Ga or liquid Ga enveloping the crystalline Bi. The third type of structures, the combination of Ga and Bi, forms during the cooling after growth since Ga and Bi are fully miscible in a liquid phase at temperatures above approximately 270 °C but separate into a solid Bi and liquid Ga phase at room temperature[36]. By the use of transmission electron microscopy and by investigation on selectively etched samples, it was shown that Bi containing droplets already start to form at the very beginning of the growth since they reach down to the GaAs buffer layer which is deposited prior to the

Ga(AsBi) layer. These droplets can also be evaporated at 625 °C after the growth leaving holes behind with volcano-like structures arising at the edges. These consist of GaAs from the Ga that was dissolved within the evaporated Bi droplet and As from the gas phase that is used for group-V stabilization. Investigation on the influence of the applied growth temperature showed that pure Bi droplets cluster at $\lesssim$400 °C, which is a hint for catalytic decomposition of the TMBi precursor by the metal droplets. From the knowledge of the droplets' composition, further experiments were carried out with drastically reduced TMBi partial pressures and carefully adjusted growth parameters, which finally enabled droplet free surfaces (Section 3.2).

3.2 MOVPE growth of Ga(AsBi)/GaAs hetero structures

This section focuses on the deposition of Ga(AsBi) layers using the MOVPE technique. Thereby the influence of several growth parameters such as the applied growth temperature (T_{gr}), the growth rate (v_{gr}), the partial pressures of the precursors (P_P) and the pulsed and continuous precursor flow was investigated. Since the value of each of the partial pressures by itself is not meaningful they are discussed in relation to each other, where in the following the TMBi/V=P_P(TMBi)/(P_P(TBAs)+P_P(TMBi)) ratio is the fraction of TMBi in the gas phase related to the total amount of group-V precursors. The V/III=(P_P(TBAs)+P_P(TMBi))/P_P(TEGa) ratio will be most often discussed in terms of the TBAs/TEGa=P_P(TBAs)/P_P(TEGa) since P_P(TMBi) is much smaller than P_P(TBAs) and varied at constant TBAs/TEGa. The total value of P_P(TEGa) will be given since group-III usually determines the growth rate and all other values can be derived directly for the given TBAs/TEGa and TMBi/V ratios.

3.2.1 Pulsed precursor flow - Bi incorporation model in GaAs

Initial experiments on the Ga(AsBi) growth on GaAs substrates did not show any Bi incorporation but segregation of Bi and formation of droplets, even though the most important parameters as the V/III and TMBi/V were varied in a wide range at sufficiently low growth temperatures (T_{gr}<450 °C). In order to reduce the segregation of Bi a pulsed growth mode was applied with the goal of burying the Bi below the group-III layer. Alternating pulses of one second TEGa and one second TBAs and TMBi were used which resulted in Ga(AsBi) layers with small Bi fractions of about 1%. Starting from these results improved growth parameters for the growth at 400 °C were established with TBAs/TEGa $\approx$ 2 and P_P(TEGa)=1.4E-2 mbar which corresponds to the GaAs growth rate of about 0.24 nm/s for continuous precursor flow. However, as Bi segregation still takes place in this growth regime, the successful deposition of Ga(AsBi) was only possible for thin layers with a few nm thickness. Since such thin layers are difficult to analyze in HR-XRD, Ga(AsBi)/GaAs multi quantum well (MQW) structures with nominal 7 nm QW and 45 nm

GaAs barrier were realized to get a significant signal. A set of samples with different TMBi supplies was deposited and analyzed by XRD, AFM and TEM in order to investigate the role of the TMBi during the growth. The results of these studies were published in *"MOVPE growth of Ga(AsBi)/GaAs multi quantum well structures"*[27] (Section 5.1).
It was found that only very low values of TMBi/V are needed to observe significant Bi incorporation. Increasing the TMBi partial pressure results in linearly increasing Bi fractions in the crystal that level out due to the metastability of the material at about 2% Bi for TMBi/V=0.01 at 400 °C. In contrast to the Bi fraction the QW thickness increases as soon as this limitation sets in, while the GaAs barrier thickness decreases. This is a result of the surplus Bi that segregates at the surface during the Ga(AsBi) QW growth and then incorporates during the growth of the subsequent nominal GaAs layer even though TMBi is no longer supplied. Since TEGa and TBAs were not changed from the QW to the barrier growth, the incorporation efficiency of Bi is the same and hence the QW growth continues until the segregated Bi is consumed. Thus, the incorporation of Bi is not determined by the gas phase concentration of the precursor, as usual for group-V elements, but by the amount of elemental Bi at the surface. The Bi incorporation thereby scales linearly with the amount of Bi at the surface but levels out due to metastability at a certain surface coverage (θ_{max}). When θ_{max} is exceeded also small droplets appear at the surface of the MQW, which form out of the surplus Bi and get larger for increasing TMBi supply.
TEM studies on a MQW grown with low TMBi supply in the unsaturated regime showed that the first grown QW is thinner than the following ones, even though the growth conditions were not changed. This surprising observation leads to the conclusion that at the very beginning of the Ga(AsBi) growth, the surface coverage is so low that Bi only acts as a surfactant and does not incorporate. Thus, when TMBi is switched on it takes some time to reach the minimal Bi coverage (θ_{min}) that is needed for the Bi incorporation. Hence, the start of the Ga(AsBi) growth is delayed, which results in a reduced QW thickness. When the TMBi is switched off, the segregated Bi gets incorporated into the GaAs barrier until the coverage falls to θ_{min}. Since Bi desorption is low at the applied growth temperatures, the left over Bi floats at the surface during the GaAs barrier growth and, therefore, θ_{min} is already reached at the beginning of the deposition of the second Ga(AsBi) QW. Hence, this QW and all the subsequent ones will have a greater thickness with respect to the first one, since the start of their growth is not delayed.
The TEM measurements furthermore showed that the upper interface between Ga(AsBi) QW and GaAs barrier is smeared due to a gradient of the Bi concentration, which fits to the other observations. When the segregated Bi gets consumed during the GaAs growth the Bi surface coverage decreases and passes through the range where a linear relation to the Bi incorporation was observed, before it finally ends up at θ_{min} and pure GaAs growth.
The growth model that can be extracted from these investigations is depicted in Figure

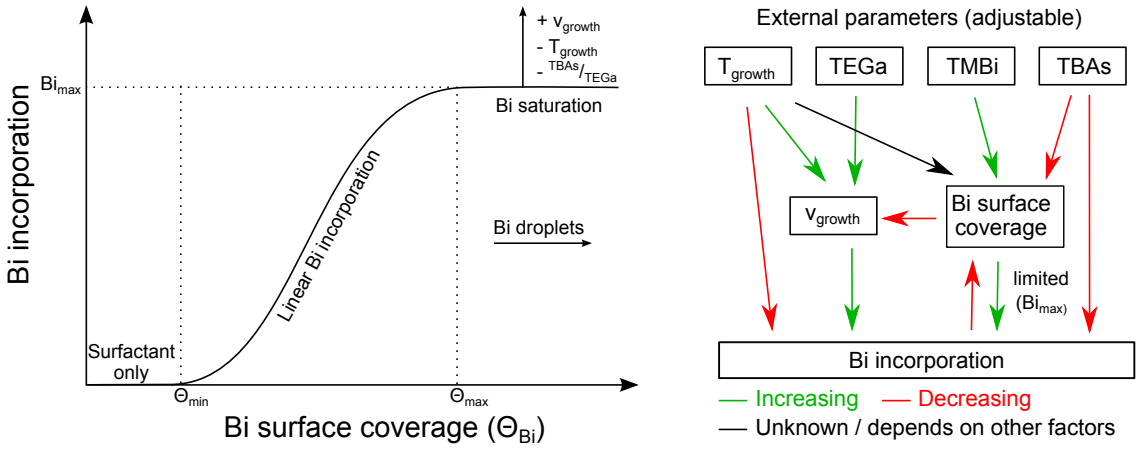

Figure 3.1: The Bi incorporation depends mainly on the Bi surface coverage. Below $\theta_{\min}$ Bi only floats at the surface, with increasing Bi coverage a linear relation to the Bi fraction was found. When $\theta_{\min}$ is exceeded the Bi fraction levels out and droplets form out of the surplus Bi at the surface. The saturation level is influenced by the growth temperature, growth rate and TBAs/TEGa ratio that are not necessarily independent, also the Bi surface coverage depends on several parameters making the control of the growth challenging.

3.1 where the Bi incorporation is plotted versus the Bi surface coverage. To begin with when the Bi surface coverage is low, the Bi only floats at the surface. As the coverage is increased, the regime is then reached where a linear trend in the Bi incorporation is observed (θ_{min}), and then it finally ends in the limited regime where Bi droplets occur (θ_{max}). The surface coverage is therefore affected by several factors making the control of the growth very complex: first of all there is the amount of TMBi given to the reactor and its decomposition rate, which may be influenced by reactions with other precursors and the growth temperature. Furthermore the incorporation rate needs to be taken into account, which is linked to the temperature, growth rate and the TBAs supply as it will be shown in the following section. Finally the growth time plays an important role on the surface coverage as long as the Bi incorporation and the Bi supply are not in balance.

3.2.2 Continuous precursor flow - improving Bi incorporation

The pulsed growth mode discussed previously with alternating group-V and group-III precursor supply brings a significant drawback. The growth rate is limited to $1\,^{\mathrm{ML}}/_{\mathrm{pulse}}$ which corresponds to $0.14\,^{\mathrm{nm}}/_{\mathrm{s}}$ for the shortest applicable pulses of 1 s. This is crucial for the Bi incorporation because at higher growth rates the time for Bi to escape the crystal would be reduced. Therefore optimized growth conditions from the pulsed growth were transferred to a continuous precursor flow growth with the result that the incorporation of Bi is only slightly lower with respect to the pulsed mode. The differences compared to the first attempts using the continuous growth are much lower V/III and TMBi/V ratios and higher growth rates. Starting from these results, the influence of several parameters such as v_{gr}, T_{gr}, V/III and TMBi/V on the Bi incorporation, crystalline structure and

optical properties was investigated systematically. The results were published in *"Growth of Ga(AsBi) on GaAs by continuous flow MOVPE"*[29] (Section 5.3).
Carefully adjusting the TMBi/V ratio within the regime where incorporation and segregation are in the same order allowed the growth of bulk-like single layer structures of more than 50 nm thickness without appearance of metallic droplets. Furthermore, in this study the subsequent GaAs layer was grown at 625 °C to avoid the incorporation of segregated Bi into the GaAs layer and to realize sharp Ga(AsBi)/GaAs hetero interfaces. It was demonstrated in *"Electrical injection Ga(AsBi)/(AlGa)As single quantum well laser"*[28] (Section 5.2, presented in Section 3.3) that heating the crystal under TBAs stabilization to 625 °C directly after the deposition of Ga(AsBi) and growing GaAs or (AlGa)As on top does not negatively influence the Ga(AsBi) and no Bi gets incorporated in the top layer. This is due to desorption of Bi during the heating and the high growth temperature of GaAs at which no Bi incorporation could be observed so far. Hence, the Ga(AsBi) layer only grows when Bi is supplied which then allows the determination of the Ga(AsBi) growth rate from the layer thickness. This was not possible for the MQW growth as the GaAs barrier was grown under the same conditions as the QW and thus the Ga(AsBi) growth continued for an unknown time until the segregated Bi was consumed.
A series of single layer structures with much higher GaAs growth rates (v_{gr}(GaAs)=0.42 nm/s for P_P(TEGa)=4.2E-2 mbar and TBAs/TEGa=1.9 at 400 °C) with varying TMBi was produced which showed the same behavior for the Bi incorporation as observed for the

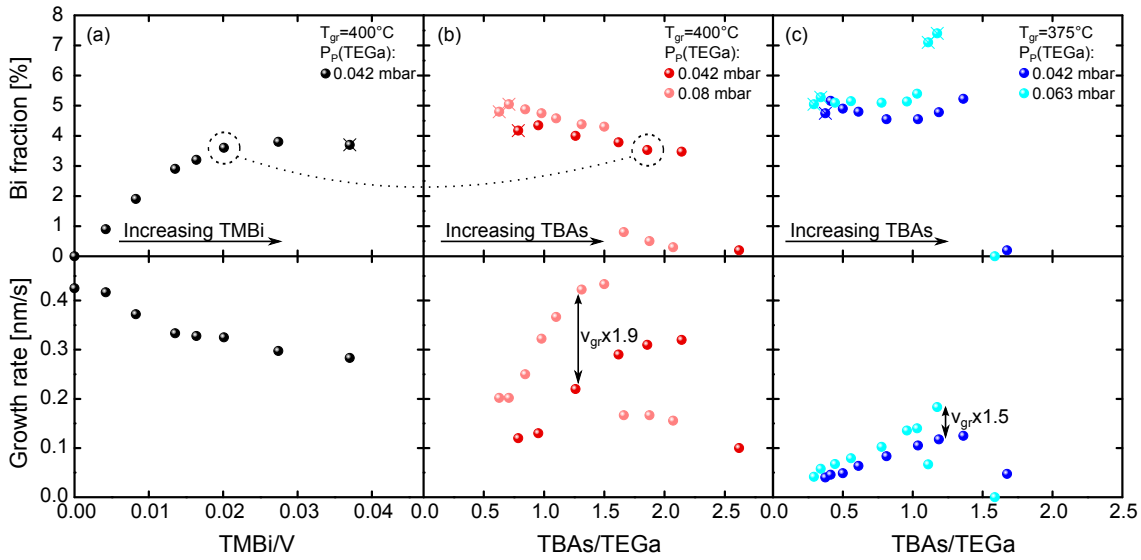

Figure 3.2: Bi fraction and growth rate of several sample series: Increasing the TMBi supply leads to increasing Bi fractions up to a limitation which is here at approximately 4%. At the same time the growth rate gets reduced by one third due to the presence of Bi at the surface (a). The Bi fraction increases with decreasing TBAs within the regime where droplet free growth is possible, doubling the growth rate allows higher maximum Bi fraction(b). At the reduced growth temperature of 375 °C more Bi can be incorporated even though the growth rate is much lower, there is also a narrow window where the Bi fraction exceeds 7% Bi (c).

pulsed MQW growth in Section 3.2.1 (Figure 3.2 (a)). The Bi fraction first scales linearly with the TMBi supply and levels out at 3.8% for high TMBi/V ratios with volcano-like structures occurring at the surface that come from evaporated Bi droplets (Section 3.1). The higher achievable Bi fraction with respect to the QW growth is related to the growth rate and will be discussed later. Having an insight on the growth rate it was found that it decreases up to 33% with increasing amount of TMBi. As v_{gr} is usually determined by the amount of the group-III elements due to the excess supply of group-V elements (here only As), it can be concluded that either the decomposition of TEGa or its ability to stick to the surface is reduced by the presence of TMBi or Bi at the surface.
This is underlined by a second sample series where the TBAs was reduced down to TBAs/TEGa=1 at constant TMBi within saturation, which led to further strong reduction of v_{gr} (Figure 3.2 (b)). As and Bi are in competition for the group-V lattice places and, hence, the surface becomes more Bi or TMBi rich if TBAs is reduced. The Bi incorporation increases for the same reason when less TBAs is present, even though the growth rate gets lower. The highest Bi fraction of 4.4% was observed for TBAs/TEGa=1 which was the minimum applicable value in order to achieve good Ga(AsBi) single layers. For even lower amounts of TBAs the surface becomes metallic (Ga and/or Bi), the previously mentioned volcano-like structures appear and the Bi fraction in the crystal decreases again. At high TBAs supplies (TBAs/TEGa>2.2) the growth rate drops more or less digitally from 0.32 nm/s to 0.1 nm/s and the Bi fraction from 3.5% to 0.2%, which is not yet understood but could be related to a change in the surface reconstruction at these growth conditions.
To investigate the influence of the growth rate on the Bi incorporation, the sample series was repeated with nearly double the amount of each precursor which results in two times higher growth rates (Figure 3.2 (b)). The curve behaves similarly to the one at lower growth rates but the Bi fraction is about 10% to 20% higher with a maximum observed Bi fraction of 5%, showing that more Bi gets incorporated when the time to escape the crystal is reduced. However, the amounts of the precursors that are carried to the reactor are limited by the machine and even higher amounts were not possible up to now for further increasing the Bi fraction.
Another way to reduce the segregation of Bi is the reduction of the energy in terms of temperature. Therefore similar studies as at 400 °C were performed at 375 °C (Figure 3.2 (c)). Due to the decomposition characteristics of the used metal organics, the GaAs growth rate at this temperature is only the half with respect to that at 400 °C. Most of the correlations stated before were also found to be true for the growth at 375 °C, with the Bi fraction being increased by about 20% to a maximum of 5.5% at comparable conditions. However, a narrow growth regime was found at TBAs/TEGa ratios just below the previously described "digital drop" where Bi fractions larger than 7% were realized. This is most probably due to the two competing processes that occur when the TBAs/TEGa is varied: on the one side the Bi fraction scales inversely to the amount of As since both are in competition for the group-V sublattice places, whilst on the other hand

the Bi fraction increases with increasing growth rate which was found to be proportional to the TBAs/TEGa ratio. So far all experiments indicated that the first of those two processes is dominating the Ga(AsBi) growth but it is presumably the other way around in this narrow regime. For the samples with Bi fraction above 7% the Ga(AsBi) layer was only found at the inner area of the wafer, which might be related to small changes in the gas phase composition and temperature that occur across the wafer and lead to unfavorable growth conditions as at too high TBAs/TEGa ratios.
There have also been experiments at even lower temperatures (350 °C) but decomposition of the precursors becomes worse, leading to another halving of the growth rate and no growth condition has been established so far to further improve the Bi content. The growth temperature has also been increased to 425 °C, 450 °C and 475 °C to enables higher growth rates, but Bi fractions of 2.5%, 2% and 0.5%, respectively, were not exceeded so far, providing a clear trend of decreasing Bi incorporation efficiency at with increasing growth temperature.
In conclusion, the above extracted growth model (Figure 3.1) can be expanded relating the maximum achievable Bi fraction to the applied growth conditions. The saturation of Bi can be increased by increasing the growth rate and decreasing TBAs/TEGa ratio and growth temperature. One therefore also has to keep in mind that the growth temperature has an impact on the decomposition characteristics and with that on the growth rate and the TBAs/TEGa ratio. Furthermore the TBAs/TEGa ratio itself directly influences the growth rate at constant offer of TMBi.

3.2.3 Optical properties and crystalline purity - Bi as surfactant

Since Ga(AsBi) is supposed to be used as active material in photonic devices, its optical properties and crystalline purity is of great interest. Therefore, room temperature PL and secondary ion mass spectroscopy (SIMS) measurements were carried out and post growth annealing was investigated. Most of the results are published in *"Growth of Ga(AsBi) on GaAs by continuous flow MOVPE"*[29] (Section 5.3) and *"Electrical injection Ga(AsBi)/(AlGa)As single quantum well laser"*[28] (Section 5.2).
Unintentional carbon (C) doping is one of the main drawbacks of the low temperature MOVPE growth. The metal organics might not fully decompose in the gas phase and C from the remaining organic groups can incorporate. In GaAs this usually happens on the group-V lattice sites which leads to a p-doping of the crystal[70], in Ga(AsBi) this is not yet known but a similar behavior is expected. The sample series introduced at the beginning of Section 3.2.2 with different offers of TMBi and therefore different Bi fractions was analyzed by the use of SIMS. Extremely high C concentrations in the range of 1E20 atoms/cm^3 were found for the low temperature grown pure GaAs sample. With increasing presence of Bi at the surface the C incorporation gets more and more reduced down to the detection limit of only 1E16 atoms/cm^3 for the sample grown in the Bi saturated regime. This is

most probably caused by the segregation of the Bi atoms that block the group-V lattice sites at the surface and hinder the C from incorporating. Thus, unintentional C doping is not a counter-argument against using Ga(AsBi) in optoelectronics, as long as it gets deposited within or close to the Bi saturated regime. All investigated samples, even those with more than 7% Bi, showed clear room temperature PL providing a very good agreement of the PL peak and the theoretically expected bandgap energy (*"Luminescence properties of dilute bismide systems"*[31], Section 5.5). The linewidth of the spectra in the range of 80 to 90 meV even at the best growth conditions is quite large but comparable to values that were reported before on Ga(AsBi)[71,72]. It is assumed that the linewidth is broadened due to the disorder in the dilute bismides[73–76] that was further investigated by temperature dependent PL investigations at a sample with 4.2% Bi (*"Thermal quenching of photoluminescence in Ga(AsBi)"*[34], Section 5.8). It turned out that the thermal quenching of the PL intensity shows an unusual behavior and a second scale of disorder needs to be introduced in order to describe the experimental observation. This implies the presence of deep-laying localized states in the bandgap of Ga(AsBi) that need to be investigated in more detail.

The intensity of the PL is strongly linked to the applied growth conditions. The most important parameter is the amount of Bi that floats at the surface during growth. The PL intensity of the sample series discussed before increases by three orders of magnitude with increasing TMBi offer. This is thought to be related to the surfactant effect of Bi[77,78] that

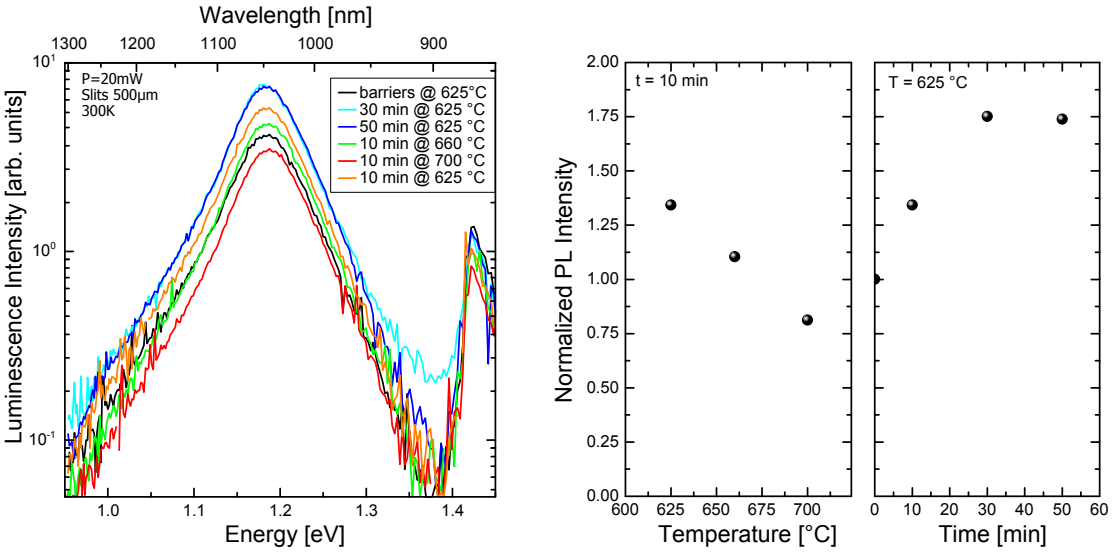

Figure 3.3: Room temperature PL spectra of a Ga(AsBi)/(AlGa)As 3QW structure with 3.9% Bi that was post growth annealed under TBAs stabilization varying annealing temperature and time. The "as grown" sample (black line) is already initially annealed for about 4 min at 625 °C since the barriers and cap were deposited at this temperature. The investigations show that annealing temperatures not greater than 625 °C and times between 30 to 50 min lead to the highest integrated intensity of the Ga(AsBi) PL signal, which corresponds to the overgrowth of the p-contact of the laser devices.

reduces the density of defects in the crystal and, as shown before, the C concentration. Especially for samples with low PL intensity a defect luminescence at about 1 eV was found. This is not directly related to the Bi as it also occurs in Bi free GaAs layers that were deposited at 400 °C and is thought to come from point defects in GaAs such as antisites and vacancies[79,80]. Higher PL intensities were also observed for samples grown at higher temperature and lower growth rates, which is also related to fewer defects and less C in the crystal.
The PL of the samples can be further improved by a post growth annealing at high temperatures. Samples with GaAs barriers or GaAs cap deposited at 625 °C already showed a 20 times higher PL signal than those that were only grown at 400 °C. Post growth reactor annealing investigations under TBAs stabilization of a Ga(AsBi)/(AlGa)As MQW structure with 3.9% Bi (Figure 3.3, unpublished) indicated that annealing temperatures greater than 625 °C are not suitable as the PL signal decreases again. The maximum PL intensity is observed after ca. 30 min but even longer times do not affect the material negatively. This is important for the growth of laser diodes as the deposition of the p-contact on top of the active region takes about 50 min at a growth temperature of 625 °C.
Concluding, from an optoelectronic point of view, the best Ga(AsBi) layers can be produced when growth takes place at the highest suitable temperature and within the saturation regime of Bi in order to benefit the most from the Bi surfactant effect. Additional improvement can be realized by post growth annealing at not more than 625 °C.

3.3 Ga(AsBi) QW laser devices

Aside from the growth studies on dilute bismides it was also of interest in this work to show that the material is suitable for the fabrication of photonic devices. Hence, the established growth processes for Ga(AsBi)/GaAs MQW structures (Section 3.2) were optimized and transferred to the deposition of laser diodes. As a result the first electrically pumped Ga(AsBi) laser was demonstrated, presented at full length in *"Electrical injection Ga(AsBi)/(AlGa)As single quantum well laser"*[28] (Section 5.2).
The first Ga(AsBi)/GaAs MQW structures discussed in Section 3.2.1 were not suitable for laser structures as they suffered from three main drawbacks due to the low temperature GaAs barriers. First, the hetero interfaces were smeared out due to the incorporation of segregated Bi during the growth of the GaAs barriers. Second, the GaAs barriers are highly C doped at the low growth temperature of only 400 °C and finally, the conduction band offset between Ga(AsBi) and GaAs and, thus, the electron confinement, is too low at small Bi fraction because Bi mainly affects the valance band of GaAs. To overcome these problems a growth interruption subsequent to the Ga(AsBi) deposition was introduced and the substrate was heated to 625 °C under TBAs stabilization for the growth of the barrier. It was already stressed in Section 3.2 that this procedure enables sharp Ga(AsBi)/GaAs

hetero interfaces and improves PL signal due to an annealing. The GaAs/Ga(AsBi) interface was addressed by growing the Ga(AsBi) QW in the saturated Bi regime so that the maximum Bi incorporation is reached immediately. The structures further benefit from the high temperature barriers as C no longer gets incorporated and the GaAs can easily be replaced by (AlGa)As, for which the growth at 625 °C is well known, in order to improve the electron confinement.

The sketch of the first laser diode with lasing operation is given in Figure 3.4. The 6.4 nm thick Ga($AsBi_{0.022}$) single quantum well (SQW) is surrounded by 150 nm ($Al_{0.2}Ga$)As barriers for carrier confinement and 1.4 µm ($Al_{0.4}Ga$)As cladding layers. An n-doped GaAs substrate was used, hence the lower cladding layer was n-doped using tellurium (Te) and the upper cladding layer p-doped with C. The structure was capped by 250 nm highly zinc (Zn) doped GaAs:Zn for good semiconductor to metal contact. Subsequent to the growth broad area laser devices of 50 µm and 100 µm width and 1000 µm cavity length were fabricated and their light-current (L-I) characteristics investigated applying 200 ns current pulses at a frequency of 10 kHz to reduce heating.

Lasing operation was observed at room temperature at a threshold current of I_{th}=1.56 kA/cm^2 (Figure 3.4). The emission wavelength of 947 nm is in perfect agreement with the PL of test structures and modeling which proves that lasing operation origins from the Ga(AsBi) QW. The threshold current is promising as it is only eight times higher than measured for a comparable laser diode at which the Ga(AsBi) QW was replaced by a GaAs QW that was grown at 625 °C, however an improvement of the growth conditions is desirable.

In the study *"Physical properties and optimization of GaBiAs/(Al)GaAs based near-infrared laser diodes grown by MOVPE with up to 4.4% Bi"*[33] (Section 5.7) further laser devices were investigated including temperature and pressure dependence measurements (per-

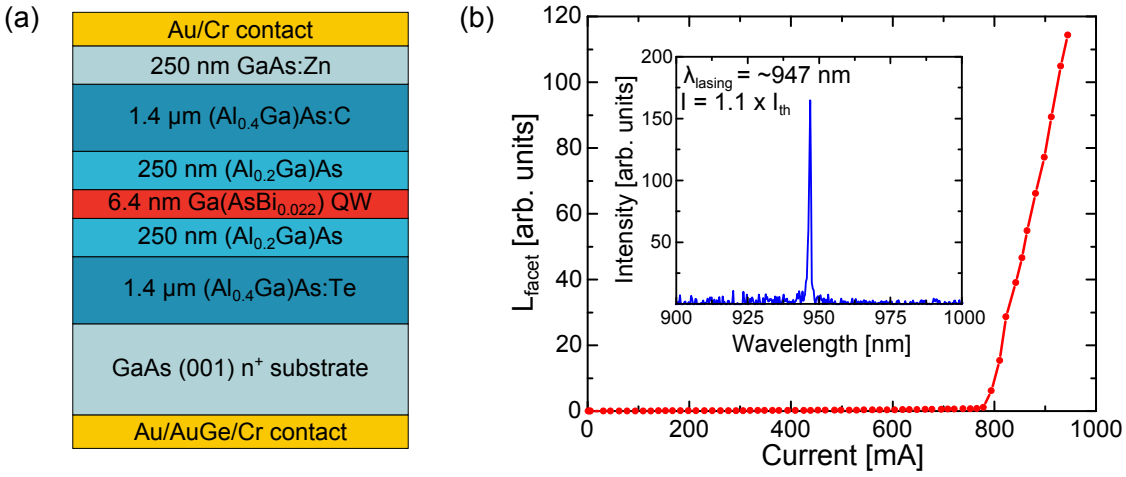

Figure 3.4: Sketch of the first realized Ga(AsBi) SQW laser with 2.2% Bi and (AlGa)As barriers (a) and the corresponding L-I characteristics (b) of a 50 µm x 1000 µm broad area laser device indicating lasing at a threshold of I_{th}=1.56 kA/cm^2 at the expected emission wavelength of 947 nm (inset).

Device	#QW	d_{QW} [nm]	Bi_{QW} [%]	Al_{bar} [%]	I_{th} [kA/cm^2]	λ_{lasing} [nm]
17275	1	8.0	0	20	0.2	854
17152	1	6.4	2.2	20	1.5-1.6	947
17273	1	6.4	2.2	12	1.0-1.1	947
17392	1	6.4	2.2	0	7.5	940
12393	1	8.0	4.4	0	4.5 at 180 K	1039 at 180 K

Table 3.1: The table summarizes the structure and lasing characteristics of the discussed Ga(AsBi) SQW laser devices.

formed at the Advanced Technology Institute (ATI), University of Surrey, UK). The Al content in the barriers was found to be a parameter for improvement and modeling showed that 10% to 15% Al fraction in the barrier brings the best compromise of electron and optical confinement for 2.2% Bi in the QW. This was confirmed experimentally as I_{th} was reduced by one third for a laser diode with 12% Al in the barrier while it increased to I_{th}=7.5 kA/cm^2 for pure GaAs barriers because of the poor electron confinement (see Table 3.1). It was further stated that about 80% of I_{th} is lost due to non-radiative recombination through defects, which underlines the necessity of improving growth and annealing conditions. The temperature dependence of the lasing photon energy of the devices was -42 meV/K and therefore no significant reduction with respect to GaAs-based devices was observed.
The improvements that were made on the incorporation efficiency enabled the heightening of the Bi fraction in the QW to 4.4%. Lasing operation of SQW devices with GaAs barriers was only observed up to 180 K with I_{th}=4.5 kA/cm^2 due to the limited applicable current of the set up. The much higher threshold with respect to the 2.2% devices is most probably related to the changes in the growth conditions that are needed for higher Bi incorporation. Furthermore, the applied GaAs barriers might not provide a sufficient electron confinement for this Bi fraction. However, the temperature dependency of the lasing energy was only -32 meV/K and therefore lower than that of the 2.2% devices.
In conclusion, a proof of principle for dilute bismide laser diodes was provided showing lasing operation for devices with up to 4.4% Bi. The lowest achieved threshold current density of about I_{th}=1.0 kA/cm^2 for a 2.2% Bi device is promising for such a new material system, however, an improvement of the applied growth conditions is necessary in order to reduce losses caused by defects in the Ga(AsBi) material.

3.4 MOVPE growth of Ga(NAsBi)/GaAs hetero structures

Additionally to the pure dilute bismide Ga(AsBi) the dilute nitride and bismide Ga(NAsBi) alloy was investigated in this work. In *"Growth and characterisation of Ga(NAsBi) alloy by metal organic vapour phase epitaxy"*[30] (Section 5.4) the growth and the subsequent

optical and structural characterization of this quaternary material are reported.
MQW structures were grown at 400 °C to 450 °C, since higher temperatures are usually favorable for dilute nitrides to reduce N related defects but significant Bi incorporation was also still desired. The deposition of MQW and bulk-like structures with smooth Ga(NAsBi)/GaAs hetero interfaces and good chemical homogeneity within the Ga(NAsBi) was realized as confirmed by STEM investigation. SIMS measurements at chosen samples showed that the Bi fraction in the crystal is not affected by the presence of N, at least within the growth regime below Bi saturation at which the experiments were carried out. This discovery allows the determination of the quaternary composition in the case that the Bi fraction of a corresponding N free sample is known. N, in contrast to Bi, desorbs from the surface and the decomposition of UDMHy is very low at the applied temperatures[69], hence, high UDMHy/TBAs ratios need to be applied for N incorporation. The relation between the gas phase fraction of the N precursor UDMHy and the N incorporation was found to be linear and the gradient of this relation decreases with increasing Bi contents. Increasing the UDMHy/TBAs up to unity, maximum N fractions of 3.7% and 2.6% for 2.6% Bi and 3.5% Bi were achieved at the growth temperature of 400 °C. At these structures, however, it was not possible to detect bandgap PL at room temperature, only the defect luminescence discussed in Section 3.2.3 was found. The absence of the PL signal was thought to be related to N induced non-radiative defects and, so far, no annealing conditions were found at which bandgap PL is observed. Therefore further experiments at 450 °C growth temperature have been performed using bulk-like single layer structures with fixed Bi fraction of 1.8% and different N contents up to 1.8%. Since room temperature PL was only detectable for that with 0.6% N, the photo reflectance (PR) signal was analyzed in order to get an insight to the electronic structure of the Ga(NAsBi) (PR measurements performed at the Advanced Technology Institute (ATI), University of Surrey, UK). It turned out that the bandgap is reduced by approximately 140 meV per % N at constant Bi fraction which is in good agreement with the predicted 130 meV from theory and supports the assumption that N and Bi act independently on the bandgap of GaAs.
These preliminary experiments show that the growth of Ga(NAsBi) on GaAs can be easily controlled by adjusting the UDMHy supply at fixed and known Bi fraction. Doing so alloys with Bi and N fractions close to 4% were already realized that would include the emission wavelength of 1.55 µm. However, the PL signal in those structures is quenched or fully suppressed by N related defects and annealing conditions improving the signal were not yet established but need to be the focus of future work.

CHAPTER 4

Summary and outlook

A lot of energy in today's optical communication is wasted due to the inefficiency of optoelectronic devices operating at the telecommunication wavelength of 1.55 µm. The novel Ga(AsBi) material system is very promising to address this as it could enable the fabrication of high efficiency IR photonic devices such as laser diodes and EAM. In the case that the Bi fraction exceeds 10%, the spin-orbit splitting becomes greater than the bandgap, which is due to band anti crossing in the valance band. Hence, loss mechanisms such as Auger recombination in the valance band and inter valance band absorption that occur in conventional devices would be suppressed. The epitaxial growth of this highly metastable material, however, is very challenging as metallic droplets can form at the surface and low deposition temperatures are required in order to incorporate a significant amount of Bi into GaAs.

In this work the growth of Ga(AsBi) and Ga(NAsBi) on GaAs substrates using MOVPE with TEGa, TBAs, TMBi and UDMHy as precursors was investigated, and thereby MQW as well as bulk-like structures were deposited. Several growth parameters were varied systematically applying pulsed as well as continuous precursor flows. Structural analysis such as HR-XRD, AFM, SEM, (S)TEM of the crystals were performed and PL spectroscopy has been carried out. Furthermore, the first electrically pumped Ga(AsBi) containing laser diode was demonstrated.

The surface of the first Ga(AsBi) samples were covered by metallic droplets consisting either of Ga, Bi or both in phase separated droplets. Drastically reducing the amounts of TMBi offer and carefully adjusting the TBAs/TEGa ratio enabled the growth of droplet free samples with measurable Bi fractions applying pulsed as well as continuous precursor flow. Bi segregates to the surface and it was found that the Bi incorporation depends on the Bi surface coverage during growth. In the case the coverage is too small, Bi only floats at the surface and does not get incorporated. At higher amounts the Bi fraction scales with the surface coverage up to a certain maximum and when it becomes too high Bi droplets begin to form. The maximum Bi fraction was found to increase with decreasing growth temperature that was varied in the range of 350 °C to 475 °C. However, at lower

temperatures more defects occur and the precursor decomposition is reduced. Thus, 375 °C and 400 °C were stated to be most suitable for the MOVPE growth of Ga(AsBi) so far and maximum Bi fractions of about 7% and 5% were realized, respectively. The incorporation efficiency also increases with the growth rate and is inversely proportional to the TBAs/TEGa ratio within a range around unity were droplet free growth of Ga(AsBi) is possible. What makes the optimization and investigation of the growth conditions more complicated is that the before mentioned parameters are not independent. For example, the presence of Bi or the not fully decomposed TMBi at the surface reduces the growth rate, which is a hint that it hinders either the decomposition of the TEGa or its approach to the surface. Furthermore, lowering the growth temperature reduces the decomposition of the precursors and, hence, has an impact on the optimum TBAs/TEGa and TMBi/V ratios and reduces the growth rate.

However, chemically homogenous Ga(AsBi) samples were realized and, if the subsequent layer was grown at temperatures as high as 625 °C, sharp hetero interfaces were found. The Bi floating at the surface acts as surfactant that quenches the unintentional C incorporation that usually occurs at the low applied temperatures in MOVPE and it reduces the point defect density. Hence, strong bandgap PL was found for samples that are grown in the regime at which the Bi saturation sets in. The PL peak fits perfectly to the prediction from theory with linewidths (FWHM) of about 80 to 90 meV that are related to the disorder in dilute bismides.

To investigate whether the dilute bismides are suitable for optoelectronic devices, broad area Ga(AsBi) QW lasers were fabricated with Bi fractions of 2.2% and 4.4%. Electrical injection lasing of dilute bismides was demonstrated for the first time on a $Ga(AsBi_{0.022})$ SQW laser with (AlGa)As barriers and cladding layers that showed room temperature lasing operation. The lowest achieved threshold current density of I_{th}=1.0 kA/cm^2 at pulsed current injection is very promising for such a new material system, however about 80% of I_{th} is lost by non-radiative recombination through defects. For devices with 4.4% Bi lasing was only found at low temperatures up to 180 K showing the necessity of further improving the growth of Ga(AsBi), especially when increasing the Bi fraction.

For the growth of Ga(NAsBi) it was stated that at constant Bi fraction the N fraction can easily be controlled by the UDMHy supply. Samples containing up to 4% Bi and N were realized, however, it was not possible to observe room temperature PL from those structures. Hence, photo reflection measurements were carried out, showing that at constant Bi fraction the bandgap reduction due to N is about 140 meV/%N confirming that N and Bi act independently on the band structure of GaAs.

Further studies need to focus on improving the MOVPE growth conditions for Ga(AsBi) in order to increase the Bi fraction above 10%. Most promising will be the growth at lower temperatures down to 350 °C, since the parameter space is quite large and there has not been much optimization for the growth at such low temperatures so far. Additionally, as the decomposition of the chosen precursors is very low at 350 °C, the introduction of new

precursors such as tritertiarybutylgallium (TTBGa), tritertiarybutylbismuth (TTBBi) and triisopropylbismuth (TIPBi), which are supposed to dissociate better at low temperatures, might bring progress on the growth. Besides that further work in the Ga(NAsBi) material system needs to be done as N reduces the strain which could be the driving force for the Bi segregation. Hence, the presence of N might allow for higher maximum Bi fractions, which has not yet been investigated. This, however, necessarily involves annealing studies in order to improve the optical properties of the quaternary material. It is also not excluded that different annealing conditions such as lower temperatures or rapid thermal annealing can further improve the ternary Ga(AsBi) and with that the so far realizable laser diodes. Altogether, this thesis shows the successful deposition of dilute bismide GaAs based alloys by MOVPE and the potential of this alloy for high efficiency photonic devices as basis for further development.

CHAPTER 5

Publications

5.1 MOVPE growth of Ga(AsBi)/GaAs multi quantum well structures[1]

P. Ludewig, N. Knaub, W. Stolz, K. Volz, Journal of Crystal Growth **370**, 186 (2013).
DOI: 10.1016/j.jcrysgro.2012.07.002.

Abstract

This paper summarizes results of the epitaxial growth of Ga(AsBi) by metal organic vapor phase epitaxy (MOVPE) using all-liquid group V precursors. Ga(AsBi)/GaAs multi quantum well (MQW) samples are grown on GaAs (001) substrates at temperatures as low as 375 °C and 400 °C using triethylgallium (TEGa), tertiarybutylarsine (TBAs) and trimethylbismuth (TMBi) as precursors. High resolution x-ray diffraction (HR-XRD), transmission electron microscopy (TEM) as well as atomic force microscopy (AFM) measurements show that MQW structures with good crystalline quality are realized. Under specific growth conditions, the Bi droplet formation can be avoided completely. The incorporated Bi-content is limited depending on the growth temperature used. Surplus Bi segregates at the surface and incorporates into the subsequent GaAs barrier when the Bi supply is stopped. The MQW samples show room temperature photoluminescence (PL) already after growth. A redshift and a decreasing PL signal intensity with increasing Bi fraction is observed.

The Authors contribution

My contribution to this work was the planning, execution and interpretation of all experiments including the MOVPE growth and analysis by HR-XRD, AFM and PL spectroscopy. The preparation and investigation of the TEM samples was performed by

1 Reprinted from *Journal of Crystal Growth **370** (2013) 186-190*, Copyright 2012, with permission from Elsevier.

Nikolai Knaub in close collaboration with me. All co-authors helped to interpret the data and to improve the manuscript that was written by me.

Journal of Crystal Growth 370 (2013) 186–190

Contents lists available at SciVerse ScienceDirect

Journal of Crystal Growth

journal homepage: www.elsevier.com/locate/jcrysgro

MOVPE growth of Ga(AsBi)/GaAs multi quantum well structures

P. Ludewig *, N. Knaub, W. Stolz, K. Volz

Material Science Center and Faculty of Physics, Philipps-Universität Marburg, Hans Meerwein Straße 6, 02D34, 35032 Marburg, Germany

ARTICLE INFO

Available online 16 July 2012

Keywords:
A3. Metalorganic vapor phase epitaxy
B1. Bismuth compounds
B2. Semiconducting III–V materials

ABSTRACT

This paper summarizes results of the epitaxial growth of Ga(AsBi) by metal organic vapor phase epitaxy (MOVPE) using all-liquid group V precursors. Ga(AsBi)/GaAs multi quantum well (MQW) samples are grown on GaAs (001) substrates at temperatures as low as 375 °C and 400 °C using triethylgallium (TEGa), tertiarybutylarsine (TBAs) and trimethylbismuth (TMBi) as precursors. High resolution x-ray diffraction (HR-XRD), transmission electron microscopy (TEM) as well as atomic force microscopy (AFM) measurements show that MQW structures with good crystalline quality are realized. Under specific growth conditions, the Bi droplet formation can be avoided completely. The incorporated Bi-content is limited depending on the growth temperature used. Surplus Bi segregates at the surface and incorporates into the subsequent GaAs barrier when the Bi supply is stopped. The MQW samples show room temperature photoluminescence (PL) already after growth. A redshift and a decreasing PL signal intensity with increasing Bi fraction is observed.

1. Introduction

Due to band anticrossing (BAC) in the valance band (VB), replacing a small amount of As by Bi highly reduces the bandgap of GaAs while the spin–orbit splitting is increased [1]. If the Bi fraction is more than 10.5% the spin–orbit splitting becomes higher the bandgap [2,3]. Hence, Bi containing laser-diodes with an increased efficiency could be realized, since Auger loss processes could be suppressed. Furthermore, the temperature sensitivity of the bandgap of dilute bismide Ga(AsBi) is reduced compared to conventional III/V semiconductors [4]. Therefore devices with increased temperature stability become possible [5].

The epitaxial growth of the metastable Ga(AsBi) is still a challenge and very low growth temperatures are required. In molecular beam epitaxy (MBE) the successful deposition of Ga(AsBi) on GaAs with Bi fractions of more than 10% has been reported [6,7]. Furthermore Ga(AsBi)/GaAs multi quantum well (MQW) structures were successfully grown[8]. The photoluminescence signal of those samples is very sensitive to the Bi content as well as the applied growth conditions [6,9]. Using metal organic vapor phase epitaxy (MOVPE) lower Bi fractions of 2.4% at reduced pressure and 3.7% at atmospheric pressure were realized since higher growth temperatures (>350 °C) are required for the decomposition of the precursors [10,11]. Furthermore the appearance of Bi droplets or whiskers at the surface could not be suppressed yet. A limited Bi content in Ga(AsBi) depending on the growth conditions was observed at atmospheric pressure MOVPE [11] as well as MBE [6,12].

In this paper we will present the successful growth of Ga(AsBi)/GaAs MQWs with up to 4.2% of Bi by MOVPE and discuss the growth mechanism as well as the structural and optical properties of the MQWs. Those Ga(AsBi)/GaAs MQW could act as active region of a high efficiency IR laser diode.

2. Experimental procedure

Ga(AsBi)/GaAs MQW structures were grown on GaAs (001) substrates by MOVPE. The samples shown in the following are 3x or 5x QW structures that were ended with a GaAs barrier. A commercially available AIX 200-GFR reactor system with Pd-purified H_2 as carrier gas at a reduced reactor pressure of 50 mbar was used. The applied growth temperatures were 375 °C and 400 °C. Triethylgallium (TEGa) was used as Gallium precursor, tertiarybutylarsine (TBAs) and trimethylbismuth (TMBi) as group V precursors since low growth temperatures were required. The growth rates were 0.88 μm/h at 400 °C and 0.41 μm/h at 375 °C, respectively, due to reduced decomposition of Ga precursor. Those were determined by the layer thicknesses in the growth regime where no segregation is observed and the growth rate of GaAs and Ga(AsBi) are the same within the accuracy of the measurement. The TBAs/TEGa ratio was varied from 1.1 to 3.6 and the TMBi/TEGa ratio was varied in the range of 2.3E-3 to 0.13 at a constant TEGa supply of 7E-3 mbar for all samples. The Ga(AsBi) QWs were all grown by pulsed growth mode supplying group III and group V precursors alternating for 1 s without any pause in between. In contrast the GaAs barriers were grown under a continuous

* Corresponding author. Tel.: +49 6421 28 25713; fax: +49 6421 28 28935.
E-mail address: peter.ludewig@physik.uni-marburg.de (P. Ludewig).

0022-0248/$ - see front matter © 2012 Elsevier B.V. All rights reserved.
http://dx.doi.org/10.1016/j.jcrysgro.2012.07.002

precursor flow. High resolution X-ray diffraction (HR-XRD) omega-2theta scans around the GaAs (004) reflection in combination with dynamical modeling of the experimental pattern was used to determine the Bi content and the layer thicknesses. The parameters of GaBi were taken from [13] and [14]. Cross-sectional transmission electron microscopy (TEM) dark field (DF) (002) images were taken in order to investigate the crystalline quality, the homogeneity of the composition as well as the layer thicknesses in more detail. The (002) reflection is chemically sensitive in III/V semiconductors with zinc-blende structures. The TEM samples were prepared conventionally, using Ar-ion milling as last preparation step. Imaging took place in a JEOL JEM 3010, which was operated at 300 keV. The surface morphology and the presence of Bi droplets were studied by atomic force microscopy (AFM). Room temperature photoluminescence spectroscopy (PL) was performed to analyze optical properties of the MQWs. The PL measurements were carried out using a continuous-wave (cw) Ar-ion laser at a wavelength of 514 nm for excitation. The PL signal was dispersed in a 1 m grating monochromator (THR 1000, Jobin-Yvon) and collected by a cooled germanium detector applying the standard lock-in technique.

3. Results and discussion

First we will discuss the influence of the V/V ratio on the growth of Ga(AsBi) by MOVPE. Therefore the TBAs partial pressure was changed with constant TMBi and TEGa supply. Following, the TBAs and TEGa partial pressures were held constant varying the TMBi supply. Furthermore the Bi incorporation in dependency of the growth temperature is discussed and finally the influence of the Bi incorporation on the optical properties.

Fig. 1(a) shows HR-XRD (004) patterns of Ga(AsBi)/GaAs 5xQWs. In all cases the growth temperature was 400 °C with constant TEGa and TMBi supply (TMBi/TEGa=0.09). Only the TBAs partial pressure was varied in order to change the V/V ratio. In case of TBAs/TEGa=1.1 the diffraction pattern shows no MQW profile. A single Ga(AsBi) layer of about 60 nm thickness and Bi content of 2% was found instead of a 5xQW. The surface of this sample is covered by Ga droplets as determined by energy dispersive X-ray spectroscopy (EDX) in scanning electron microscopy (SEM) (not shown here) indicating a too low V/III ratio. If the TBAs/TEGa ratio is increased to 2.1 the diffraction pattern of a 5xQW with a Bi fraction of 2.7% is found. The pendellösung fringes are clearly resolved indicating good crystalline structure and sharp hetero interfaces. This is no longer the case when the TBAs partial pressure is further raised to TBAs/TEGa=3.6. In this case the pendellösung fringes are broadened and TEM investigations of this sample shows that the topmost barrier is missing. Dynamical modeling of the XRD profiles show that the shift of the zero order peak which occurs by increasing the TBAs/TEGa from 2.1 to 3.6 only results from an increased GaAs barrier thickness (31 nm instead of 25 nm). The reason for this behavior as well as the missing topmost barrier is not understood so far. However the Bi content (2.7%) is not changed by the increased TBAs supply. This demonstrates that the structure of the Ga(AsBi)/GaAs MQWs is very sensitive to the chosen TBAs/TEGa ratio due to the required low growth temperatures while the Bi incorporation cannot be raised by decreasing the TBAs partial pressure under the growth conditions used here.

Fig. 1(b) shows the HR-XRD (004) patterns of Ga(AsBi)/GaAs 5xQWs where the V/V ratio was only changed by varying the TMBi supply. The TBAs/TEGa ratio was set to 2.1 following the discussion before. In this case all three profiles show clearly resolved pendellösung fringes indicating that there is no change in the layer sequence of these samples. Dynamical modeling of these patterns shows that the layer thicknesses of these samples differ.

This is shown in Fig. 2 in more detail. The QW-, barrier and super lattice (SL) thicknesses, as well as the Bi fraction of several 5xQW structures are plotted versus the TMBi/(TMBi+TBAs) ratio with constant TBAs and TEGa supply (TBAs/TEGa=2.1). The graph

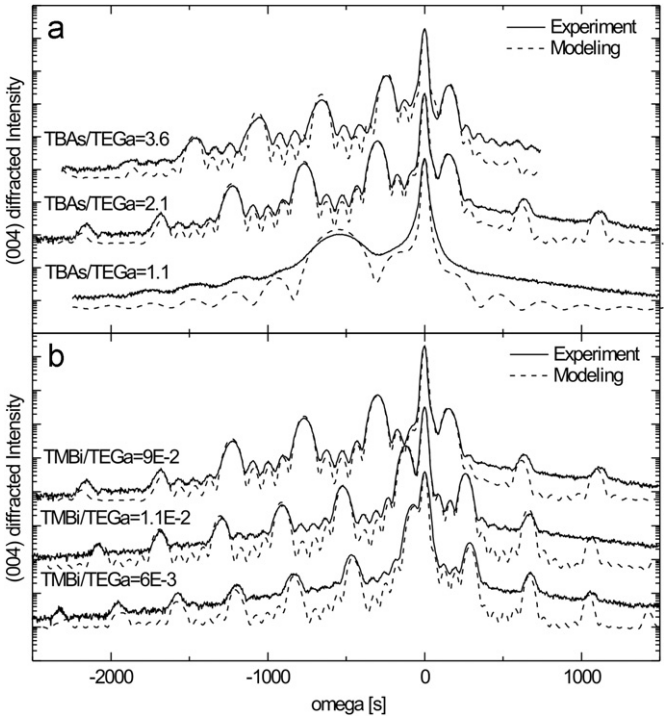

Fig. 1. HR XRD (004) pattern of Ga(AsBi)/GaAs MQWs grown with different TBAs/TEGa ratios (a) and different TMBi/TEGa ratios (b). (a) T_{growth} = 400°C TMBi/TEGa = 0.09, (b) T_{growth} = 400°C TBAs/TEGa = 2.1.

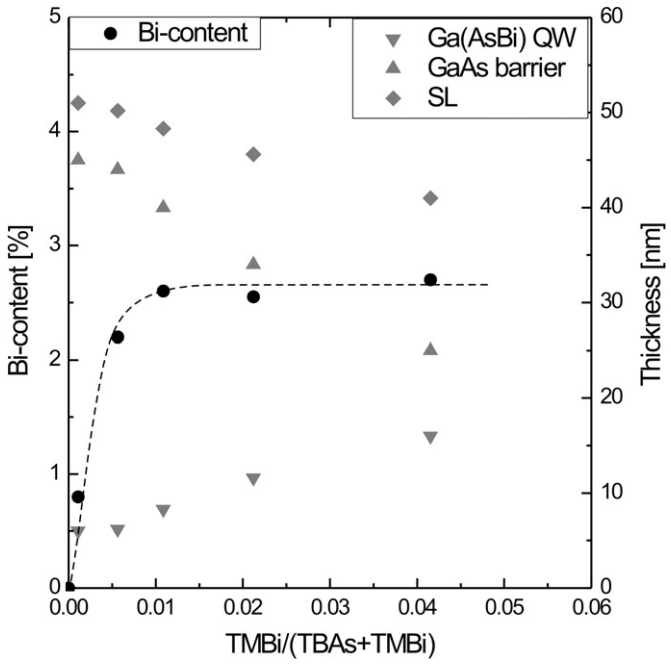

Fig. 2. Thicknesses and Bi fraction of several Ga(AsBi)/GaAs MQWs depending on the TMBi partial pressure. Above a TMBi/V ratio of 0.005 surpluses Bi segregates at the surface and incorporates into the subsequent GaAs barrier. The dashed line is only a guide to the eye.

shows, that an increasing TMBi partial pressure leads in the beginning to an increasing Bi content. At a TMBi/(TMBi+TBAs) ratio of approximately 5E-3 a saturation of the Bi content occurs at about 2.7%. At this point, where the saturation of the Bi content sets in, the thickness of the QWs increases linearly with the TMBi partial pressure while the barrier as well as the SL thickness decreases. Obviously only a given amount of Bi can be incorporated into GaAs under the chosen growth conditions. Since there is no desorption of Bi expected at that low growth temperatures, surplus Bi segregates at the surface and then incorporates in the subsequent GaAs barriers when TMBi is no longer supplied. As soon as the Bi surface coverage falls below a certain value the incorporation stops immediately and Bi acts as a surfactant; so pure GaAs can be grown. Hence only the QW and barrier thicknesses are affected by raising the Bi supply. Furthermore the growth rate of the MQWs is reduced when there is too much Bi at the surface, since the SL thickness is decreasing and the growth times are not changed. This indicates that the Ga does not reach the GaAs growth front effectively anymore. The limitation of the Bi content was already discussed in [11] for AP-MOVPE and [15] for MBE growth. Our studies show that this limitation does not occur from the formation of a liquid Bi phase at the surface as proposed in [11] but from the metastability of the material leading to the formation of a liquid Bi phase and Bi droplets as the result.

The surface morphologies of some of these samples are shown in Fig. 3. In Fig. 3(a) there is no segregation of surpluses Bi so this sample shows a very smooth surface (topmost GaAs barrier). If the TMBi flow is raised (Fig 3(b)) and segregation sets in, small dots at the surface can be found, which are a hint for the formation of Bi droplets. Further increasing the TMBi partial pressure leads to less but much bigger droplets (Fig. 3(c)) which could be ascribed to Ostwald ripening of the droplets. Fig. 3(d) shows the surface morphology of a sample with a Bi fraction of 4.2% that was grown at 375 °C. In this case also droplet free surfaces are possible. The RMS roughnesses of the droplet free samples are in the range of 0.25 nm.

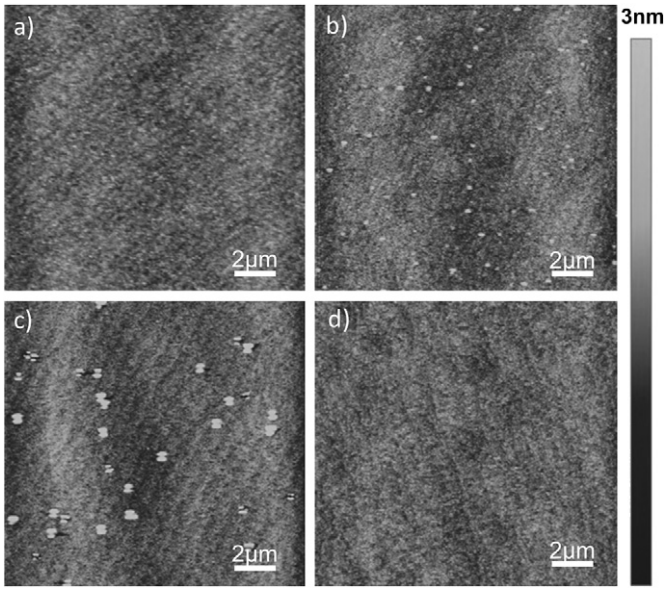

Fig. 3. Surface morphology of the Ga(AsBi)/GaAs MQWs depending on the TMBi partial pressure and the growth temperature. (a)–(c) were grown at a temperature of 400 °C with TMBi/V ratios of (a) 0.0056; (b) 0.021 and (c) 0.042. (d) was grown at a reduced temperature of 375 °C. For low TMBi/V ratio smooth surfaces with no droplet formation were observed. If the TMBi partial pressure is increased Bi droplets occur. For the low temperature growth with a Bi concentration of 4.2% also droplet free surfaces were realized.

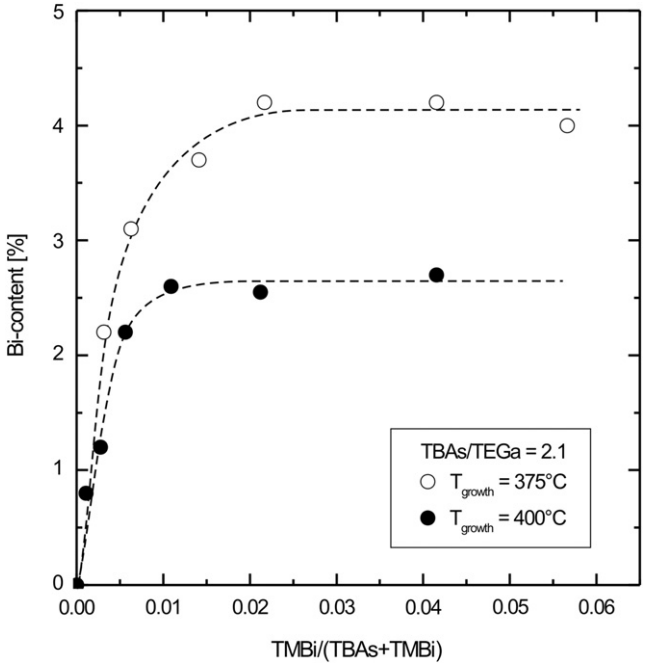

Fig. 4. Bi fraction depending on the TMBi partial pressure for samples grown at 375 °C and 400 °C. If the temperature is only reduced by 25 °C the Bi fraction can be raised from 2.7% to 4.2%. The dashed lines are again only guides to the eye.

In Fig. 4 the Bi fraction of Ga(AsBi)/GaAs MQW is plotted versus the TMBi/V ratio for growth temperatures of 400 °C and 375 °C, respectively. The TBAs supply and the TEGa supply were not changed (TBAs/TEGa=2.1). The results are consistent with the assumption of a limited Bi fraction in Ga(AsBi) which is independent of the TMBi supply. This limitation can be raised from 2.7% of Bi to 4.2% by reducing the temperature from 400 °C to 375 °C. More experiments will be done here to extrapolate an activation energy.

Fig. 5 displays TEM DF (002) images in [010] direction of two Ga(AsBi)/GaAs 3xQWs. The sample shown in Fig. 5(a) was grown at 400 °C with a TMBi partial pressure of 3.3E-4 mbar (TMBi/(TMBi+TBAs)=0.011) and a Bi fraction of 2.7% while the sample shown in Fig. 5(b) was grown at 375 °C with a much higher TMBi supply of 1.3E-3 mbar and a Bi fraction of 4.2%. In both cases the interfaces from GaAs barriers (dark) to Ga(AsBi) QWs (bright) are very smooth while the upper ones seems to be a little smeared out which is a hint for a gradient of the Bi fraction. Perpendicular to the growth direction Bi gets incorporated very homogeneously for layers with 2.7% of Bi as well as for 4.2%. The comparison of the QW thicknesses in Fig. 5(a) confirms the assumption, that a certain coverage of Bi is needed before the Bi incorporation starts, as the first QW is much thinner than the other two. When TMBi is supplied in the first place it takes some time until this critical surface coverage is reached and Bi incorporates which leads to a delay of the Ga(AsBi) growth. After the TMBi supply is stopped, surplus Bi still incorporates as demonstrated before, until the Bi coverage is again below this critical surface coverage. Hence a certain amount of Bi stays on the surface and acts as a surfactant during the growth of the first barrier. When now TMBi is again supplied for the second QW the critical amount of Bi at the surface is reached immediately and therefore the growth of Ga(AsBi) starts without delay. This assumption is supported by Fig. 5(b). In this case the TMBi supply is four times higher while the growth rate is less than the half due to the lower applied temperature. So in this case the critical coverage of Bi is reached much faster and no difference in the QW thicknesses is observed. In addition the gradient of the Bi fraction at the upper interfaces

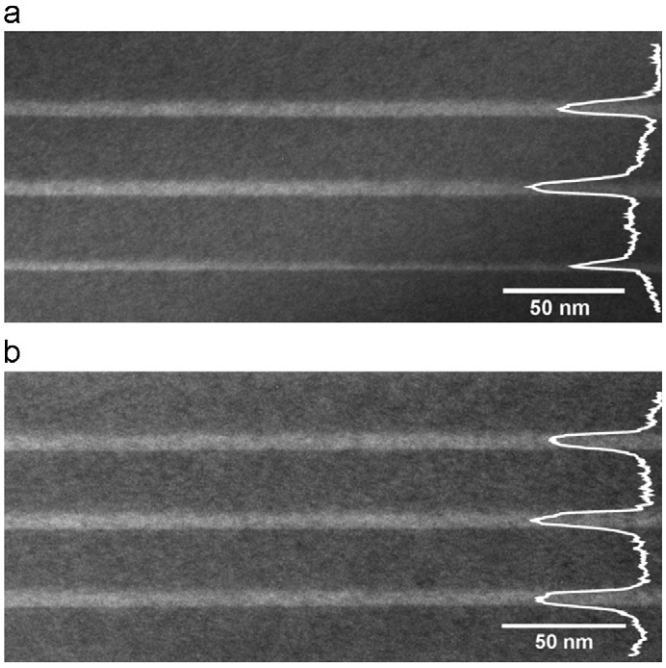

Fig. 5. Cross-sectional TEM DF (002) images of Ga(AsBi)/GaAs 3xQWs grown at 400 °C with a small TMBi supply (a) and at 375 °C with a higher TMBi supply (b). The Ga(AsBi) QWs appear brighter than the GaAs barriers in the DF images.

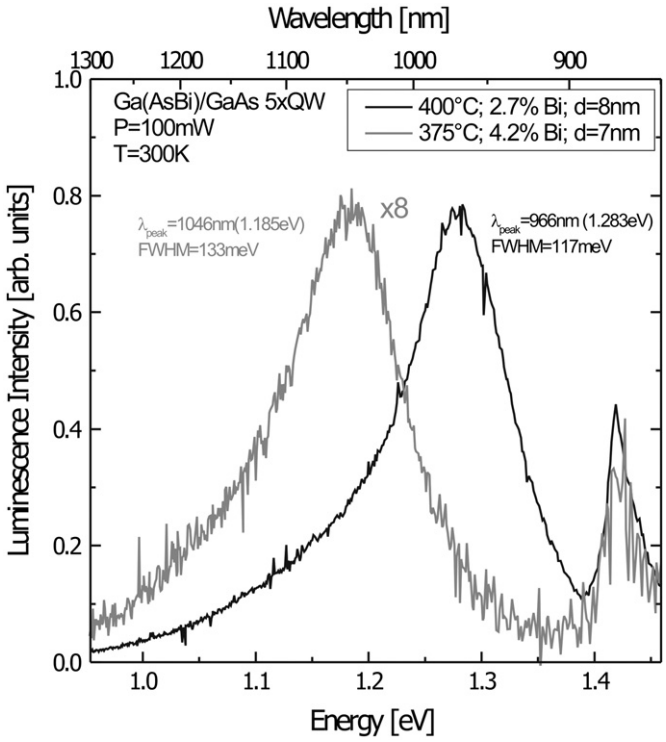

Fig. 6. Room-temperature photoluminescence spectra of Ga(AsBi)/GaAs 5xQWs with Bi fractions of 2.7% and 4.2%.

can be explained since during the time where the TMBi supply stops and the time where the surface coverage of Bi falls below the critical Bi coverage, the Bi fraction decreases.

Fig. 6 shows room temperature photoluminescence spectra of a sample with a Bi content of 2.7% grown at 400 °C and a sample

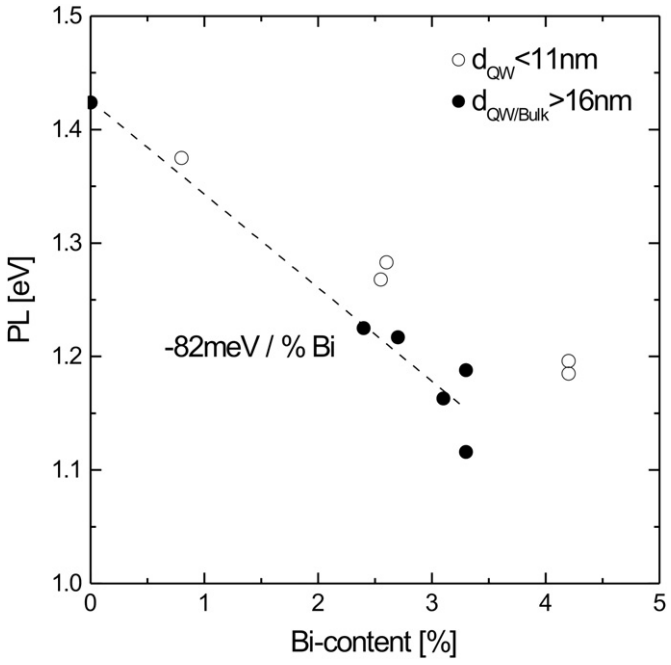

Fig. 7. Dependency of the photoluminescence peak on the Bi content.

with 4.2% of Bi grown at 375 °C. Both are as grown 5xQWs with QW thickness of 8 nm (2.7% Bi) and 7 nm (4.2% Bi). The PL peak position shifts from 1.283 eV to 1.185 eV when the Bi fraction is raised from 2.7% to 4.2%. Furthermore the integrated photoluminescence intensity decreases by more than one order of magnitude which is explained by Bi related defects as well as by the lower growth temperature. Especially for the sample with a Bi fraction of 2.7% a defect level in the range of 1.1 eV can be found which might be due to Bi clusters. The large line width of the emission of these MQWs is comparable to the literature [9]. This broadening might be due to Bi clusters and inhomogeneity of the Bi incorporation especially at the QW to barrier interfaces as discussed before.

The PL peak position of several MQW and bulk layers is shown in Fig. 7 in dependency of the Bi fraction. In this case one has to distinguish between thick layers where no quantization takes place (filled circles) and thinner layers where quantization effects have to be taken into account (empty circles). For the bulk and thick MQW layers a reduction of the emission energy of about 82 meV with 1% of Bi can be found which is in good agreement with the literature [16]. In case of the QW samples this effect is much lower which is due to the quantization.

4. Summary

We have demonstrated the growth of droplet free Ga(AsBi)/GaAs MQW on GaAs (001) substrates by MOVPE with Bi contents of up to 4.2%. Under optimized growth parameters layers with good crystalline quality are realized. The TMBi/TEGa and TBAs/TBAs ratios have to be adjusted very carefully in order to avoid Ga droplets (too low TBAs/TEGa ratio) as well as Bi droplets (too high TMBi/TEGa ratio). A limitation of the Bi content was found that is independent on V/III and V/V ratio but can be increased by reducing the growth temperature. In order to grow Ga(AsBi) a critical Bi coverage of the surface is needed whereas surplus Bi segregates at the surface and leads to a carry-over into the subsequent GaAs barriers. Room temperature photoluminescence

was observed where the peak position shifts to lower energy and the integrated PL signal drops by increasing the Bi fraction.

Acknowledgments

This work was founded by the European Union Project No. BIANCHO (FP7-257974) and the German Science Foundation (DFG: VO805/4 and VO/805/5).

References

[1] K. Alberi, O.D. Dubon, W. Walukiewicz, K.M. Yu, K. Bertulis, A. Krotkus, Applied Physics Letters 91 (5) (2007) 051909.
[2] S. Sweeney, In Semiconductor Laser Conference (ISLC), 2010 22nd IEEE International, 111 –112, Sept. (2010).
[3] M. Usman, C.A. Broderick, A. Lindsay, E.P. O'Reilly, Physical Review B 84 (245202) (2011).
[4] K. Oe, H. Okamoto, Japanese Journal of Applied Physics 37 (Part 2, No. 11A) (1998) L1283–L1285.
[5] Y. Tominaga, K. Oe, M. Yoshimoto, Applied Physics Express 3 (6) (2010) 062201.
[6] X. Lu, D.A. Beaton, R.B. Lewis, T. Tiedje, Y. Zhang, Applied Physics Letters 95 (4) (2009) 041903.
[7] A. Ptak, R. France, D. Beaton, K. Alberi, J. Simon, A. Mascarenhas, C.-S. Jiang, Journal of Crystal Growth 338 (1) (2012) 107–110.
[8] Y. Tominaga, Y. Kinoshita, K. Oe, M. Yoshimoto, Applied Physics Letters 93 (13) (2008) 131915.
[9] A.R. Mohmad, F. Bastiman, C.J. Hunter, J.S. Ng, S.J. Sweeney, J.P.R. David, Applied Physics Letters 99 (4) (2011) 042107.
[10] K. Oe, Journal of Crystal Growth 237-239 (Part 2(0)) (2002) 1481–1485.
[11] H. Fitouri, I. Moussa, A. Rebey, A. Fouzri, B.E. Jani, Journal of Crystal Growth 295 (2) (2006) 114–118.
[12] F. Bastiman, A. Mohmad, J. Ng, J. David, S. Sweeney, Journal of Crystal Growth 338 (1) (2012) 57–61.
[13] S. Tixier, M. Adamcyk, T. Tiedje, S. Francoeur, A. Mascarenhas, P. Wei, F. Schiettekatte, Applied Physics Letters 82 (14) (2003) 2245–2247.
[14] S.Q. Wang, H.Q. Ye, Physica Status Solidi (B) 240 (1) (2003) 45–54.
[15] X. Lu, D.A. Beaton, R.B. Lewis, T. Tiedje, M.B. Whitwick, Applied Physics Letters 92 (19) (2008) 192110.
[16] S. Francoeur, M.-J. Seong, A. Mascarenhas, S. Tixier, M. Adamcyk, T. Tiedje, Applied Physics Letters 82 (22) (2003) 3874–3876.

5.2 Electrical injection Ga(AsBi)/(AlGa)As single quantum well laser[1]

P. Ludewig, N. Knaub, N. Hossain, S. Reinhard, L. Nattermann, I. P. Marko, S.R. Jin, K. Hild, S. Chatterjee, W. Stolz, S.J. Sweeney, K. Volz, Applied Physics Letters **102**, 242115 (2013). DOI: 10.1063/1.4811736.

Abstract

The Ga(AsBi)material system opens opportunities in the field of high efficiency infrared laser diodes. We report on the growth, structural investigations, and lasing properties of dilute bismide Ga(AsBi)/(AlGa)As single quantum well lasers with 2.2% Bi grown by metal organic vapor phase epitaxy on GaAs (001) substrates. Electrically injected laser operation at room temperature is achieved with a threshold current density of 1.56 kA/cm^2 at an emission wavelength of 947 nm. These results from broad area devices show great promise for developing efficient IR laser diodes based on this emerging materials system.

The Authors contribution

My contribution to this work was the development and MOVPE growth of the laser diode and its test structure. Furthermore I was responsible for the characterization of those structures using HR-XRD and PL spectroscopy supported by Lukas Nattermann, the preparation and investigation of the STEM samples was performed by Nikolai Knaub. Stefan Reinhard did the fabrication of the broad area laser structures. The investigations in the laser characteristics were performed by me as well as by Nadir Hossain from the University of Surrey, UK, whose results are published in this work. All co-authors also helped to interpret the data and to improve the manuscript that I wrote in cooperation with Nadir Hossain.

1 Reprinted with permission from *Applied Physics Letters **102** (2013) 242115.* Copyright 2013, AIP Publishing LLC.

Electrical injection Ga(AsBi)/(AlGa)As single quantum well laser

P. Ludewig,[1] N. Knaub,[1] N. Hossain,[2] S. Reinhard,[1] L. Nattermann,[1] I. P. Marko,[2] S. R. Jin,[2] K. Hild,[2] S. Chatterjee,[1] W. Stolz,[1] S. J. Sweeney,[2] and K. Volz[1,a)]
[1]*Material Sciences Center and Faculty of Physics, Philipps-Universität Marburg, 35032 Marburg, Germany*
[2]*Advanced Technology Institute and Department of Physics, University of Surrey, Guildford, Surrey GU2 7XH, United Kingdom*

(Received 9 April 2013; accepted 6 June 2013; published online 20 June 2013)

The Ga(AsBi) material system opens opportunities in the field of high efficiency infrared laser diodes. We report on the growth, structural investigations, and lasing properties of dilute bismide Ga(AsBi)/(AlGa)As single quantum well lasers with 2.2% Bi grown by metal organic vapor phase epitaxy on GaAs (001) substrates. Electrically injected laser operation at room temperature is achieved with a threshold current density of 1.56 kA/cm^2 at an emission wavelength of ~947 nm. These results from broad area devices show great promise for developing efficient IR laser diodes based on this emerging materials system. © *2013 AIP Publishing LLC*. [http://dx.doi.org/10.1063/1.4811736]

Dilute bismide Ga(AsBi) based lasers diodes are promising candidates for high efficiency infrared (IR) light sources. The incorporation of only a small amount of Bi into GaAs causes a large reduction in the band gap due to valence band anti-crossing[1] and, in addition, decreases the temperature sensitivity of the emission wavelength compared to conventional III/V semiconductors,[2] making temperature stabilization more straightforward. Furthermore, for Bi fractions above approximately 10%, the spin-orbit splitting becomes larger than the bandgap.[3–6] Under such conditions it is expected that troublesome hot-hole generating Auger recombination and inter-valence band absorption (IVBA) processes may be suppressed leading to higher efficiencies and more temperature stable power output of lasers for optical communications applications.[6–8] Ga(AsBi) light-emitting diodes (LEDs)[9,10] and optically pumped laser diodes[11] have been demonstrated with promising optical material qualities. In order to exploit the beneficial properties of this metastable material system, which has to be grown under highly non-equilibrium growth conditions, it is however necessary to demonstrate that electrically pumped lasing at room temperature can be achieved.

In this work we will present an electrically pumped Ga(AsBi)/(AlGa)As laser with a Bi fraction of 2.2% in the active material. Single quantum well (SQW) laser devices as well as Ga(AsBi)/(AlGa)As multi QW test structures were grown by metal organic vapor phase epitaxy (MOVPE) on exact GaAs (001) substrates. A commercially available AIX 200-GFR reactor system with Pd-purified H_2 as carrier gas at a reduced reactor pressure of 50 mbar was used. Trimethylaluminum (TMAl) and triethylgallium (TEGa) were used as group III precursors, tertiarybutylarsine (TBAs), and trimethylbismuth (TMBi) as group V precursors since low growth temperatures were required. Diethyl tellurium (DETe) and diethyl zinc (DEZn) were used as n- and p-type dopants, respectively. Furthermore p-type doping with carbon was realized by a reduced V/III ratio in the p-contact (AlGa)As layer.

Adding Bi to GaAs mainly affects the valence band and for low Bi concentration, the conduction band (CB) offset is small; we estimate the e1-CB(GaAs)-separation to be 12 meV. Therefore, to provide a suitable electron confinement (AlGa)As barriers were used. Adding Al into the barriers improves the electron confinement; however, this leads to a lower refractive index contrast relative to the cladding and hence causes poorer optical confinement. A reasonable compromise was found to be to use 20% Al in the barriers which significantly increases e1-CB($Al_{0.2}Ga_{0.8}As$) to approximately 144 meV. The quantum well was selected to be thick enough to avoid inhomogeneity effects. A schematic of the layer structure of the laser diode grown on n^+ substrate is given in Figure 1. The 6.4 nm thick Ga($AsBi_{0.022}$) QW is embedded between 150 nm thick ($Al_{0.2}Ga$)As barriers for electrical confinement in the active region. The 1.4 μm thick ($Al_{0.4}Ga$)As:Te and ($Al_{0.4}Ga$)As:C layers serve as waveguides as well as n and p contact layers, respectively. 250 nm of highly p-doped GaAs:Zn were grown on top of the structure to improve the metal-semiconductor contact. All (AlGa)As and GaAs layers were grown at 625 °C, adjusting the Al fraction by the ratio of the group III vapor pressures. In contrast, the Ga($AsBi_{0.022}$) QW was deposited at 400 °C using a pulsed growth mode where group III and group V precursors were alternately supplied to the reactor for 1 s without any pause in between. Subsequently, TEGa and TBAs were supplied for a few seconds with continuous precursor flow in order to consume the segregated Bi. This growth methodology of Ga(AsBi) QW structures using MOVPE was described earlier in more detail.[12] The temperature changes applied before and after the growth of the QW were performed during TBAs stabilized growth interruptions. It is assumed that the segregated Bi that is left at the surface after the QW growth is stopped gets evaporated during the heating to 625 °C. So far no influence of segregated Bi on the growth of the (AlGa)As barrier was found which supports this assumption.

To form broad area laser structures, 50 μm and 100 μm wide Au/Cr metal stripes were deposited on the top contact, and an Au/AuGe/Cr-based contact was deposited on the substrate backside. The sample was alloyed at 400 °C for ohmic contact formation. To avoid current spreading the GaAs:Zn-contact layer was etched-off using the metal stripes as mask. Since the device was grown on GaAs-substrates the laser

a)E-mail: kerstin.volz@physik.uni-marburg.de

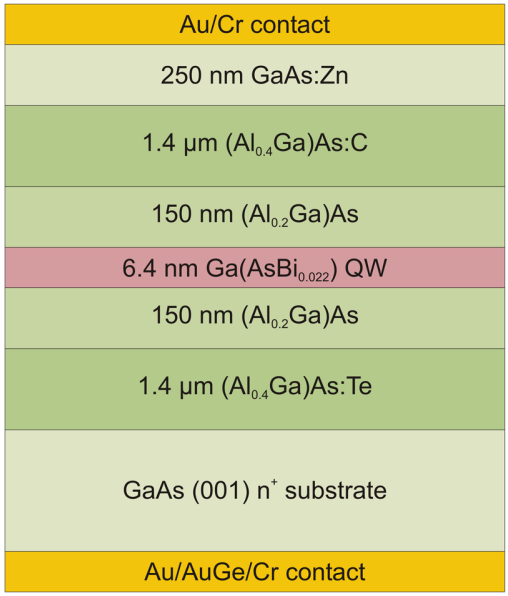

FIG. 1. Schematic view of the electrically pumped $Ga(AsBi_{0.022})$/(AlGa)As SQW laser diode.

facets were cleaved using standard techniques with a cavity length of 1 mm. The devices were measured *as-cleaved*.

Figure 2 shows high resolution X-ray diffraction (HR-XRD) omega-2theta scans around the GaAs (004) reflection, which were performed to investigate a Ga(AsBi)/(AlGa)As 5 × QW test structure that was grown under the same growth conditions as the active region of the device. Dynamical modeling of the experimental pattern allowed the determination of the Bi-fraction to 2.2% and layer thickness of 6.4 nm of the QW assuming GaBi lattice constant of 6.33 Å.[13]

Cross-sectional [-110] scanning transmission electron microscopy (STEM) high angle annular dark field (HAADF) images were taken in order to investigate the crystalline quality, the homogeneity of the composition, as well as the

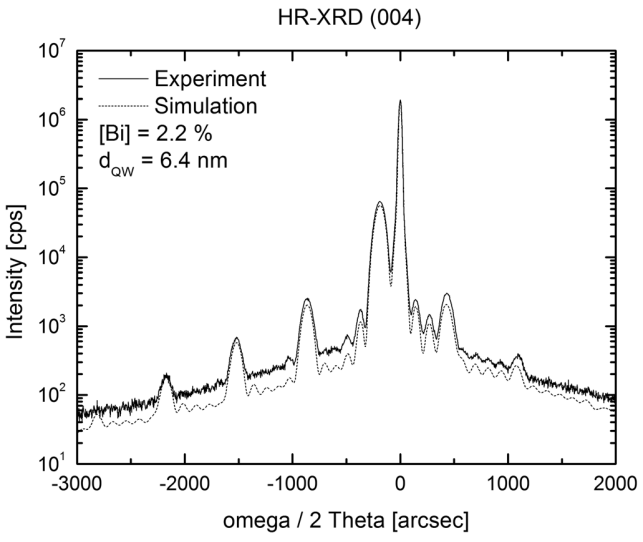

FIG. 2. HR-XRD (004) pattern of a Ga(AsBi)/(AlGa)As 5 × QW. The diffraction pattern is in good agreement with the dynamical simulation of a 5 × QW structure with a Bi fraction of 2.2 and a Ga(AsBi) layer thickness of 6.4 nm. The (AlGa)As barriers contain about 20% Al with a thickness of 22 nm, the sample is capped by a 7 nm thin GaAs layer.

layer thicknesses of the laser in more detail. Imaging took place with a JEOL JEM 2200 FS, which was operated at 200 keV using an aberration corrector for the probe. Figure 3 shows an overview HAADF [-110] STEM image of the laser device (a) as well as a high resolution image of the Ga(AsBi) QW (b). Since the contrast in the STEM HAADF mode is highly sensitive to the chemical composition of the layer (Z-contrast) a very high chemical homogeneity of the quantum well can be concluded from these investigations. In addition, the Ga(AsBi)/(AlGa)As transition can be clearly seen, indicating good control of the growth process. Furthermore, it is obvious that there is no degradation of the crystalline structure occurring during the TBAs stabilized growth interruptions that were applied during changes of the growth temperature.

Room temperature photoluminescence (PL) spectroscopy was performed using a continuous-wave (cw) 100 mW Ar-ion laser at a wavelength of 514 nm for excitation. The PL signal was dispersed in a 1 m grating monochromator (THR 1000, Jobin-Yvon) and collected by a cooled germanium detector applying standard lock-in techniques. The PL spectra of two 5 × QWs samples with Ga(AsBi) QW grown under the same growth conditions are shown in Figure 4. In contrast to the laser test structure with (AlGa)As barriers (black line), the sample with GaAs barriers was completely grown at 400 °C (grey line). The blue shift of the PL signal is explained by a thinner QW thickness using $(Al_{0.2}Ga)As$ barriers since the growth is interrupted and the sample heated to $(Al_{0.2}Ga)As$ growth temperature before all segregated Bi is consumed. Furthermore the higher confinement of the $(Al_{0.2}Ga)As$ barriers compared to GaAs lead to a blue shift.

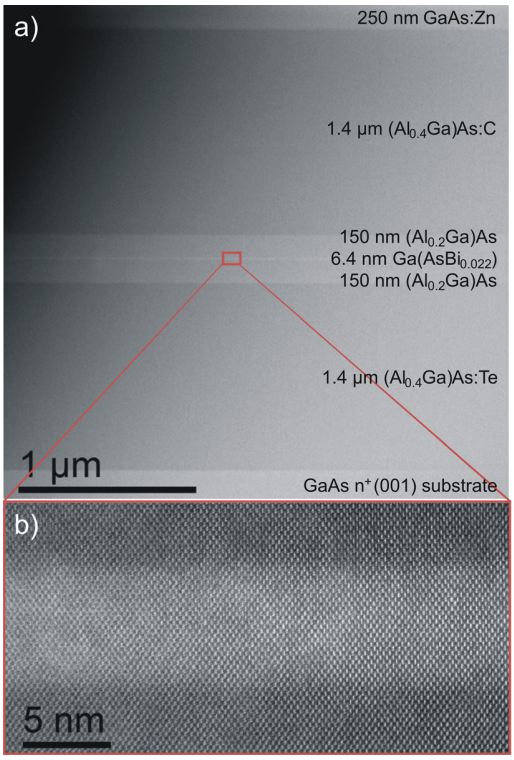

FIG. 3. (a) STEM HAADF overview image of the laser structure. (b) High resolution STEM image of the Ga(AsBi) QW showing smooth interfaces and a high chemical homogeneity.

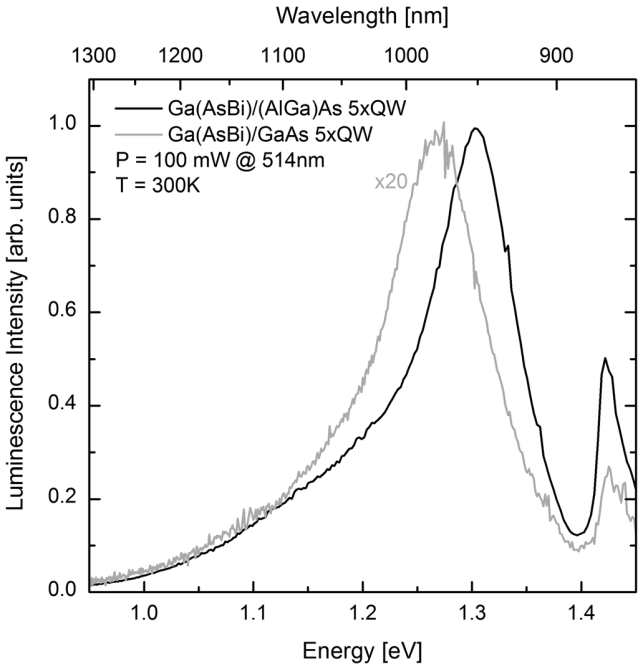

FIG. 4. Photoluminescence spectra of a Ga(AsBi)/GaAs and a Ga(AsBi)/(AlGa)As 5 × QW as test structure for the SQW laser diode.

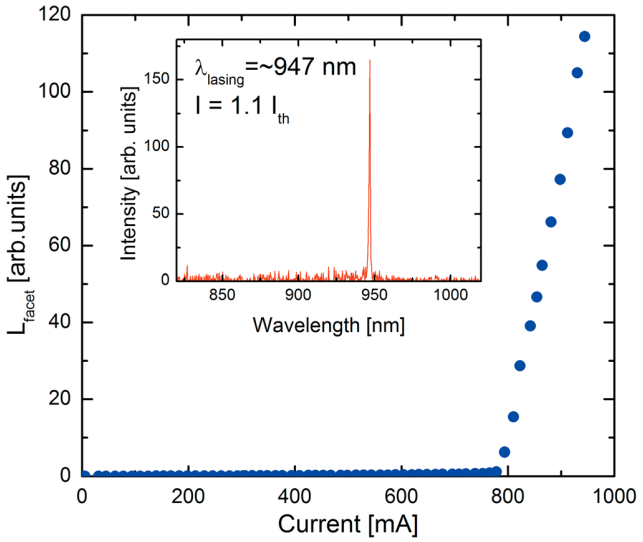

FIG. 5. L-I curve for a 50 × 1000 μm Ga(AsBi)/(AlGa)As SQW laser diode at room temperature and corresponding lasing spectrum (inset).

The integrated PL intensity is increased by a factor of 20 using $(Al_{0.2}Ga)As$ barriers. This is most likely due to improved carrier confinement and an annealing effect of the Ga(AsBi) QW due to the higher growth temperature of the $(Al_{0.2}Ga)As$ barrier. The relatively large full width at half maximum (FWHM) of about 120 meV might be related to disorder within the QW; however, comparable values were observed before in the Ga(AsBi) material system.[13,14]

The devices were measured as-cleaved under pulsed operation (200 ns long pulses at a frequency of 10 kHz) in order to reduce current heating effects. RT measurements were carried out on a probe station, where the facet emission was detected with a large area (InGa)As detector. Figure 5 shows the light-current (L-I) characteristic and the laser emission spectrum (inset) recorded at an injection current of ~1.1 J_{th} (where J_{th} is the threshold current density) at RT. Clear threshold behavior of the integrated emission intensity as a function of drive current is observed at RT as shown in Figure 5. This threshold behavior also corresponds to a pronounced spectral narrowing of the facet emission above threshold (as shown in the inset of Figure 5) providing further verification of laser action. J_{th} for the broad area SQW devices was measured to be ~1.56 kA/cm^2 with a lasing wavelength of 947 nm at RT. The voltage drop across devices at threshold was measured to be approximately 2 V. The J_{th} of these devices is relatively high compared to the standard (InGa)As lasers. However, we believe that room temperature lasing in such a complex material system, for which only one quantum well provides optical gain, is encouraging. This shows great promise for developing efficient IR lasers with this materials system. Investigations are currently underway to determine the cause of the high threshold currents; however, we expect that the device performance is affected by non-radiative defect-related recombination due to unoptimised low temperature growth.

In summary, we have developed high optical quality Ga(AsBi) (2.2% Bi) quantum well material using the MOVPE growth technique. Based upon this material development we have gone on to demonstrate electrically pumped lasing at room temperature with a threshold current density of 1.56 kA/cm^2 at an emission wavelength of 947 nm. These initial results show great promise for this material in laser applications, and further research is now focused on demonstrating longer wavelength lasers where higher bismuth fractions are expected to eliminate some of the major losses plaguing lasers in the near-infrared.

This work was funded by the European Union Framework 7 Project BIANCHO (FP7-257974), the Engineering and Physical Sciences Research Council (EPSRC), UK (EP/H005587/1 and EP/G064725/01), and the German Science Foundation (DFG: GRK1782 and VO805/4).

[1]K. Alberi, O. D. Dubon, W. Walukiewicz, K. M. Yu, K. Bertulis, and A. Krotkus, Appl. Phys. Lett. **91**, 051909 (2007).
[2]K. Oe, Jpn. J. Appl. Phys. **41**, 2801 (2002).
[3]S. J. Sweeney, "Bismide-alloys for higher efficiency infrared semiconductor lasers," in *22nd IEEE International Semiconductor Laser Conference (ISLC)*, 2010, pp. 111–112.
[4]Z. Batool, K. Hild, T. J. C. Hosea, X. Lu, T. Tiedje, and S. J. Sweeney, J. Appl. Phys. **111**, 113108 (2012).
[5]M. Usman, C. A. Broderick, A. Lindsay, and E. P. O'Reilly, Phys. Rev. B **84**, 245202 (2011).
[6]S. J. Sweeney and S. R. Jin, J. Appl. Phys. **113**, 043110 (2013).
[7]S. J. Sweeney, patent W02010/149978 (2010).
[8]A. F. Phillips, S. J. Sweeney, A. R. Adams, and P. J. A. Thijs, IEEE J. Sel. Top. Quantum Elect. **5**, 401 (1999).
[9]R. Lewis, D. Beaton, X. Lu, and T. Tiedje, J. Cryst. Growth **311**, 1872 (2009).
[10]N. Hossain, I. P. Marko, S. R. Jin, K. Hild, S. J. Sweeney, R. B. Lewis, D. A. Beaton, and T. Tiedje, Appl. Phys. Lett. **100**, 51105 (2012).
[11]Y. Tominaga, K. Oe, and M. Yoshimoto, Appl. Phys. Express **3**, 62201 (2010).
[12]P. Ludewig, N. Knaub, W. Stolz, and K. Volz, J. Cryst. Growth **370**, 186 (2013).
[13]S. Tixier, M. Adamcyk, T. Tiedje, S. Francoeur, A. Mascarenhas, P. Wei, and F. Schiettekatte, Appl. Phys. Lett. **82**, 2245 (2003).
[14]I. Moussa, H. Fitouri, Z. Chine, A. Rebey, and B. El Jani, Semicond. Sci. Technol. **23**, 125034 (2008).

5.3 Growth of Ga(AsBi) on GaAs by continuous flow MOVPE[1]

P. Ludewig, Z. L. Bushell, L. Nattermann, N. Knaub, W. Stolz, K. Volz, Journal of Crystal Growth **396**, 95 (2014). DOI: 10.1016/j.jcrysgro.2014.03.041.

Abstract

In this paper we discuss the epitaxial growth of Ga(AsBi) on GaAs under continuous precursor gas supply by metal organic vapor phase epitaxy (MOVPE). Due to the required low growth temperatures the all liquid precursors triethylgallium (TEGa), tertiarybutylarsine (TBAs) and trimethylbismuth (TMBi) were chosen. The influence of several growth parameters such as V/V and V/III ratio, the applied growth temperature and growth rate on the Bi incorporation was investigated. Layers containing up to 5% Bi with good chemical homogeneity and smooth Ga(AsBi)/GaAs hetero interfaces without metallic droplet formation were realized and beyond that incorporation of more than 7% Bi was shown. Furthermore it was found, that Bi acts as surfactant during the growth, reducing the growth rate and impurity incorporation and improving the integrated photoluminescence signal by several orders of magnitude.

The Authors contribution

My contribution to this work was the planning, execution and interpretation of all experiments including the MOVPE growth and analysis by HR-XRD, AFM and PL spectroscopy that were performed in close collaboration with Zoe Bushell supported by Lukas Natterman. The preparation and investigation of the STEM samples was performed by Nikolai Knaub in close collaboration with me. All co-authors helped to interpret the data and to improve the manuscript that was written by me.

1 Reprinted from *Journal of Crystal Growth **396** (2014) 95-99*, Copyright 2014, with permission from Elsevier.

Journal of Crystal Growth 396 (2014) 95–99

Contents lists available at ScienceDirect

Journal of Crystal Growth

journal homepage: www.elsevier.com/locate/jcrysgro

Growth of Ga(AsBi) on GaAs by continuous flow MOVPE

P. Ludewig [a,*], Z.L. Bushell [a,b], L. Nattermann [a], N. Knaub [a], W. Stolz [a], K. Volz [a]

[a] Material Science Center and Faculty of Physics, Philipps-Universität Marburg, Hans-Meerwein-Straße, Mehrzweckgebäude 02D34, 35032 Marburg, Germany

[b] Advanced Technology Institute and Department of Physics, University of Surrey, Guildford, Surrey GU2 7XH, United Kingdom

ARTICLE INFO

Article history:
Received 30 January 2014
Received in revised form
23 March 2014
Accepted 24 March 2014
Communicated by: C. Caneau
Available online 1 April 2014

Keywords:
A3. Metalorganic vapor phase epitaxy
B1. Bismuth compounds
B2. Semiconducting III–V materials
B2. Semiconducting gallium arsenide
B2. Semiconducting ternary compounds

ABSTRACT

In this paper we discuss the epitaxial growth of Ga(AsBi) on GaAs under continuous precursor gas supply by metal organic vapor phase epitaxy (MOVPE). Due to the required low growth temperatures, liquid precursors triethylgallium (TEGa), tertiarybutylarsine (TBAs) and trimethylbismuth (TMBi) were chosen. The influence of several growth parameters such as TMBi/V and V/III ratios, the applied growth temperature and growth rate on the Bi incorporation was investigated. Layers containing up to 5% Bi with good chemical homogeneity and smooth Ga(AsBi)/GaAs hetero-interfaces without metallic droplet formation were realized and beyond that incorporation of more than 7% Bi was shown. Furthermore it was found that Bi acts as surfactant during the growth, reducing the growth rate and impurity incorporation and improving the integrated photoluminescence signal by several orders of magnitude.

1. Introduction

The strong impact of Bi on the band structure of GaAs makes the Ga(AsBi) material system of interest for several applications, especially high efficiency infra red light sources. For Bi fractions exceeding approximately 10% the band gap becomes smaller than the spin–orbit splitting; hence Auger loss processes and intervalance band absorption involving transitions to the spin–orbit band could be suppressed [1,2]. Furthermore, it was shown that the temperature sensitivity of the band gap of this alloy is reduced with respect to the one of GaAs [3], allowing better control of the emission wavelength. However, the growth of high quality Ga(AsBi) crystals is still challenging. Recently we reported on room temperature lasing operation of a Ga($As_{0.978}Bi_{0.022}$) single quantum well (SQW) laser diode [4]. Optical pumped lasing has already been demonstrated on Ga($As_{0.941}Bi_{0.059}$) grown by molecular beam epitaxy (MBE) [5]. In MBE, growth Bi fractions $>10\%$ were already reported but growth temperatures as low as 200 °C are required. In metal organic vapor phase epitaxy (MOVPE) much higher growth temperatures (>350 °C) are needed in order to decompose the metal organic precursors; hence only Bi fractions up to 4% were reported so far [6–9]. In addition, the formation of metallic Bi droplets causes problems since surplus Bi segregates to the surface but does not desorb due to the low temperatures. In earlier studies we presented the growth of droplet free Ga(AsBi)/GaAs multi-quantum well structures that were grown in a pulsed growth mode [8]. In this case surplus Bi was consumed during the growth of the nominally Bi free GaAs barriers. However, the growth rate is limited to one monolayer per pulse and the control of the layer thickness as well as the deposition of bulk layers is very challenging. Furthermore this growth mode, where the Bi surface coverage changes all the time, is not recommendable for the deposition of quaternary material systems as e.g. Ga(NAsBi) and (GaIn)(AsBi) which extend the usage of the dilute bismides [1,2,10,11].

In the present work we will discuss the MOVPE growth of Ga(AsBi) layers where all growth parameters are adjusted very carefully and therefore continuous growth of high quality and droplet free bulk structures is possible. This not only enables investigations of Bi incorporation and the optical properties depending on several parameters but also analysis of the impact of Bi on the growth rate and the impurity incorporation.

2. Experimental procedure

Ga(AsBi) single layers of about 50–100 nm thickness were grown by MOVPE on exact GaAs (001) substrates. Growth took place in a commercially available horizontal reactor system with gas flow rotation (AIX 200-GFR-reactor) at a reduced reactor pressure of 50 mbar using Pd purified H_2 as carrier gas. Due to the required low growth temperatures of 375 °C and 400 °C, liquid precursors triethylgallium (TEGa), tertiarybutylarsine (TBAs) and

* Corresponding author. Tel.: +49 6421 2825713.
E-mail address: peter.ludewig@physik.uni-marburg.de (P. Ludewig).

http://dx.doi.org/10.1016/j.jcrysgro.2014.03.041
0022-0248/

trimethylbismuth (TMBi) were chosen. Most of the samples were heated to 625 °C under TBAs stabilization after the Ga(AsBi) deposition in order to grow a 20 nm thick GaAs capping layer. The heating process takes about 2 min and enables desorption of surplus Bi from the surface. In contrast to our earlier studies, where the segregated Bi is also incorporated during the growth of the subsequent GaAs layers that were grown at the same temperature as that of the Ga(AsBi) layer [8], here one can be sure that the Bi is incorporated only in the nominal Ga(AsBi) layers and therefore determine the growth rates. It was already shown before that the Ga(AsBi) material is not negatively affected by these temperature changes and sharp Ga(AsBi)/GaAs hetero-interfaces can be realized [4]. The Bi fraction and layer thickness were determined by modeling the high resolution x-ray diffraction (HR-XRD) pattern around the (004) GaAs substrate peak assuming 6.33 Å as GaBi lattice constant [12]. In some cases cross sectional scanning transmission electron microscopy (STEM) investigations were carried out to confirm these measurements and to analyze the homogeneity of the Bi incorporation as well as the Ga(AsBi)/GaAs interfaces. Surface morphologies and the presence of metal droplets were studied by atomic force microscopy (AFM). Room temperature photoluminescence (PL) measurements were then performed to relate the optical properties of the samples to the composition and the applied growth conditions. The PL measurements were carried out using a continuous-wave (cw) Ar-ion laser at a wavelength of 514 nm for excitation. The PL signal was dispersed in a 1 m grating monochromator and collected by a cooled germanium detector applying the standard lock-in technique.

3. Results and discussion

First the Bi incorporation and growth rate using optimized continuous growth conditions will be discussed in relation to the TMBi/V and V/III ratios as well as the temperature. Then we will address the structural quality and finally the effect of Bi as a surfactant on the carbon incorporation and the optical properties.

The filled circles in Fig. 1 show the dependence of the Bi fraction of the Ga(AsBi) layers on the TMBi/V ratio when only TMBi was changed. All samples were grown at 400 °C and capped with GaAs at 625 °C; the Ga(AsBi) layer thickness varies between 50 nm and 80 nm. Compared to the samples discussed in [8] the growth parameters were optimized to reduce Bi segregation and enable the growth of thick single layer samples under continuous precursor supply. The TEGa partial pressure here was increased to 0.042 mbar, which corresponds to a GaAs growth rate of 0.43 nm/s at 400 °C and the TBAs/TEGa ratio was slightly reduced to 1.9. As for the pulsed growth of the MQW structures the Bi fraction first increases with the amount of TMBi in the reactor and then levels out at about 3.8% in the present case. Since the GaAs cap is grown at 625 °C where the segregated Bi is not incorporated into the crystal it is possible to determine the Ga(AsBi) growth rate directly from its layer thickness and growth time (open circles Fig. 1). We find that with increasing TMBi the growth rate is reduced by about 33% and levels out as the Bi fraction does. As the growth rate is usually determined only by the group III precursor, we assume that the presence of Bi or the not yet fully decomposed TMBi at the surface either reduces the decomposition of TEGa or hinders it from sticking to the surface. Gas phase reactions seem unlikely here since the maximum applied TMBi/TEGa ratio is only 0.031.

In order to investigate the influence of the applied V/III ratio the TBAs partial pressure was varied starting from the sample with TMBi/V = 0.02 and TBAs/TEGa = 1.9 in Fig. 1, where the Bi limitation has already set in (marked with *). The determined Bi fractions and growth rates of this series are plotted in Fig. 2 (black circles). We observe that the Bi fraction increases nearly linearly up to 4.4% with decreasing TBAs, which is due to the fact that As and Bi are in competition for the group V sublattice places. When the TBAs gets too low the Bi fraction decreases again, which could be related to the low V/III (< 1) ratio leading to a Ga rich surface. At this point it needs to be pointed out that the given numbers are the gas phase ratios of the precursors, which are not necessarily the same as the pure metal ratios at the surface since the decomposition characteristics need to be taken into account at these low growth temperatures. Besides the increasing Bi fraction the growth rate is reduced even more than observed from the variation of the TMBi. The sample with the maximum Bi fraction of 4.4% has a growth rate of only 25% of that of the pure GaAs sample. This underlines the assumption that the more Bi or TMBi rich the surface the less the decomposition of TEGa or sticking to the surface; however, an influence of the low V/III ratio is not excluded. On the other hand, if the TBAs supply is too high (here TBAs/TEGa > 2.5) the growth rate drops along with the Bi fraction. This behavior is not yet understood and still under investigation but was also observed for

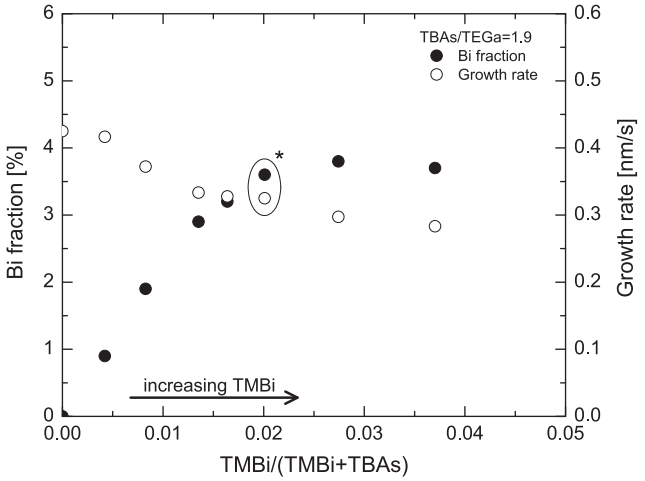

Fig. 1. Bi fraction (filled circles) and growth rate (open circles) of Ga(AsBi) samples grown at 400 °C where only the TMBi partial pressure was varied. Under the given growth conditions the Bi fraction levels out at about 3.8%. In addition, one can see that the growth rate decreases with increasing amount of TMBi.

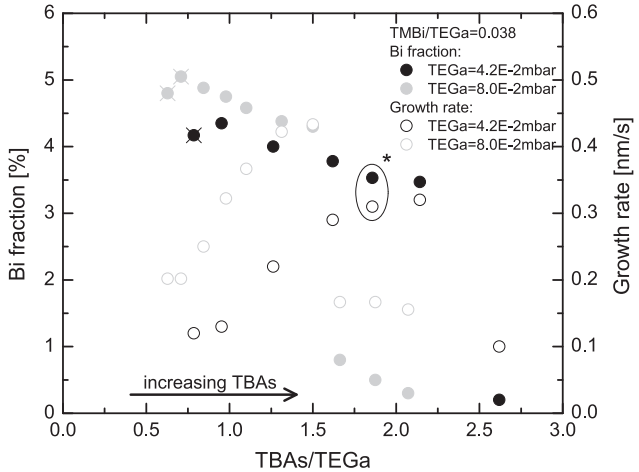

Fig. 2. Bi fraction (filled circles) and growth rate (open circles) of Ga(AsBi) samples grown at 400 °C where only the TBAs partial pressure was varied. In a narrow range of TBAs/TEGa ratios the Bi fraction increases while the growth rate decreases. Outside this range the Bi incorporation drops. The same behavior is observed for higher growth rates (gray circles) where the Bi fraction rises up to 5%. Data points of samples with volcano-like structures at the surface are crossed.

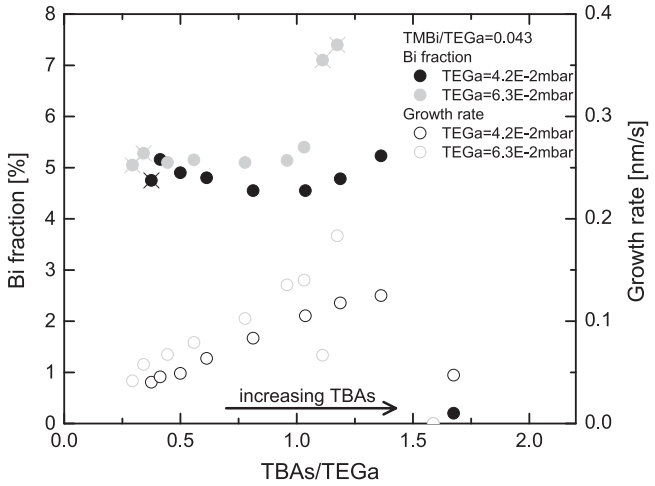

Fig. 3. Bi fraction (filled circles) and growth rate (open circles) of Ga(AsBi) samples grown at 375 °C where only the TBAs partial pressure was varied. We observe the same trend as that at 400 °C (Fig. 2). In addition, there is a small range where the higher growth rate due to the higher TBAs partial pressure leads to again increasing Bi fraction of up to 7.4%. Data points of samples with Bi droplets at the surface are crossed.

several sets of other samples. The gray circles in Fig. 2 show a series where the amount of all precursors given to the reactor was increased by a factor of 1.9. (Within the range of conditions of our study, we found a clear linear relation between the amount of TEGa in the reactor and the growth rate under a given TMBi/V ratio.) The growth rate and Bi incorporation behave in the same manner for the lower precursor flows but are shifted to lower TBAs/TEGa ratio. Increasing the growth rate also increases the Bi fraction for the same V/III ratio, as expected for this metastable material since there is less time for the Bi to escape the crystal.

Further investigations on the Ga(AsBi) growth were carried out at a reduced growth temperature of 375 °C. Fig. 3 summarizes the results of the TBAs variation for partial pressure of TEGa =0.042 mbar (black circles) and the 1.5 times higher value of 0.063 mbar (gray circles). The TMBi partial pressure is again chosen such that the Bi incorporation is in the saturated regime. The trend is very similar to what was observed for the growth at 400 °C: the growth rate decreases with decreasing TBAs supply and also drops at too high TBAs values (here TBAs/TEGa > 1.5) and the Bi fraction increases at low TBAs values and then decreases at approximately TBAs/TEGa < 0.4. However, in contrast to the observation at 400 °C the Bi fraction shows differing behavior for higher TBAs/TEGa ratios in the range of 1–1.5. In this growth regime we find a very narrow window where the Bi incorporation rises to values above 7% before it is suppressed by too much As. An explanation would be that in this regime the increasing growth rate, which supports the Bi incorporation, overbalances the higher amount of As that would suppress the Bi incorporation. In contrast to all other samples discussed so far, in this growth regime the samples show very inhomogeneous Bi distributions, especially those with Bi fractions higher than 7%. Whereas the plotted values were determined in the center region of the 50 mm wafer of 15–20 mm diameter, the outer area shows no presence of Ga(AsBi). Either no growth takes place at all in the outer area or no Bi gets incorporated. The reasons might be small changes in the gas phase composition and temperature across the wafer that lead to disadvantageous growth conditions as in the range of TBAs/TEGa > 1.5.

The surface morphologies of all samples discussed above were investigated by atomic force microscopy. For the series where only the amount of TMBi was varied, all samples up to TMBi/V=0.027 show smooth surfaces of the GaAs cap (Fig. 4(a)). In case of the sample with TMBi/V=0.037 we find volcano-like structures at the surface (Fig. 4(b)) which originate most likely from evaporated Bi droplets that leave holes behind. The structures consist of GaAs as confirmed by STEM investigations (not shown here) and arise most probably by crystallization of liquid Ga that was dissolved in the evaporated Bi droplets and As that is used for group V stabilization [13]. These structures are observed also in the sample series where the TBAs is varied (Fig. 2) on those samples with low V/III-ratios where the Bi fraction slightly decreases again. The sample series at 375 °C (Fig. 3) was grown without GaAs cap, and we find Bi droplets not only for this low V/III regime but also for the high V/III region, for the samples with Bi fractions above 7%. The surface morphologies of the samples in between these ranges do not show any indication of metallic droplet formation during the growth. In Fig. 4(c) the high angle annular dark field (HAADF) STEM image in [−110] direction of a sample with about 5% Bi is shown. The sample was grown at 400 °C in the TMBi/V regime, where the growth rate levels out, the Bi incorporation has its maximum (see Fig. 2) and already small amounts of the volcano-like structures appear at the surface. The contrast in this imaging mode is dependent on the atomic number Z of the atoms, making those group V columns with Bi atoms appear brighter than pure As columns. We find smooth and abrupt heterointerfaces between the Ga(AsBi) and GaAs layers showing again the stability of this material system versus the change of the growth temperature from 400 °C to 625 °C. In addition the contrast in the Ga(AsBi) layer is homogenous and no signs of Bi clustering could be found. Overall this structural analysis shows that at least up 5% Bi can be incorporated into GaAs by MOVPE growth with high crystalline quality.

One main issue that occurs in low temperature MOVPE is the unintentional incorporation of C into the crystal from the organic groups of the precursors. In order to determine the amount of C in the Ga(AsBi) layers, secondary ion mass spectroscopy (SIMS) measurements were carried out on structures containing different amounts of Bi. The results for five samples from the series where the solid Bi fraction was adjusted by the TMBi partial pressure (see Fig. 1) including the Bi free sample, are plotted in Fig. 5. Interestingly the highest amount of C with about 5×10^{19} C atoms/cm^2 was found in the low temperature (LT) GaAs sample, which shows that the main C doping seems to come from the TEGa precursor since an incorporation of C from the tertiarybutyl-group of the TBAs is very unlikely. The more the Bi added to the surface during the growth, the lower the amount of C incorporated in the epilayer. For the sample with the highest TMBi/V ratio of 0.0275, which was grown in the Bi saturation regime, the C level is only 2×10^{16} C atoms/cm^2 (close to the detection limit) in the layer and therefore more than three orders of magnitude lower than in the LT GaAs sample. This might be related to the fact that the segregated Bi occupies the group V sites at the surface during growth and with that hinders the incorporation of C, which is incorporated on group V lattice sites in GaAs [14]. Only at the lower interface could a C doping of about 10^{18} C atoms/cm^2 be detected since it takes some time at the beginning of the Ga(AsBi) layer growth until a certain Bi coverage is reached [8].

In addition, room temperature photoluminescence (PL) measurements of these samples were performed to investigate their optical properties (Fig. 6(a)). With increasing TMBi partial pressure the integrated PL signal monotonically increases by several orders of magnitude even though the Bi fraction again decreases for the highest TMBi/V ratio. These investigations show that the often observed effect of improved PL intensity with increasing Bi fraction [16,17] is most probably not related to the Bi fraction in the crystal, but instead to the larger amount of Bi at the surface during growth that is needed for higher Bi incorporation. The Bi

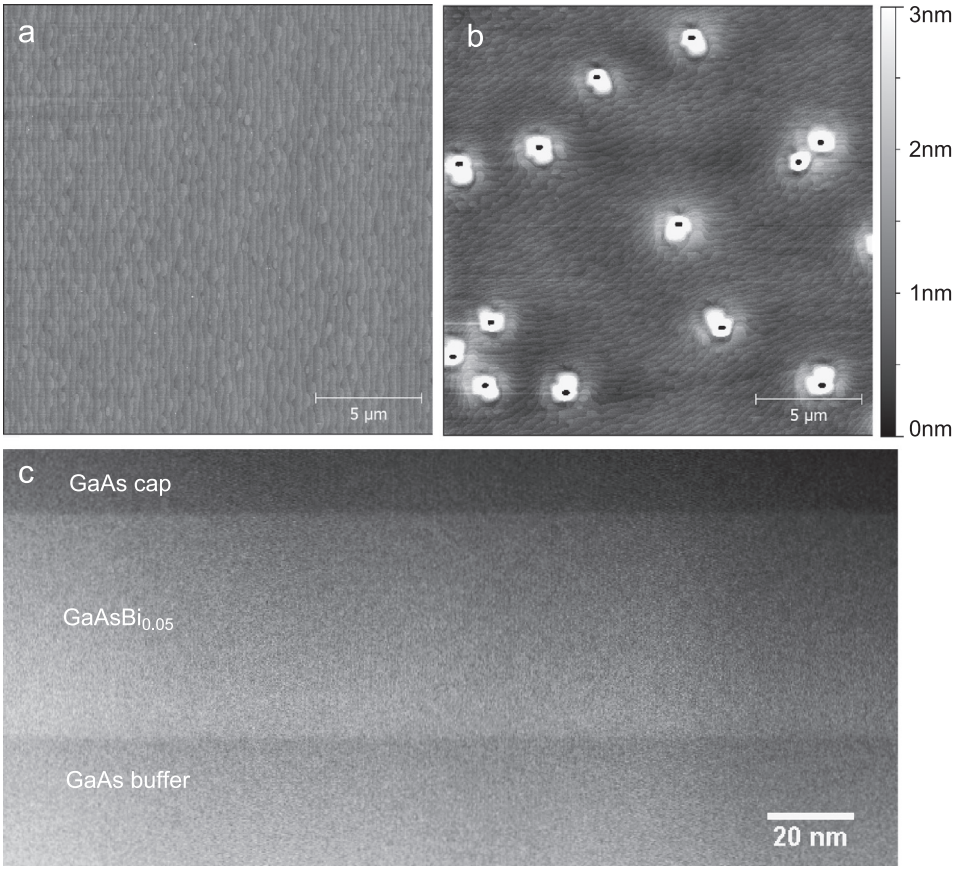

Fig. 4. Surface morphologies of the GaAs cap of the sample with TMBi/V=0.027 (a) and TMBi/V=0.037 (b) from the series in Fig. 1 where only TMBi was varied. While in (a) no signs of metallic droplets can be found, the volcano-like structures in (b) form when Bi droplets are evaporated at the higher temperatures. The cross section HAADF-STEM image in [−110] direction of a sample with 5% Bi (c) shows smooth interfaces and high chemical homogeneity.

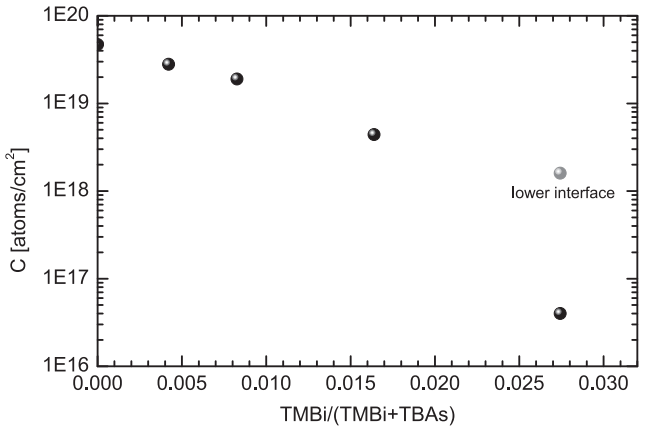

Fig. 5. Carbon incorporation dependence on the TMBi partial pressure. With increasing amount of Bi on the surface during the growth, the unintentional C incorporation decreases by several orders of magnitude.

acts as a surfactant and hence reduces the amount of defects such as antisites or vacancies and also the incorporation of C, which then leads to an improved PL intensity.

The PL peak energy of several samples discussed above is plotted in Fig. 6(b). We find a very good agreement of our measurements with calculations of the Ga(AsBi) bandgap taken from [15] (dashed line) which confirms the investigation of the composition by HR-XRD. In addition the linewidth (full width at half maximum, FWHM) of the PL spectra is plotted versus the Bi fraction. Here we find quite high values in the low Bi fraction regime (< 3.5%) of about 130–140 meV. These values might be due to the superposition of the PL signal coming from the Ga(AsBi) layer with the signal from a defect level at roughly 0.97 eV that is observed in Fig. 6(a). This defect level also appears in the PL spectrum of a Bi free GaAs sample that was grown at the same conditions as those of the Ga(AsBi) samples; hence it must be related to a defect occurring in the low temperature growth of GaAs such as e.g. antisites or vacancies. For higher Bi fractions the Ga(AsBi) peak becomes more intense and therefore the defect level has less influence on the PL spectra and the linewidth shrinks to about 80–90 meV which is often observed in this material system [16–18] and is most probably due to the disorder.

4. Summary

The growth of Ga(AsBi) by MOVPE applying continuous precursor flows is dominated by the surface Bi. The Bi fraction increases with the amount of Bi at the surface, reaching a maximum value depending on the applied growth conditions. This maximum increases with the growth rate and increases with decreasing temperature and TBAs supply. Applying relatively high growth rates and V/III ratios in the range of 0.5–2, we were able to deposit homogenous Ga(AsBi) layers with up to 5% Bi and smooth Ga(AsBi)/GaAs heterointerfaces. There is a very narrow growth regime at 375 °C where even more than 7% of Bi was incorporated but at the cost of homogeneity and morphology. It was also found that besides the Bi incorporation, the growth rate of the Ga(AsBi) depends on the TMBi partial pressure, which is most likely related to a suppressed TEGa decomposition due to the

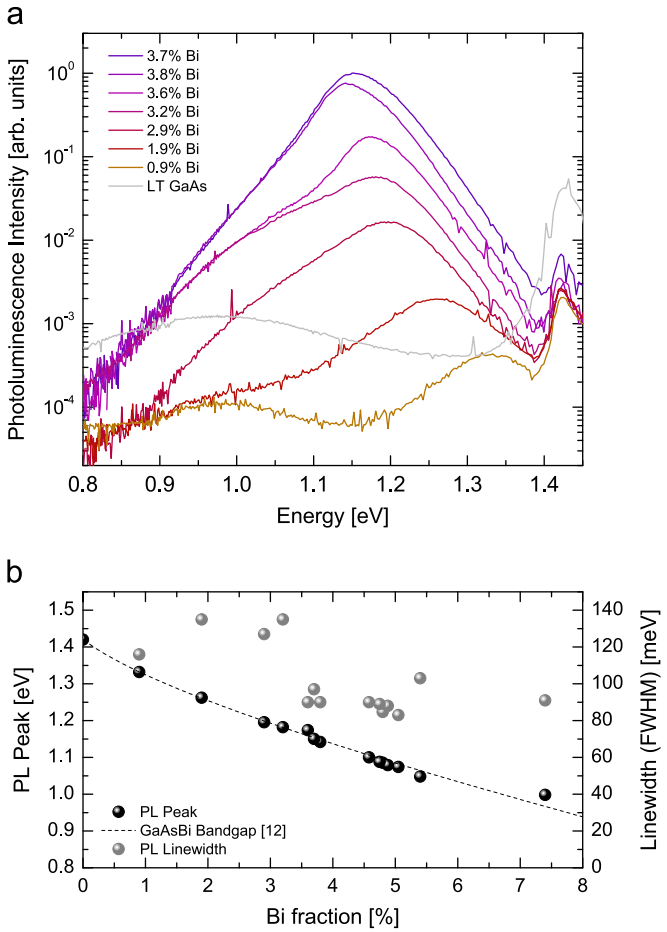

Fig. 6. Room temperature photoluminescence spectra (a) of the Ga(AsBi) samples plotted in Fig. 1. The integrated PL intensity does not scale with the Bi fraction but with the applied TMBi partial pressure due the surfactant effect of Bi. The peak positions (b) of the samples are in very good agreement with the calculated values taken from [15]. The quite high linewidth of the PL spectra for samples with low Bi fraction could be due to a superposition of the PL of the Ga(AsBi) layer and an additional peak at about 0.97 eV. This peak is most likely due to a defect level such as antisites or vacancies since it is also observed in the spectra of a GaAs sample that was grown under the same conditions as those of the Ga(AsBi) samples but without TMBi (LT GaAs).

presence of (TM)Bi at the surface. Bi acts as a surfactant during the growth and improves the photoluminescence signal and quenches the C incorporation.

Acknowledgments

This work was funded by the European Union Framework 7 Project BIANCHO (FP7-257974) and the German Science Foundation (DFG: VO805/4 and DFG: GRK1782). Z.L. Bushell acknowledges financial support from an ERASMUS grant through the European Commission Lifelong Learning Programme.

References

[1] C.A. Broderick, M. Usman, S.J. Sweeney, E.P. O'Reilly, Semicond. Sci. Technol. 27 (2012) 094011, http://dx.doi.org/10.1088/0268-1242/27/9/094011.
[2] S.J. Sweeney, S.R. Jin, J. Appl. Phys. 113 (2013) 043110, http://dx.doi.org/10.1063/1.4789624.
[3] K. Oe, H. Okamoto, Japn. J. Appl. Phys. 37 (1998) L1283–L1285, http://dx.doi.org/10.1143/JJAP.37.L1283.
[4] P. Ludewig, N. Knaub, N. Hossain, S. Reinhard, L. Nattermann, I.P. Marko, S.R. Jin, K. Hild, S. Chatterjee, W. Stolz, S.J. Sweeney, K. Volz, Appl. Phys. Lett. 102 (2013) 242115, http://dx.doi.org/10.1063/1.4811736.
[5] T. Fuyuki, R. Yoshioka, K. Yoshida, M. Yoshimoto, Appl. Phys. Lett. 103 (2013) 202105, http://dx.doi.org/10.1063/1.4830273.
[6] K. Oe, J. Cryst. Growth 239 (2002) 1481–1485, http://dx.doi.org/10.1016/S0022-0248(01)02301-6.
[7] I. Moussa, H. Fitouri, A. Rebey, B. El Jani, Thin Solid Films 516 (2008) 8372–8376, http://dx.doi.org/10.1016/j.tsf.2008.04.062.
[8] P. Ludewig, N. Knaub, W. Stolz, K. Volz, J. Cryst. Growth 370 (2013) 186–190, http://dx.doi.org/10.1016/j.jcrysgro.2012.07.002.
[9] K. Forghani, A. Anand, L.J. Mawst, T.F. Kuech, J. Cryst. Growth 380 (2013) 23–27, http://dx.doi.org/10.1016/j.jcrysgro.2013.05.033.
[10] I.P. Marko, Z. Batool, K. Hild, S.R. Jin, N. Hossain, T.J.C. Hosea, J.P. Petropoulos, Y. Zhong, P.B. Dongmo, J.M.O. Zide, S.J. Sweeney, Appl. Phys. Lett. 101 (2012) 221108, http://dx.doi.org/10.1063/1.4768532.
[11] Z.L. Bushell, P. Ludewig, N. Knaub, Z. Batool, K. Hild, W. Stolz, S.J. Sweeney and K. Volz, Growth and characterisation of Ga(NAsBi) alloy by metal organic vapour phase epitaxy, J. Cryst. Growth. http://dx.doi.org/10.1016/j.jcrysgro.2014.03.038, in press.
[12] S. Tixier, M. Adamcyk, T. Tiedje, S. Francoeur, A. Mascarenhas, P. Wei, F. Schiettekatte, Appl. Phys. Lett. 82 (2003) 2245–2247, http://dx.doi.org/10.1063/1.1565499.
[13] K. Reyes, P. Smereka, D. Nothern, J.M. Millunchick, S. Bietti, C. Somaschini, S. Sanguinetti, C. Frigeri, Phys. Rev. B 87 (2013) 165406, http://dx.doi.org/10.1103/PhysRevB.87.165406.
[14] T.F. Kuech, M.a. Tischler, P.-J. Wang, G. Scilla, R. Potemski, F. Cardone, Appl. Phys. Lett. 53 (1988) 1317, http://dx.doi.org/10.1063/1.100008.
[15] C.A. Broderick, M. Usman, E.P. O'Reilly, Semicond. Sci. Technol. 28 (2013) 125025, http://dx.doi.org/10.1088/02681242/28/12/125025.
[16] A.R. Mohmad, F. Bastiman, C.J. Hunter, J.S. Ng, S.J. Sweeney, J.P.R. David, Appl. Phys. Lett. 99 (2011) 42107, http://dx.doi.org/10.1063/1.3617461.
[17] X. Lu, D.A. Beaton, R.B. Lewis, T. Tiedje, Y. Zhang, Appl. Phys. Lett. 95 (2009) 41903, http://dx.doi.org/10.1063/1.3191675.
[18] A.R. Mohmad, F. Bastiman, J.S. Ng, S.J. Sweeney, J.P.R. David, Appl. Phys. Lett. 98 (2011) 122107, http://dx.doi.org/10.1063/1.3565244.

5.4 Growth and characterisation of Ga(NAsBi) alloy by metal organic vapour phase epitaxy[1]

Z. L. Bushell, P. Ludewig, N. Knaub, Z. Batool, K. Hild, W. Stolz, S. J. Sweeney, K. Volz, Journal of Crystal Growth **396**, 79 (2014). DOI: 10.1016/j.jcrysgro.2014.03.038.

Abstract

This paper summarises results of the epitaxial growth of Ga(NAsBi) by metal organic vapour phase epitaxy (MOVPE) and the subsequent optical and structural characterisation of the samples. Ga(NAsBi)/GaAs multi quantum well (MQW) samples are grown at 400 °C and single layers at 450 °C on GaAs (001) substrates. Triethylgallium (TEGa), tertiarybutylarsine (TBAs), trimethylbismuth (TMBi) and unsymmetrical dimethylhydrazine (UDMHy) are used as precursors. Secondary ion mass spectrometry (SIMS) shows that the Bi content is independent of the N content in the alloy. It is found that the N content depends on both UDMHy and TMBi supply during growth. High resolution X-ray diffraction (HR-XRD), scanning transmission electron microscopy (STEM) and atomic force microscopy (AFM) measurements show that samples with good crystalline quality can be realised. For samples containing 1.8% Bi and up to 1.8% N grown at 450 °C, photoreflectance spectroscopy (PR) shows a decrease in the band gap with increasing N content of -141±22 meV/%N.

The Authors contribution

Zoe Bushell did the planning, execution and interpretation of the experiments including the MOVPE growth and analysis by HR-XRD, AFM and PL spectroscopy under my supervision and in close collaboration. The preparation and investigation of the STEM samples was performed by Nikolai Knaub. The PR measurements were done at the University of Surrey by Zahida Batool. The co-authors, including me, helped to interpret the data and to improve the manuscript written by Zoe Bushell.

1 Reprinted from *Journal of Crystal Growth **396** (2014) 79-84*, Copyright 2014, with permission from Elsevier.

Journal of Crystal Growth 396 (2014) 79–84

Contents lists available at ScienceDirect

Journal of Crystal Growth

journal homepage: www.elsevier.com/locate/jcrysgro

Growth and characterisation of Ga(NAsBi) alloy by metal–organic vapour phase epitaxy

Z.L. Bushell [a,b,*], P. Ludewig [a], N. Knaub [a], Z. Batool [b], K. Hild [b], W. Stolz [a], S.J. Sweeney [b], K. Volz [a]

[a] Material Science Center and Faculty of Physics, Philipps-Universität Marburg, 35032 Marburg, Germany
[b] Advanced Technology Institute and Department of Physics, University of Surrey, Guildford, Surrey GU2 7XH, United Kingdom

ARTICLE INFO

Article history:
Received 31 January 2014
Received in revised form
21 March 2014
Accepted 25 March 2014
Communicated by: C. Caneau
Available online 1 April 2014

Keywords:
A3. Metal–organic vapour phase epitaxy
B1. Bismuth compounds
B1. GaNAsBi
B1. Nitrides
B2. Semiconducting III–V materials
B2. Semiconducting quaternary alloys

ABSTRACT

This paper summarises results of the epitaxial growth of Ga(NAsBi) by metal–organic vapour phase epitaxy (MOVPE) and the subsequent optical and structural characterisations of the samples. Ga(NAsBi)/GaAs multi-quantum well (MQW) samples are grown at 400 °C and single layers at 450 °C on GaAs (001) substrates. Triethylgallium (TEGa), tertiarybutylarsine (TBAs), trimethylbismuth (TMBi) and unsymmetrical dimethylhydrazine (UDMHy) are used as precursors. Secondary ion mass spectrometry (SIMS) shows that the Bi content is independent of the N content in the alloy. It is found that the N content depends on both UDMHy and TMBi supply during growth. High resolution X-ray diffraction (HR-XRD), scanning transmission electron microscopy (STEM) and atomic force microscopy (AFM) measurements show that samples with good crystalline quality can be realised. For samples containing 1.8% Bi and up to 1.8% N grown at 450 °C, photoreflectance spectroscopy (PR) shows a decrease in the band gap with increasing N content of 141 ± 22 meV/% N.

1. Introduction

The III–V alloy Ga(NAsBi) has several important properties that make it an interesting material for infrared photonic devices. Band anticrossing (BAC) interactions in both the conduction band and valence band due to the incorporation of dilute amounts of nitrogen and bismuth, respectively, into GaAs lead to a strong reduction in the bandgap [1]. Due to the compensation in strain between the relatively small N atoms and relatively large Bi atoms, it is predicted to be possible to cover a range of bandgaps from 0.2 eV to 1.4 eV whilst keeping the strain on GaAs to within ± 1.5% [1]. The incorporation of bismuth also increases the spin–orbit splitting [2], which could allow suppression of Auger recombination and inter-valence band absorption [3]. The bandgap of Ga(NAsBi) is also less temperature sensitive than conventional III–V alloys [4], which offers the potential for devices with improved temperature stability.

The growth of Ga(AsBi) has been demonstrated by both molecular beam epitaxy (MBE) and metal–organic vapour phase epitaxy (MOVPE), with Bi content of more than 10% in MBE growth [5,6] and up to 7.4% by MOVPE [7]. For successful growth of the metastable Ga(AsBi), growth conditions must be carefully controlled within a narrow range with low growth temperatures and low V/III ratios required [7–9]. Ga(NAsBi) bulk layers have previously been grown successfully by MBE [10,11] but there have been no previous reports on growth by MOVPE. In this paper we present the successful growth of Ga(NAsBi) MQWs and single layers by MOVPE and discuss their structural and optical properties.

2. Experimental procedure

Ga(NAsBi)/GaAs multi-quantum well (MQW) and single layer samples were grown on semi-insulating GaAs (001) substrates by MOVPE. Growth took place in a commercially available AIX 200-GFR horizontal reactor system, using Pd-purified H_2 carrier gas at a reduced reactor pressure of 50 mbar. Triethylgallium (TEGa), tertiarybutylarsine (TBAs), trimethylbismuth (TMBi) and unsymmetrical dimethylhydrazine (UDMHy) were used as precursors for Ga, As, Bi and N respectively, since these decompose at the low growth temperatures required. Growth temperatures of 400 °C and 450 °C were used for the Ga(NAsBi) layers and 625 °C for GaAs. Temperature changes before and after the Ga(NAsBi) growth were performed during TBAs stabilised growth interruptions. The UDMHy/TBAs ratio was varied up to a maximum of 1.0 and the TMBi/TBAs ratio was varied in the range of 7.7×10^{-3} – 3.0×10^{-2}.

* Corresponding author.
E-mail address: zb00031@surrey.ac.uk (Z.L. Bushell).

http://dx.doi.org/10.1016/j.jcrysgro.2014.03.038
0022-0248/

The MQW samples grown at 400 °C had a constant TEGa supply of 4.2×10^{-2} mbar and TBAs/TEGa ratio of 1.2 and the growth rate was around 1 μm/h. The single layer samples grown at 450 °C had a constant TEGa supply of 3.2×10^{-2} mbar and TBAs/TEGa ratio of 1.9 and the growth rate was in the range of 2–3 μm/h in order to incorporate sufficient Bi at the higher growth temperature.

Dynamical modelling to fit the experimental results from high resolution X-ray diffraction (HR-XRD) omega–2theta scans around the GaAs (004) reflection was used to determine the layer thicknesses and relationship between Bi and N contents. Two samples containing Ga(NAsBi) and Ga(AsBi) layers were also analysed by secondary ion mass spectrometry (SIMS) to investigate the relative Bi and N contents of the layers. Cross-sectional [010] scanning transmission electron microscopy (STEM) high angle annular dark field (HAADF) images were obtained using a JEOL JEM 2200 FS in order to investigate the crystalline quality and layer thicknesses in more detail. In the STEM HAADF mode the intensity is sensitive to the chemical composition of the layer (Z-contrast) so it can be used to investigate chemical homogeneity in the material. STEM samples were prepared conventionally, using Ar-ion milling as the final preparation step. Atomic force microscopy was used to study the surface morphology. Room temperature (RT) photoluminescence spectroscopy (PL) and photomodulated reflectance (PR) were performed to analyse the optical properties of the samples. The PL measurements were carried out using the 514 nm line of a continuous-wave Ar-ion laser for excitation. The PL signal was dispersed in a 1 m grating monochromator (THR 1000, Jobin-Yvon) and collected by a cooled germanium detector applying the standard lock-in technique. In addition to PL, PR, a form of modulation spectroscopy [12], is a very useful non-destructive technique to determine the band gap and other critical points in the band structure of semiconductors. To modulate the sample dielectric function a 514 nm argon ion laser chopped at a frequency of 333 Hz with output power of 113 mW was used, illuminating the same spot on the sample where a monochromatic probe beam was reflected off the sample. The output PR signal, the fractional change in the reflectivity $\Delta R/R$, was measured with a lock-in amplifier connected to an InGaAs detector.

3. Results and discussion

In this section the influence of N content on Bi incorporation in Ga(NAsBi) is first discussed. The influence of both UDMHy and TMBi supply on the growth of Ga(NAsBi) MQWs at 400 °C is then investigated and the structural properties are examined by STEM. Finally, the growth of Ga(NAsBi) single layers at 450 °C is investigated and the optical properties are discussed.

Dynamical modelling of HR-XRD results can only determine a linear relationship between Bi and N contents in the quaternary alloy, not the absolute values of each. Therefore a sample was produced for SIMS analysis with both Ga(AsBi) and Ga(NAsBi) ~30 nm layers separated by a 100 nm GaAs barrier. Both layers were grown under identical conditions at 400 °C apart from the addition of N to the Ga(NAsBi) layer with UDMHy/TBAs = 1. The results of the SIMS analysis are shown in Fig. 1. It can be seen that the Bi content of the two layers is approximately equal, independent of the addition of N. It is therefore assumed when performing subsequent fitting of dynamical modelling to the HR-XRD results that the Bi content of Ga(NAsBi) is the same as that of an equivalent N-free sample grown under the same conditions.

3.1. Growth of Ga(NAsBi) MQW samples at 400 °C

Starting from a Ga(AsBi)/GaAs MQW sample with Bi content of 3.5%, as determined from HR-XRD, a set of samples (#1–4 in Table 1) were grown varying only the UDMHy supply. A second

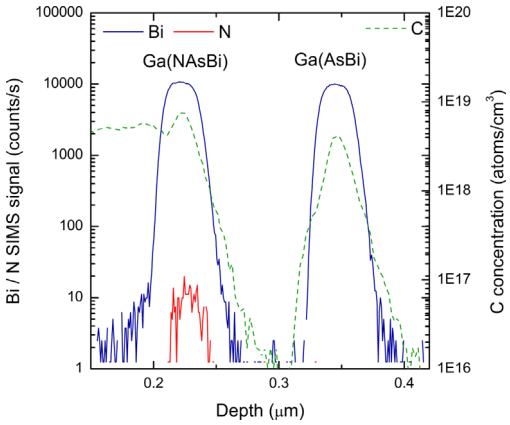

Fig. 1. SIMS profile of Ga(NAsBi) and Ga(AsBi) layers grown at 400 °C surrounded by GaAs barriers.

set of samples (#5–8 in Table 1) were also produced with increasing UDMHy supply, but in this case with Bi content of 2.6%. Fig. 2(a) and (b) shows the experimental HR-XRD (004) patterns (solid lines) of these sets of Ga(NAsBi) MQW samples along with the best fit simulations (dashed lines). The main features of the XRD patterns identified in Fig. 2 are as follows: (1) GaAs substrate peak and (2) broad peak from Ga(NAsBi) QWs, superimposed with fringes due to the layer thicknesses. It is possible to achieve a good fit of the simulated curve to the experimental result in all cases, allowing for accurate determination of the layer compositions and thicknesses. Further detail on the dynamical theory of XRD and interpretation of the XRD profiles for multi-layer structures can be found, for example, in Ref. [13]. In all cases the diffraction patterns show a 3 × QW profile with clearly resolved pendellosung fringes, indicating good crystalline quality and sharp heterointerfaces. It can be seen that with increasing UDMHy supply, the samples change from being compressively strained (broad QW peak on left, lower angle side of substrate peak), through almost lattice matched to GaAs for the sample with UDMHy/TBAs = 0.75, towards tensilely strained (broad QW peak on right, larger angle side of substrate peak).

The resulting N content, as determined from dynamical modelling of the HR-XRD results assuming that the Bi content is independent of N, for these two sets of samples is plotted in Fig. 3(a). Details of all samples are also summarised in Table 1 for reference. It can be seen that there is a linear increase in the N content with increasing UDMHy supply during growth. In contrast to the Bi incorporation, which is independent of N, it is found that for a given UDMHy/TBAs ratio the N content is higher in the sample with lower Bi content. In order to investigate this further, additional samples (#9–10 in Table 1) were grown with a constant UDMHy/TBAs ratio of 0.75 and the TMBi/TBAs ratio was instead varied. Fig. 3(b) shows the resulting N content in these samples and it can be seen that there is an approximately linear decrease in the N content with increasing TMBi supply. The growth rate of these Ga(NAsBi) layers, also plotted in Fig. 3(b), decreases with increasing TMBi supply as has previously been observed in the growth of Ga(AsBi) QWs [8]. This suggests that there is increased Bi surface coverage that may be reducing the rate of diffusion of atoms to the growth surface or reducing decomposition of the precursors, and this could be inhibiting the N incorporation. There may also be more chance for N desorption from the surface at lower growth rates, as is observed in the growth of (GaIn)(NAs) where the N content approximately doubles as growth rate is doubled [14]. In addition there is increased competition between Bi and N atoms for group V lattice sites, which could lead to reduced N incorporation.

Table 1
Summary of properties for all samples discussed in this work.

Sample #	QW/single layer	T_{growth} (°C)	UDMHy/TBAs	TMBi/TBAs	Bi (%)	N (%)
1	3QW	400	0.00	0.030	3.5	0.0
2	3QW	400	0.50	0.030	3.5	1.3
3	3QW	400	0.75	0.030	3.5	1.8
4	3QW	400	1.00	0.030	3.5	2.7
5	3QW	400	0.00	0.015	2.6	0.0
6	3QW	400	0.50	0.015	2.6	2.0
7	3QW	400	0.75	0.015	2.6	2.7
8	3QW	400	1.00	0.015	2.6	3.7
9	3QW	400	0.75	0.008	1.4	3.5
10	3QW	400	0.75	0.000	0.0	4.1
11	Single layer	450	0.00	0.008	1.8	0.0
12	Single layer	450	0.30	0.008	1.8	0.6
13	Single layer	450	0.61	0.008	1.8	1.2
14	Single layer	450	1.00	0.008	1.8	1.8
SIMS	4× 30 nm Ga(NAsBi) layers grown under the same conditions as *A*: 2, *B*: 9, *C*: 4, and *D*: 7					

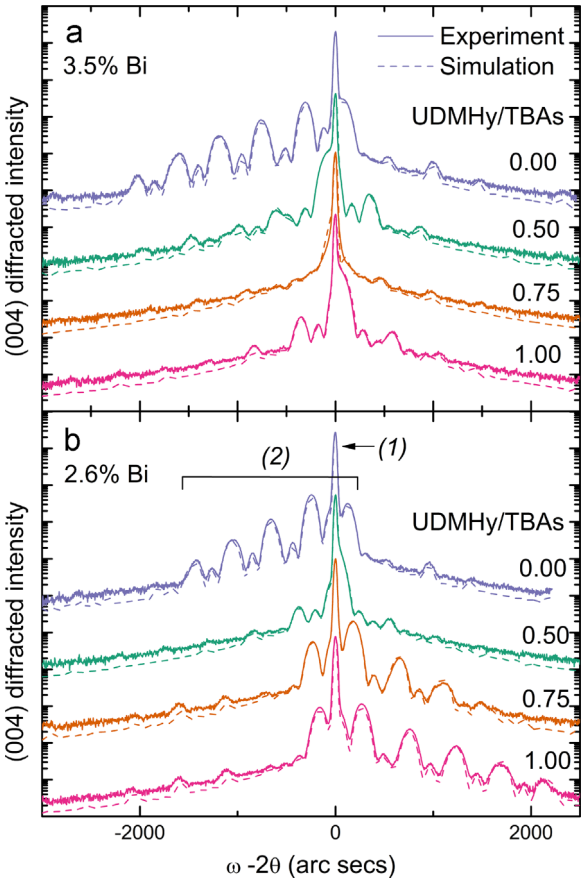

Fig. 2. HR-XRD (004) patterns of Ga(NAsBi)/GaAs MQWs grown at 400 °C with different UDMHy/TBAs ratios for (a) TMBi/TBAs=0.03, 3.5% Bi and (b) TMBi/TBAs=0.015, 2.6% Bi. The features (1) and (2) are the GaAs substrate peak and broad Ga(NAsBi) QW peak, respectively.

A second sample was investigated with SIMS analysis, which contained four ~30 nm Ga(NAsBi) layers, grown under the same conditions as (*A*): #2, (*B*): #9, (*C*): #4, and (*D*): #7 as listed in Table 1 and labelled in Fig. 3, separated by 100 nm GaAs barriers. The SIMS depth profile is shown in Fig. 4(a) and in Fig. 4(b) the average SIMS signal from the Bi (N) in each layer is plotted against the expected Bi (N) content as determined from HR-XRD of the MQW sample grown under the same conditions. There is a clear linear relationship between the Bi (N) signal and Bi (N) content, which provides additional evidence that composition as

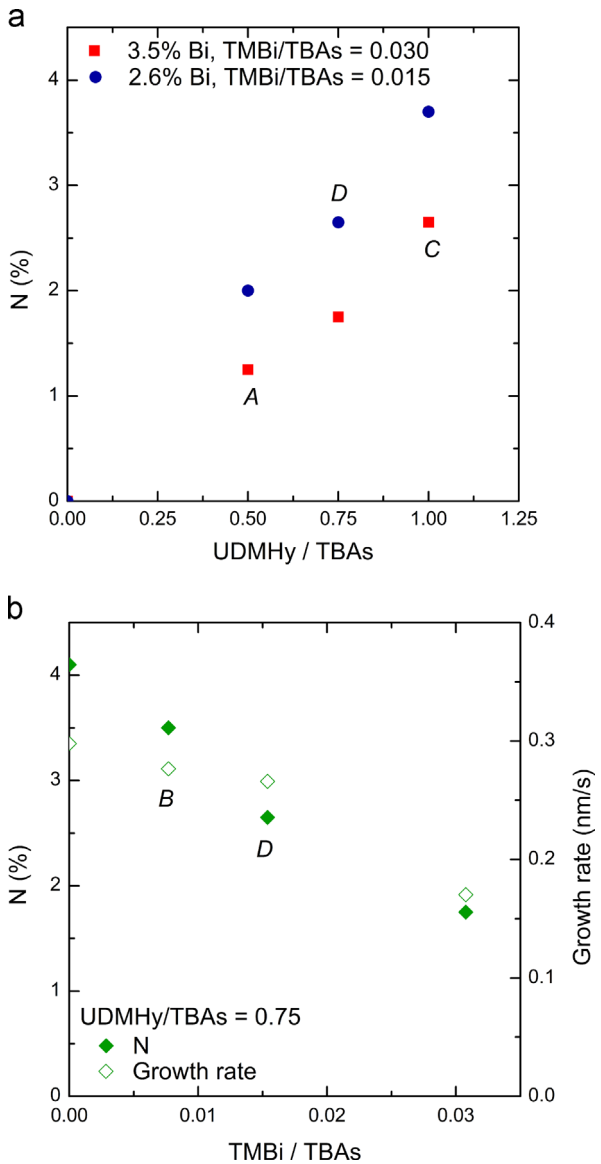

Fig. 3. (a) Dependence of N content of Ga(NAsBi)/GaAs MQWs grown at 400 °C on UDMHy/TBAs ratio. Red squares: TMBi/TBAs=0.030, 3.5% Bi, blue circles: TMBi/TBAs=0.015, 2.6% Bi. (b) Dependence of N content (filled markers) and growth rate (open markers) on TMBi/TBAs ratio for constant UDMHy/TBAs=0.75. (For interpretation of the references to colour in this figure legend, the reader is referred to the web version of this article.)

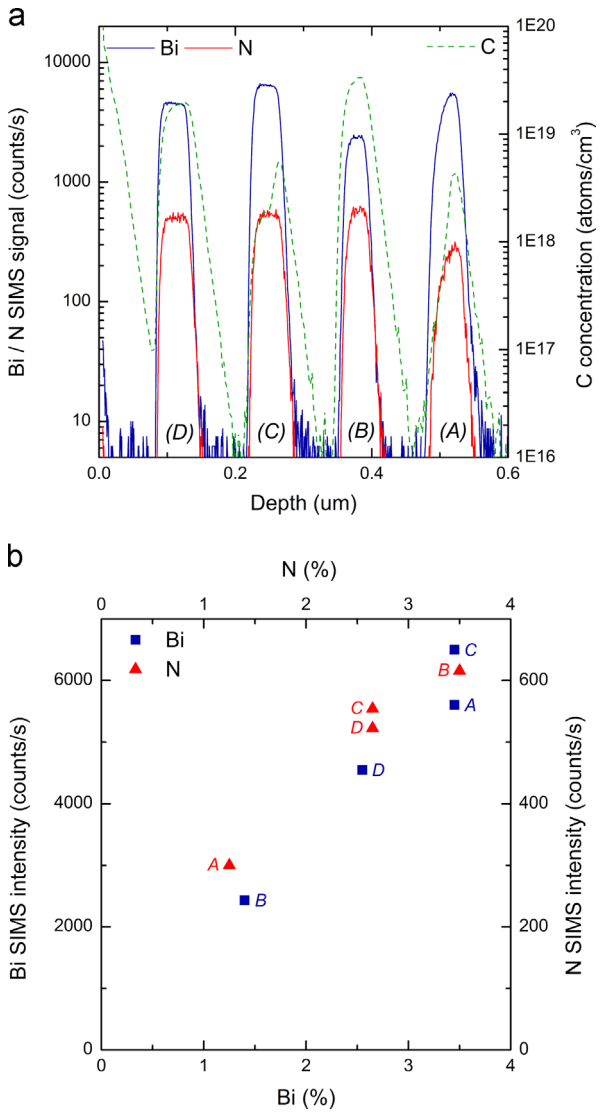

Fig. 4. (a) SIMS profile of Ga(NAsBi) layers with (A) 3.5% Bi, 1.2% N, (B)1.4% Bi, 3.6% N, (C)3.5% Bi, 2.7% N and (D) 2.6% Bi, 2.7% N. (b) Average intensity of Bi (N) SIMS signal plotted against Bi (N) content as determined from XRD.

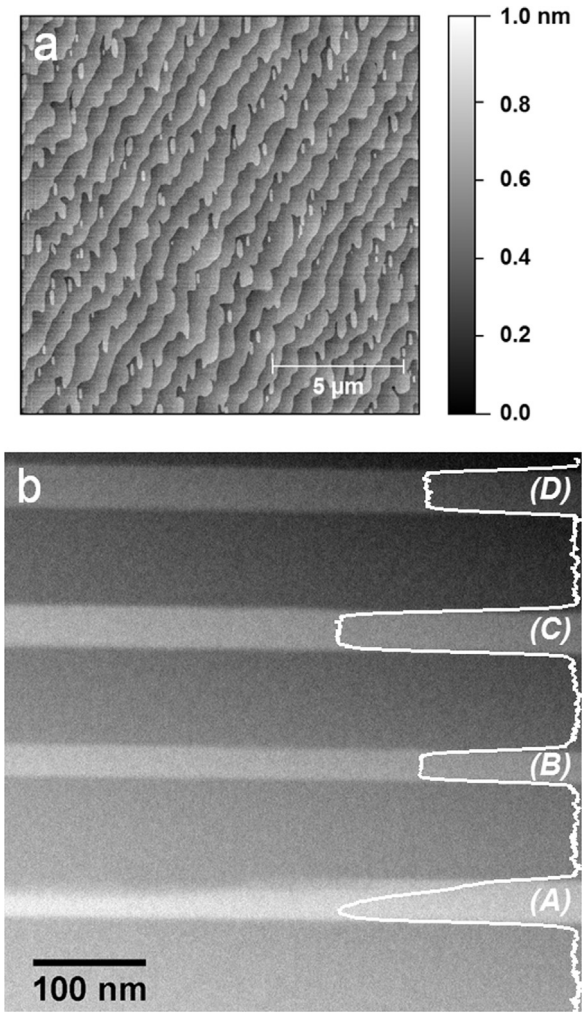

Fig. 5. (a) 15 × 15 μm AFM image showing the surface morphology of the GaAs cap layer on sample #4. (b) STEM HAADF image of Ga(NAsBi)/GaAs SIMS sample.

determined by HR-XRD is correct and the Bi content does indeed remain the same as in an equivalent N-free sample. In particular, layers (*C*) and (*D*) have different Bi contents but are expected to have the same N content and from the SIMS analysis it can be seen that the N content is approximately equal in the two layers.

Atomic force microscopy was used to study the surface morphology of the GaAs cap layer on all of the MQW samples. It was found that all samples had very low surface roughness, comparable to Ga(AsBi)/GaAs samples reported in Ref. [7], and no Bi droplets were present. An example AFM image of sample #4 is shown in Fig. 5(a) for a $15 \times 15\ \mu m^2$ area. To investigate the internal structure, STEM HAADF images were made of the SIMS sample from Fig. 4 and an overview is shown in Fig. 5(b). The Ga(NAsBi) layers appear brighter than the GaAs barriers due to the presence of Bi atoms with higher atomic number. Since the contrast is highly sensitive to the atomic number, uniform brightness within a layer indicates good chemical homogeneity in the material. The layers (*B*), (*C*) and (*D*) all have very good homogeneity in composition and thickness with relatively sharp interfaces, demonstrating that it is possible to grow Ga(NAsBi) with good crystalline quality by MOVPE. Layer (*A*), however, has significant variations in thickness at different positions, which is also reflected in the SIMS results where there is a gradient in Bi and N contents at the upper interface. Since this is one of the layers with higher TMBi supply, it is thought this may be due to the Bi surface coverage increasing during the growth time and possibly becoming too great, causing the formation of Bi droplets on the surface. Layer (*C*), which has the same TMBi supply, does not suffer from such problems showing that it is possible to successfully produce material with higher Bi content so further investigation will be required to achieve this over a wider range of compositions.

Attempts were made to measure room temperature PL from the Ga(NAsBi)/GaAs MQW samples (#1–10) but no signal could be detected with the apparatus. It is thought that the incorporation of N into the crystal has introduced non-radiative defects such as N interstitials and Ga vacancies that significantly reduce the PL intensity, as also occurs in other N containing materials such as Ga(NAs) and (GaIn)(NAs) [15–18]. Another factor which acts to decrease PL intensity is unintentional incorporation of carbon from the metal–organic precursors. It has previously been found in MOVPE growth of Ga(NAs) and (GaIn)(NAs) that the C content increases strongly with decreasing growth temperature and is significantly higher than that in GaAs due to the strength of the C–N bond [19]. The directly comparable Ga(AsBi) and Ga(NAsBi) layers grown under identical conditions apart from the addition of N, for which the SIMS profile is plotted in Fig. 1, provide some evidence of increased C incorporation with approximately twice as

much C in the N containing layer. Note that the high C concentration in the left-most GaAs barrier in the figure occurs because this was grown at 400 °C instead of the usual 625 °C to check C incorporation in GaAs at this temperature. The SIMS analysis of the other Ga(NAsBi) layers, shown in Fig. 4(a), found them to have C concentrations of 5×10^{18}–4×10^{19} atoms/cm^3, whereas previous SIMS analysis of Ga(AsBi) layers with a similar range of Bi contents showed them to have typically 5×10^{16}–2×10^{19} atoms/cm^3 depending on TMBi supply [7]. Although there is slightly greater C incorporation in the Ga(NAsBi) material, it is still of the same order of magnitude as for Ga(AsBi) samples from which good RT PL can be detected, so it is unlikely to have a significant effect on the PL intensity from the Ga(NAsBi) samples. It is therefore thought that other non-radiative defects introduced by the presence of N are the dominant reason for the absence of RT PL.

3.2. Ga(NAsBi) single layer growth at 450 °C

Other N containing materials, such as Ga(NAs) and (GaIn)(NAs), are typically grown at higher temperatures of 500–600 °C [20–22] so it was thought that by increasing the growth temperature of Ga(NAsBi) it may be possible to improve the material quality through decreasing non-radiative defects and also carbon incorporation. The higher temperature presents a problem for Bi incorporation, however, which requires a low growth temperature. Previous investigations of the MOVPE growth of Ga(AsBi) have focused on growth at 400 °C and 375 °C [8], so it was first necessary to perform initial investigations on the growth of Ga(AsBi) at 450 °C. After some optimisation of precursor partial pressures, the growth of a sample with 1.8% Bi and a droplet free surface was achieved so this was used as the starting point for the growth of Ga(NAsBi) samples. All 450 °C samples (#11–14 in Table 1) are single layers with thickness in the range 40–70 nm, capped with 20 nm GaAs. The results of N content determined from simulation of the XRD data are shown in Fig. 6. A linear increase in N content with UDMHy supply is again observed, as it was at 400 °C.

Room temperature PL measurements were performed and the spectra are shown in Fig. 7. There is a clear redshift in the PL peak from 1.27 eV for the Ga(AsBi) sample to 1.19 eV for the Ga(NAsBi) sample with the lowest N content of 0.6%. The peak intensity also decreases significantly with the addition of N, which could be explained by the presence of N-related defects and increased C incorporation. It is interesting to note that the PL intensity from

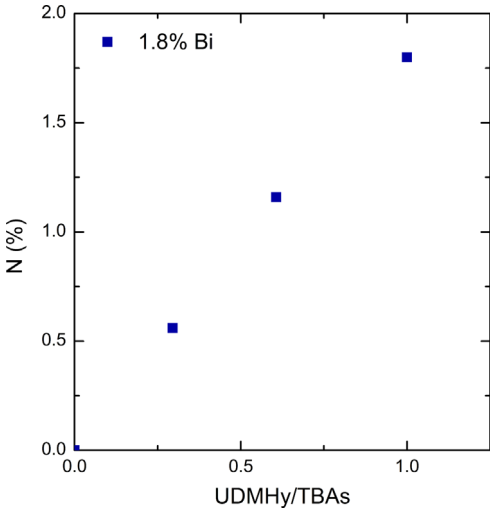

Fig. 6. Dependence of N content of Ga(NAsBi) single layers with 1.8% Bi grown at 450 °C on UDMHy/TBAs ratio.

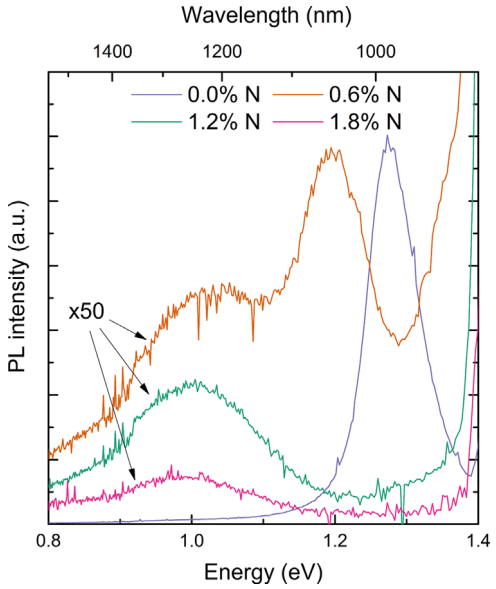

Fig. 7. Room temperature photoluminescence spectra of Ga(NAsBi) single layers with 1.8% Bi grown at 450 °C. PL intensity ×50 for N-containing samples.

the N-free sample is an order of magnitude greater than for previous Ga(AsBi) samples with similar Bi content grown at 400 °C [7]. This suggests that there is an improvement in material quality and probable reduction in C incorporation at the higher growth temperature. All spectra have a broad peak at ~1 eV, which is thought to be related to a defect and is also observed in pure GaAs grown at 400 °C by MOVPE [7]. According to theoretical calculations, the samples with 1.2% and 1.8% N are expected to have band gaps that lie within the broad feature around 1 eV and as such it is not possible to distinguish a separate peak due the Ga(NAsBi).

In order to determine the band gap in all samples even where there is no clear PL peak, RT photoreflectance spectroscopy (PR) was also performed. PR spectra were analysed by a third derivative functional form (TDFF) to determine the energy transition values [23] as shown in Fig. 8(a). The band gap as determined by PR of the four samples as a function of N content is plotted in Fig. 8(b). There is a reduction in band gap of 141 ± 22 meV/% N over the range studied, which is in good agreement with the redshift in PL peak energy of 130 meV/% N measured previously for MBE-grown samples with up to 4.5% Bi and 2% N [4] and smaller than the 180 meV decrease in band gap for 1% N in GaAs [24]. In other dilute nitride materials, as well as MBE grown Ga(NAsBi), previous investigations have shown that annealing can significantly improve PL intensity [17,25,26]. It is therefore planned to carry out annealing studies on this material in future, with the expectation that this may improve the optical properties of the material.

4. Summary

We have discussed the growth by MOVPE of Ga(NAsBi)/GaAs MQWs and Ga(NAsBi) single layers on GaAs (001) substrates using growth temperatures of 400 °C and 450 °C. Beginning from Ga(AsBi) samples with known Bi content, it was found that N incorporation can easily be controlled by varying UDMHy supply during growth with a linear relationship between UDMHy supply and N content over the range investigated, whilst Bi content remains constant. Samples have been shown to have good chemical homogeneity and relatively sharp Ga(NAsBi)/GaAs interfaces can be achieved. By increasing the growth temperature to 450 °C it

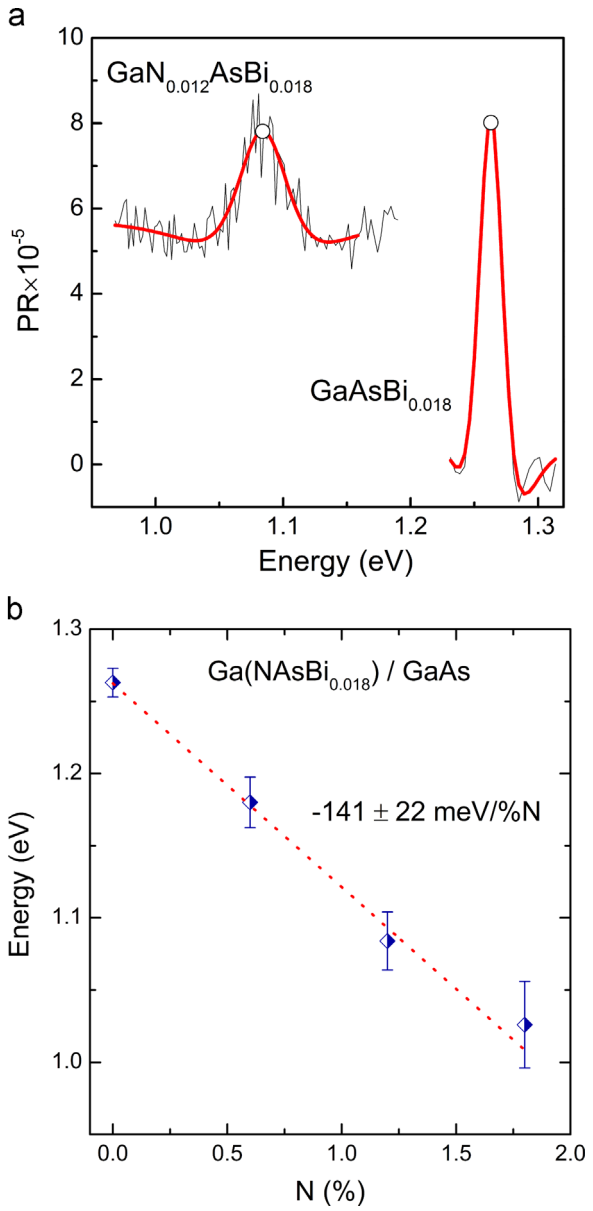

Fig. 8. (a) PR spectra (black lines) and corresponding fits (red lines) for a sample without and with 1.2% N (both containing 1.8% Bi). The open circles denote the position of the band gap energy as determined by the fitting. (b) Dependence of band gap on N content for Ga(NAsBi) single layers with 1.8% Bi as measured by PR. (For interpretation of the references to colour in this figure legend, the reader is referred to the web version of this article.)

was possible to detect RT photoluminescence from a Ga(NAsBi) sample with 0.6% N. Photoreflectance spectroscopy showed a decrease in the band gap of 141 ± 22 meV/% N for Ga(NAsBi) single layer samples with 1.8% Bi and up to 1.8% N. These preliminary results illustrate the potential of Ga(NAsBi) alloys for infrared band gap materials that can be lattice-matched to GaAs with applications in photonic devices.

Acknowledgements

This work was funded by the European Union Framework 7 Project BIANCHO (FP7-257974), the German Science Foundation (DFG: VO805/4 and DFG: GRK1782) and EPSRC-UK Projects EP/H005587/1 and EP/G064725/1. Z.L. Bushell acknowledges financial support from an ERASMUS grant through the European Commission Lifelong Learning Programme. Z. Batool is grateful to the Kwan Trust and the Islamia University of Bahawalpur, Pakistan for supporting her Ph.D. studentship.

References

[1] S.J. Sweeney, S.R. Jin, Bismide–nitride alloys: promising for efficient light emitting devices in the near- and mid-infrared, J. Appl. Phys. 113 (2013) 043110.
[2] B. Fluegel, S. Francoeur, A. Mascarenhas, S. Tixier, E. Young, T. Tiedje, Giant spin–orbit bowing in $GaAs_{1-x}Bi_x$, Phys. Rev. Lett. 97 (2006) 067205.
[3] M. Usman, C.A. Broderick, A. Lindsay, E.P. O'Reilly, Tight-binding analysis of the electronic structure of dilute bismide alloys of GaP and GaAs, Phys. Rev. B 84 (2011) 245202.
[4] M. Yoshimoto, W. Huang, G. Feng, K. Oe, New semiconductor alloy GaNAsBi with temperature-insensitive bandgap, Phys. Status Solidi 243 (2006) 1421–1425.
[5] X. Lu, D.A. Beaton, R.B. Lewis, T. Tiedje, Y. Zhang, Composition dependence of photoluminescence of $GaAs_{1-x}Bi_x$ alloys, Appl. Phys. Lett. 95 (2009) 041903.
[6] A.J. Ptak, R. France, D.A. Beaton, K. Alberi, J. Simon, A. Mascarenhas, et al., Kinetically limited growth of GaAsBi by molecular-beam epitaxy, J. Cryst. Growth 338 (2012) 107–110.
[7] P. Ludewig, Z.L. Bushell, L. Nattermann, N. Knaub, W. Stolz, K. Volz, Growth of Ga(AsBi) on GaAs by continuous flow MOVPE, J. Cryst. Growth. http://dx.doi.org/10.1016/j.jcrysgro.2014.03.041, accepted for publication.
[8] P. Ludewig, N. Knaub, W. Stolz, K. Volz, MOVPE growth of Ga(AsBi)/GaAs multiquantum well structures, J. Cryst. Growth 370 (2012) 186–190.
[9] K. Oe, Metalorganic vapor phase epitaxial growth of metastable $GaAs_{1-x}Bi_x$ alloy, J. Cryst. Growth 237–239 (2002) 1481–1485.
[10] S. Tixier, S.E. Webster, E.C. Young, T. Tiedje, S. Francoeur, A. Mascarenhas, et al., Band gaps of the dilute quaternary alloys $GaN_xAs_{1-x-y}Bi_y$ and $Ga_{1-y}In_yN_xAs_{1-x}$, Appl. Phys. Lett. 86 (2005) 112113.
[11] M. Yoshimoto, W. Huang, Y. Takehara, J. Saraie, A. Chayahara, Y. Horino, et al., New semiconductor GaNAsBi alloy grown by molecular beam epitaxy, Jpn. J. Appl. Phys. 43 (2004) L845–L847.
[12] F.H. Pollak, in: T.S. Moss (Ed.), Handbook on Semiconductors, 2nd ed., Elsevier, Amsterdam, 1994, p. 527.
[13] P.F. Fewster, Analysis of nearly perfect semiconductor multi-layer structures, X-Ray Scattering from Semiconductors, 2nd ed., Imperial College Press, London (2003) 200–247.
[14] K. Volz, J. Koch, F. Hohnsdorf, B. Kunert, W. Stolz, MOVPE growth of dilute nitride III/V semiconductors using all liquid metalorganic precursors, J. Cryst. Growth 311 (2009) 2418–2426.
[15] W. Li, M. Pessa, T. Ahlgren, J. Decker, Origin of improved luminescence efficiency after annealing of Ga(In)NAs materials grown by molecular-beam epitaxy, Appl. Phys. Lett. 79 (2001) 1094.
[16] N.Q. Thinh, I.A. Buyanova, W.M. Chen, H.P. Xin, C.W. Tu, Formation of nonradiative defects in molecular beam epitaxial GaN_xAs_{1-x} studied by optically detected magnetic resonance, Appl. Phys. Lett. 79 (2001) 3089.
[17] S.G. Spruytte, C.W. Coldren, J.S. Harris, W. Wampler, P. Krispin, K. Ploog, et al., Incorporation of nitrogen in nitride–arsenides: origin of improved luminescence efficiency after anneal, J. Appl. Phys. 89 (2001) 4401.
[18] J. Toivonen, T. Hakkarainen, M. Sopanen, H. Lipsanen, J. Oila, K. Saarinen, Observation of defect complexes containing Ga vacancies in GaAsN, Appl. Phys. Lett. 82 (2003) 40.
[19] K. Volz, T. Torunski, B. Kunert, O. Rubel, S. Nau, S. Reinhard, et al., Specific structural and compositional properties of (GaIn)(NAs) and their influence on optoelectronic device performance, J. Cryst. Growth 272 (2004) 739–747.
[20] F. Hohnsdorf, J. Koch, C. Agert, W. Stolz, Investigations of (GaIn)(NAs) bulk layers and (GaIn)(NAs)/GaAs multiple quantum well structures grown using tertiarybutylarsine (TBAs) and 1,1-dimethylhydrazine (UDMHy), J. Cryst. Growth 195 (1998) 391–396.
[21] T. Miyamoto, T. Kageyama, S. Makino, D. Schlenker, F. Koyama, K. Iga, CBE and MOCVD growth of GaInNAs, J. Cryst. Growth 209 (2000) 339–344.
[22] A. Moto, S. Tanaka, N. Ikoma, T. Tanabe, S. Takagishi, Metalorganic vapor phase epitaxial growth of GaNAs using tertiarybutylarsine (TBA) and dimethylhydrazine (DMHy), Jpn. J. Appl. Phys. 38 (1999) 1015–1018.
[23] D.E. Aspnes, Third-derivative modulation spectroscopy with low-field electroreflectance, Surf. Sci. 37 (1973) 418–442.
[24] J. Wu, W. Shan, W. Walukiewicz, Band anticrossing in highly mismatched III–V semiconductor alloys, Semicond. Sci. Technol. 17 (2002) 860–869.
[25] K. Volz, D. Lackner, I. Németh, B. Kunert, W. Stolz, C. Baur, et al., Optimization of annealing conditions of (GaIn)(NAs) for solar cell applications, J. Cryst. Growth 310 (2008) 2222–2228.
[26] G. Feng, K. Oe, M. Yoshimoto, Influence of thermal annealing treatment on the luminescence properties of dilute GaNAs–bismide alloy, Jpn. J. Appl. Phys. 46 (2007) L764–L766.

5.5 Luminescence properties of dilute bismide systems[1]

B. Breddermann, A. Bäumner, S. W. Koch, P. Ludewig, W. Stolz, K. Volz, J. Hader, J. V. Moloney, C. A. Broderick, E. P. O'Reilly, Journal of Luminescence **154**, 95 (2014), DOI: 10.1016/j.jlumin.2014.04.012

Abstract

Systematic photoluminescence measurements on a series of $GaBi_xAs_{1-x}$ samples are analyzed theoretically using a fully microscopic approach. Based on sp^3s^* tight-binding calculations, an effective $\mathbf{k}\cdot\mathbf{p}$ model is set up and used to compute the band structure and dipole matrix elements for the experimentally investigated samples. With this input, the photoluminescence spectra of a number of $GaBi_xAs_{1-x}$ samples are calculated using a detailed microscopic approach based on the semiconductor luminescence equations. Very good agreement between theory and experiment is obtained, in particular with respect to the variation of the energy of the luminescence peaks with Bi composition.

The Authors contribution

My contribution to this work was the MOVPE growth of the discussed samples and their characterization concerning the composition and layer thickness. Furthermore, I carried out the PL measurements that were used to validate the calculations of the PL spectra performed by Benjamin Breddermann. Benjamin Breddermann as well wrote the manuscript to which I contributed the experimental description. The further co-authors helped to interpret the data and to improve the manuscript.

1 Reprinted from *Journal of Luminescence **154** (2014) 95-98*, Copyright 2014, with permission from Elsevier.

Journal of Luminescence 154 (2014) 95–98

Contents lists available at ScienceDirect

Journal of Luminescence

journal homepage: www.elsevier.com/locate/jlumin

Luminescence properties of dilute bismide systems

B. Breddermann [a,*], A. Bäumner [a], S.W. Koch [a], P. Ludewig [a], W. Stolz [a], K. Volz [a], J. Hader [b], J.V. Moloney [b], C.A. Broderick [c,d], E.P. O'Reilly [c,d]

[a] Faculty of Physics, Philipps-Universität Marburg, 35032 Marburg, Germany
[b] Nonlinear Control Strategies Inc, 3542 N. Geronimo Ave., Tucson, AZ 85705, USA
[c] Tyndall National Institute, Lee Maltings, Dyke Parade, Cork, Ireland
[d] Department of Physics, University College Cork, Cork, Ireland

ARTICLE INFO

Article history:
Received 7 February 2014
Received in revised form
7 April 2014
Accepted 9 April 2014
Available online 18 April 2014

Keywords:
Dilute bismides
Optical properties
Photoluminescence
Band structure

ABSTRACT

Systematic photoluminescence measurements on a series of $GaBi_xAs_{1-x}$ samples are analyzed theoretically using a fully microscopic approach. Based on sp^3s^* tight-binding calculations, an effective $\mathbf{k}\cdot\mathbf{p}$ model is set up and used to compute the band structure and dipole matrix elements for the experimentally investigated samples. With this input, the photoluminescence spectra are calculated using a systematic microscopic approach based on the semiconductor luminescence equations. The detailed theory-experiment comparison allows us to quantitatively characterize the experimental structures and to extract important sample parameters.

1. Introduction

Besides interest in the fundamental material properties of the $GaBi_xAs_{1-x}$ alloy, the investigation of this and related materials containing bismuth (Bi) is also driven by the promise of these so-called dilute bismide alloys for possible applications in active and passive semiconductor optical devices [1]. Not only should the strong modifications of the material band structure induced by Bi incorporation [2–4] allow for long-wavelength operation of GaAs-based optical devices [5], but it is also expected that the $GaBi_xAs_{1-x}$ band structure can be engineered in such a way that non-radiative Auger recombination (occurring in the valence band) can be suppressed [6,7]. Since the control and limitation of Auger losses is crucial to reduce the threshold current and increase the temperature stability of III–V lasers [8,9], the composition range in $GaBi_xAs_{1-x}$ for which Auger losses are suppressed offers opportunities for designing efficient and thermally stable optoelectronic devices [5,7,9].

In this paper, we present a systematic experimental and theoretical analysis of the luminescence properties of a series of $GaBi_xAs_{1-x}$ samples. The theoretical analysis of the band structure in these samples is based upon the sp^3s^* tight-binding (TB) supercell and $\mathbf{k}\cdot\mathbf{p}$ approaches of Refs. [5,3]. This approach is used to parametrize an effective $\mathbf{k}\cdot\mathbf{p}$ band structure model which provides the basis for the microscopic calculations of the optical response of each of the $GaBi_xAs_{1-x}$ samples studied.

2. Experimental

The $GaBi_xAs_{1-x}$/GaAs heterostructures were grown by metal organic vapor phase epitaxy (MOVPE) on undoped, exact (001) GaAs substrates. For each sample, the $GaBi_xAs_{1-x}$ layer (which is between 50 and 80 nm thick) was deposited on a 250 nm thick GaAs buffer and capped by 20 nm of GaAs. The sample growth took place in a commercially available Aix 200 GFR system at a reduced reactor pressure of 50 mbar using Pd-purified H_2 as the carrier gas. Triethylgallium (TEGa), tertiarybutylarsine (TBAs) and trimethylbismuth (TMBi) were used as precursors. The growth temperature was set to 400 °C for the $GaBi_xAs_{1-x}$ layer, whereas the GaAs buffer and cap were grown at 625 °C. The TEGa partial pressure for the $GaBi_xAs_{1-x}$ growth was 4.2×10^{-2} mbar at a TBAs/TEGa ratio of 1.9 which led to growth rates between 0.32 and 0.42 nm s^{-1}, depending on the applied TMBi partial pressure. High resolution X-ray diffraction ω-2θ scans around the (004) reflection peak of GaAs were performed to determine the Bi compositions and layer thicknesses in each of the samples. Table 1 contains the structural parameters determined in this manner for the samples under investigation. Further details regarding the growth and characterization of the samples can be found in Refs. [10,11].

* Corresponding author. Tel.: +49 6421 28 22025; fax: +49 6421 28 27076.
E-mail address: benjamin.breddermann@physik.uni-marburg.de (B. Breddermann).

http://dx.doi.org/10.1016/j.jlumin.2014.04.012
0022-2313/

Table 1
Structural details of the $GaBi_xAs_{1-x}$ samples studied, including Bi compositions and layer thicknesses determined using X-ray diffraction measurements.

Sample	Bi content (%)	Thickness (nm)
1	0.9	75
2	1.9	67
3	2.9	60
4	3.2	59
5	4.4	49
6	5.0	55

The room temperature photoluminescence (PL) spectrum for each of the samples of Table 1 was measured using a continuous-wave Ar-ion laser at a wavelength of 514 nm for excitation. In each case the PL signal was dispersed in a 1 m grating monochromator and collected by a liquid nitrogen cooled germanium detector using the standard lock-in technique.

3. Theory

To analyze the experimental data, we employ a systematic microscopic approach. We use a multi-band $\mathbf{k}\cdot\mathbf{p}$ model to calculate the single-particle band structure, which is then used as input to a detailed microscopic calculation of the optical response of the material.

3.1. Band structure

Following the methodology introduced in Refs. [4,12], we use a 14-band $\mathbf{k}\cdot\mathbf{p}$ Hamiltonian to calculate the $GaBi_xAs_{1-x}$ band structure. This model includes the effects of Bi-related resonant states on the band structure explicitly, with these localized states undergoing valence band anti-crossing (VBAC) interactions with the extended states of the GaAs valence band edge. The VBAC parameters for this 14-band model have been determined by fitting to the results of the detailed TB supercell and $\mathbf{k}\cdot\mathbf{p}$ calculations of Ref. [5].

In this way, we obtain the following 14×14 Hamiltonian matrix for $GaBi_xAs_{1-x}$:

$$H=\begin{bmatrix} H_{\mathrm{CB}} & V_{\mathrm{CB}} & 0 & 0 \\ V_{\mathrm{CB}}^{*} & H_{6\times 6} & V_{\mathrm{Bi,SO}} & V_{\mathrm{Bi}} \\ 0 & V_{\mathrm{Bi,SO}}^{*} & H_{\mathrm{Bi,SO}} & 0 \\ 0 & V_{\mathrm{Bi}}^{*} & 0 & H_{\mathrm{Bi}} \end{bmatrix}. \tag{1}$$

Here, $H_{6\times 6}$ is the block of the Hamiltonian containing the contributions and coupling matrix elements related to the valence bands of the GaAs host matrix, including spin-degenerate light (LH), heavy (HH) and split-off (SO) hole states. The 2×6 block V_{CB} couples these valence states to the 2×2 block H_{CB} containing the spin-degenerate lowest conduction band states of the host matrix, expanding the Hamiltonian to the standard 8-band $\mathbf{k}\cdot\mathbf{p}$ model for the Bi-free GaAs host matrix.

In addition to the VBAC effect occurring in the $GaBi_xAs_{1-x}$ valence band, incorporation of Bi to form $GaBi_xAs_{1-x}$ introduces biaxial compressive strain when the material is grown on a GaAs substrate. The incorporation of Bi modifies the GaAs-related 8×8 block of the Hamiltonian by the addition of (i) Bi-related virtual crystal (VC) shifts to the band edge energies and (ii) strain-induced shifts to the energies of the VC band edges.

These VC shifts (full details of which can be found in Ref. [5]) are composed of Bi-related terms which are directly proportional to the Bi concentration x and are added to the diagonal elements of the $H_{8\times 8}$ block of the $GaBi_xAs_{1-x}$ Hamiltonian. The VC shifts to the host matrix band edge energies constitute a minor contribution to the decrease in the $GaBi_xAs_{1-x}$ band gap with increasing x. The majority of the band gap reduction is the result of VBAC effects, with additional minor modifications arising due to the effects of strain. We denote the total VC contribution to the reduction of the band gap by $\Delta E_g\cdot x$ and note that this consists of (i) a valence band contribution $\Delta E_{\mathrm{VB}}\cdot x=\Delta E_g(1-r_{\mathrm{CB}})x$ and (ii) a conduction band contribution $\Delta E_{\mathrm{CB}}\cdot x=r_{\mathrm{CB}}\cdot\Delta E_g\cdot x$, where r_{CB} is the ratio of the VC conduction band offset ΔE_{CB} to ΔE_g. In addition to these VC shifts to the LH, HH and conduction band edge energies there is a VC shift to the host matrix SO band edge energy, which we denote by $\Delta E_{\mathrm{SO}}\cdot x$. The effects of strain on the VC band edge energies determined in this manner are taken into account following Ref. [13].

Finally, the VBAC interactions between localized Bi-related states and the extended valence states of the GaAs host matrix represented by $H_{6\times 6}$ lead to a 14-band $\mathbf{k}\cdot\mathbf{p}$ model for $GaBi_xAs_{1-x}$. In the 14-band model the extended GaAs valence states of $H_{6\times 6}$ undergo VBAC interactions with the LH-/HH- and SO-like Bi-related states at energies E_{Bi} and $E_{\mathrm{Bi,SO}}$, which are contained in the diagonal blocks H_{Bi} and $H_{\mathrm{Bi,SO}}$ of dimensions 4×4 and 2×2 respectively. The VBAC interaction matrix elements between the GaAs LH and HH bands and the LH- and HH-like Bi resonant states of H_{Bi} are contained in the V_{Bi} block of the Hamiltonian, while the interaction matrix elements between the GaAs SO band and the SO-like Bi resonant states of $H_{\mathrm{Bi,SO}}$ are contained in $V_{\mathrm{Bi,SO}}$. The composition dependent VBAC matrix elements vary with Bi composition as $V(x)=\beta\sqrt{x}$.

The Bi-related parameters were determined by using this 14-band model to fit to the results of the TB and 12-band $\mathbf{k}\cdot\mathbf{p}$ calculations of Ref. [5], giving $\Delta E_g=3.83$ eV, $\Delta E_{\mathrm{SO}}=0.55$ eV, $r_{\mathrm{CB}}=0.736$, $E_{\mathrm{Bi}}=-0.183$ eV, $E_{\mathrm{Bi,SO}}=-1.9$ eV, and $\beta=1.13$ eV. We note that the chosen combination of values for $E_{\mathrm{Bi,SO}}$ and the VBAC coupling parameter β ensures that the effects of Bi incorporation on the energy and character of the alloy SO band are minimal. This then brings the 14-band model into close agreement with the detailed analysis of Ref. [5], which demonstrated that (i) SO-like Bi-related resonant states could not be explicitly identified in supercell calculations and (ii) the $GaBi_xAs_{1-x}$ SO band is described well by a conventional VC approach. As a result of this, as well as the energy separation between the alloy valence band maximum and SO band which increases strongly with x, any impact from the SO-like Bi-related resonant states on the calculated PL spectra is negligible.

3.2. Photoluminescence

We calculate the optical response of each of the samples of Table 1 by solving the equations of motion for the dynamics of the photon-assisted polarizations $\Pi_{\mathbf{k},q}\equiv\langle\hat{b}_q^{\dagger}\hat{P}_{\mathbf{k}}\rangle$, the photon-number-like correlations $\mathcal{N}_{q',q}\equiv\langle\hat{b}_q^{\dagger}\hat{b}_{q'}\rangle$, and the carrier distributions $f_{\mathbf{k}}^{e(h)}$ of electrons (holes), with $\hat{b}_q(\hat{b}_q^{\dagger})$ and $\hat{P}_{\mathbf{k}}$ being operators representing photon annihilation (creation) and microscopic polarization, respectively. The coupled equations of motion for these quantities – the semiconductor luminescence can be written in the form [14–16]:

$$\begin{aligned} \mathrm{i}\hbar\frac{\partial}{\partial t}\Pi_{\mathbf{k},q}&=(\tilde{\epsilon}_{\mathbf{k}}-\hbar\omega_q)\Pi_{\mathbf{k},q}+\Omega_{\mathbf{k},q}^{\mathrm{sp}}-(1-f_{\mathbf{k}}^{e}+f_{\mathbf{k}}^{h})\Omega_{\mathbf{k},q}^{\mathrm{st}},\\ \frac{\partial}{\partial t}\mathcal{N}_{q',q}&=\mathrm{i}(\omega_q-\omega_{q'})\Delta\mathcal{N}_{q',q}+\sum_{\mathbf{k}}(\mathcal{F}_q\Pi_{\mathbf{k},q'}^{*}+\mathcal{F}_{q'}^{*}\Pi_{\mathbf{k},q}),\\ \mathrm{i}\hbar\frac{\partial}{\partial t}f_{\mathbf{k}}^{e(h)}&=-2\mathrm{Re}\left\{\sum_q\mathcal{F}_q^{*}\Pi_{\mathbf{k},q}\right\}, \end{aligned} \tag{2}$$

where $\tilde{\epsilon}_{\mathbf{k}}$ are the renormalized single-particle energies obtained from the calculated $GaBi_xAs_{1-x}$ band structure, and $\omega_q=cq$ is the

frequency of photon mode q. $\Omega^{\mathrm{sp}}_{\mathbf{k},q}$ and $\Omega^{\mathrm{st}}_{\mathbf{k},q}$ are, respectively, the spontaneous emission source and renormalized field describing stimulated emission or absorption, while for a given photon mode $\mathcal{F}_q$ comprises the dipole matrix element between electron and hole states, the mode function and the vacuum-field amplitude. Coulomb scattering effects are treated in the second Born–Markov approximation [17,18].

The numerical evaluation of the equations allows us to extract the intrinsically homogeneously broadened luminescence spectra. To account for the disorder effects in the samples [10], the microscopically computed PL spectra can be inhomogeneously broadened by convolving them with a Gaussian distribution [19].

4. Results and discussion

Fig. 1 depicts (a) the measured and (b) the calculated PL spectra for the six samples with systematic variation of the Bi composition x, as characterized in Table 1. The cases of lower [higher] Bi contents are depicted in subframe (i) [(ii)], for both experiment and theory, respectively. In order to compare both measured and calculated PL on the same scale among all of the samples with different Bi content, a single overall scaling factor – one for experiment and one for theory – was extracted by normalizing all spectra with respect to the respective peak value of the sample with highest overall intensity, i.e., sample 5. The fully computed results including the inhomogeneous broadening are shown as solid lines in Fig. 1(b-i/ii), while the intrinsically homogeneously broadened results corresponding to the full ones are added as dotted lines. We obtain the best overall theory-experiment agreement by choosing the width of the inhomogeneous distribution as 50 meV.

As a general trend, we observe a strong redshift of the PL peak with increasing x. Furthermore, we note that the measured PL intensity shows a strong bleaching with decreasing x, at least in the range of dilute Bi contents up to $x = 4.4\%$. The most likely explanation for this observed reduction in PL efficiency is the sample-dependent carrier excitation efficiencies [20]. For decreasing x the purity of the samples decreases, which is related to the presence of a higher density of defects in samples with low x. Localized growth-condition related defect states can trap carriers or induce dephasing processes, thereby reducing the effective carrier density in the material. Since the defect density is higher for the samples with lower Bi compositions, this results in strongly reduced effective carrier densities at low x. The comparison to experimental results from the literature, see e.g. Ref. [20], reveals that our Bi-dependent PL-bleaching effect is significantly stronger for most of the samples studied here. We tentatively attribute these features to the differences in sample quality. However, as already mentioned, the uniform intensity trend is only observed up to $x = 4.4\%$ (sample 5). For higher Bi content, the intensity trend is reversed to a bleaching for *increasing* (instead of decreasing) Bi content, as it is corroborated by the intensity reduction from $x = 4.4\%$ (sample 5) to $x = 5\%$ (sample 6). This trend reversal between 4 and 5% is in full agreement to the experimental findings of Ref. [20].

To account for the sample-dependent, experimentally available effective carrier densities in the theoretical analysis, we have to adjust the optically active electron–hole plasma densities. Therefore, the computed spectra in Fig. 1(b-i/ii) were determined under adaption of the carrier density yielding $1.5 \times 10^{11}\ \mathrm{cm}^{-2}$ for samples 1 and 2, i.e, the lowest Bi contents, and $5 \times 10^{11}\mathrm{cm}^{-2}$, $8.0 \times 10^{11}\ \mathrm{cm}^{-2}$, and $3.5 \times 10^{12}\ \mathrm{cm}^{-2}$ for samples 3, 4, and 5 with increasing x. Finally, for sample 6 at $x = 5\%$, the experimentally observed intensity trend reversal is reflected by the underlying

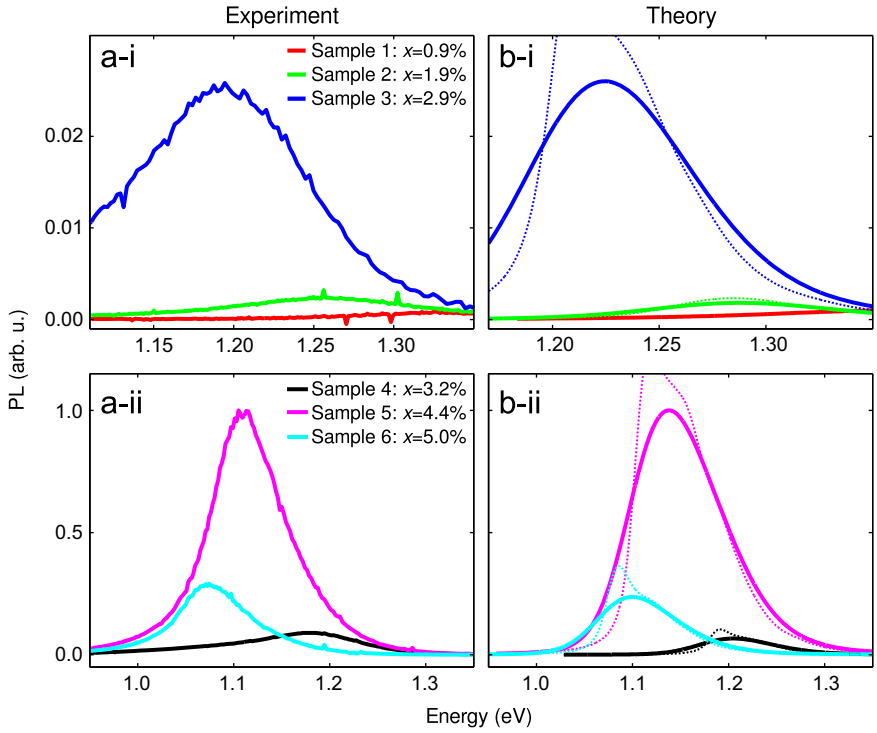

Fig. 1. Comparison of (a) measured and (b) calculated photoluminescence (PL) spectra for the $GaBi_xAs_{1-x}$ samples of Table 1 (lower Bi contents in subframe (i), higher ones in (ii), for both experiment and theory, respectively). Red, green, blue, black, magenta, and cyan lines denote the PL spectra for samples 1, 2, 3, 4, 5, and 6, respectively. The solid (dotted) lines in (b) denote the case with (without) inhomogeneous broadening, as described in the text. In order to compare the measured and calculated PL on the same scale, all of the spectra were normalized with respect to the respective peak PL of the case with the highest peak intensity, i.e, sample 5, as clarified in the text. (For interpretation of the references to color in this figure caption, the reader is referred to the web version of this article.)

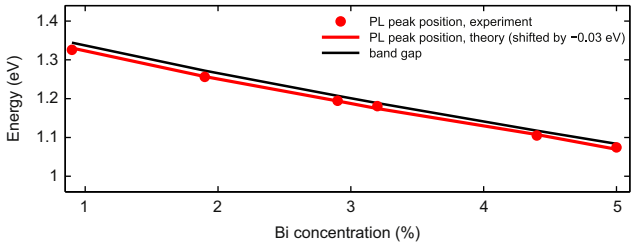

Fig. 2. Variation of the peak photoluminescence energy with increasing Bi composition, determined from experiment (closed red circles) and theory (red solid line) for all of the six samples of samples of Table 1, compared to the material band gap calculated using the 14-band $\mathbf{k}\cdot\mathbf{p}$ model (black solid line). (For interpretation of the references to color in this figure caption, the reader is referred to the web version of this article.)

excitation density condition yielding 1.5×10^{12} cm^{-2}. This adaption to the experimental conditions enters non-trivially into the fully microscopic calculation of the optical spectra. It is therefore not a simple fitting approach but an experimentally motivated determination of the carrier density, which cannot be computed microscopically.

Fig. 2 compares the measured and computed shift of the peak PL energy as a function of Bi-concentration x. In order to obtain the excellent agreement seen in the figure, we had to shift all spectra by the same constant value of 30 meV. This overall offset can be readily accounted for by small modifications of the exact material parameters. We could have adjusted the material-parameter input into the microscopic theory accordingly, however, we preferred to use the nominal experimental values to document the degree of uncertainty. Most importantly, however, and without any adjustments, we obtain the shown excellent theory-experiment agreement in the overall trend – i.e. the rate at which the peak PL energy redshifts with increasing x.

The black solid line in Fig. 2 depicts the corresponding variation of the material band gap with increasing x, calculated using the $\mathbf{k}\cdot\mathbf{p}$ model of Eq. (1). We find that the material band gap decreases by approximately 60–70 meV per % Bi across the investigated composition range, in agreement with previous work [12,5].

5. Conclusions

Overall, our systematic analysis allows for a detailed comparison between the measured and calculated composition dependence of the PL spectra in $GaBi_xAs_{1-x}$. We consistently use a fully microscopic approach not only for the band structure but also for the calculation of the optical spectra. This, and the quantitative theory-experiment comparison clearly goes beyond the scope of earlier publications like Ref. [5]. The calculated composition dependence of the peak PL energy is in excellent agreement with experiment. This level of agreement between the experimental and theoretical results is remarkable since disorder effects undoubtedly play an increasingly important role as the Bi composition decreases [10]. The interesting – and at first sight counterintuitive – observation that increasing the Bi composition improves the purity and thus the quality of the samples [10,20] is corroborated by microscopic calculations of the optical response.

Based on these results one can expect that the growth of better quality samples could open up opportunities for subsequent studies yielding an even greater degree of agreement between the experimental and theoretical results. Moreover, the analysis of the optical gain properties of $GaBi_xAs_{1-x}$ based on similar samples should pave the way towards new laser device applications.

Acknowledgments

The Marburg collaboration was supported by the Research Training Group (RTG) 1782 “Functionalization of semiconductors”, funded by the Deutsche Forschungsgemeinschaft (DFG). P.L., K.V. and E.P.O.R. acknowledge support from the European Union Seventh Framework Programme (BIANCHO; FP7-257974), and C.A.B. acknowledges support from the Irish Research Council under the Embark Initiative (RS/2010/2766).

References

[1] Y. Tominaga, K. Oe, M. Yoshimoto, Photo-pumped $GaAs_{1-x}Bi_x$ lasing operation with low-temperature-dependent oscillation wavelength, in: International Society for Optics and Photonics, SPIE OPTO, Bellingham, Washington, p. 827702.
[2] C.A. Broderick, M. Usman, S.J. Sweeney, E.P. O'Reilly, Semicond. Sci. Technol. 27 (2012) 094011.
[3] M. Usman, C.A. Broderick, A. Lindsay, E.P. O'Reilly, Phys. Rev. B 84 (2011) 245202.
[4] K. Alberi, J. Wu, W. Walukiewicz, K.M. Yu, O.D. Dubon, S.P. Watkins, C.X. Wang, X. Liu, Y.-J. Cho, J. Furdyna, Phys. Rev. B 75 (2007) 045203.
[5] C.A. Broderick, M. Usman, E.P. O'Reilly, Semicond. Sci. Technol. 28 (2013) 125025.
[6] Z. Batool, K. Hild, T.J.C. Hosea, X. Lu, T. Tiedje, S.J. Sweeney, J. Appl. Phys. 111 (2012).
[7] M. Usman, C.A. Broderick, Z. Batool, K. Hild, T.J.C. Hosea, S.J. Sweeney, E.P. O'Reilly, Phys. Rev. B 87 (2013) 115104.
[8] A.F. Phillips, S.J. Sweeney, A.R. Adams, P.J.A. Thijs, IEEE J. Sel. Top. Quantum Electron. 5 (1999) 401.
[9] S.J. Sweeney, Z. Batool, K. Hild, S.R. Jin, T.J.C. Hosea, The potential role of bismide alloys in future photonic devices, in: 13th International Conference on Transparent Optical Networks (ICTON), IEEE, 2011, pp. 1–4.
[10] P. Ludewig, Z.L. Bushell, L. Nattermann, N. Knaub, W. Stolz, K. Volz, Growth of Ga(AsBi) on GaAs by continuous flow MOVPE, J. Cryst. Growth 396 (2014) 95–99.
[11] P. Ludewig, N. Knaub, W. Stolz, K. Volz, J. Cryst. Growth 370 (2013) 186 (16th International Conference on Metalorganic Vapor Phase Epitaxy).
[12] S. Imhof, C. Bückers, A. Thränhardt, J. Hader, J.V. Moloney, S.W. Koch, Semicond. Sci. Technol. 23 (2008) 125009.
[13] M.P.C.M. Krijn, Semicond. Sci. Technol. 6 (1991) 27.
[14] M. Kira, F. Jahnke, S.W. Koch, J.D. Berger, D.V. Wick, T.R. Nelson, G. Khitrova, H. M. Gibbs, Phys. Rev. Lett. 79 (1997) 5170.
[15] M. Kira, S.W. Koch, Prog. Quantum Electron. 30 (2006) 155.
[16] M. Kira, S.W. Koch, Semiconductor Quantum Optics, Cambridge University Press, Cambridge, UK, 2011.
[17] A. Girndt, F. Jahnke, A. Knorr, S.W. Koch, W.W. Chow, Phys. Status Solidi (B) 202 (1997) 725.
[18] W.W. Chow, S.W. Koch, Semiconductor-Laser Fundamentals: Physics of the Gain Materials, Springer, Berlin, Heidelberg, New York, 1999.
[19] J. Hader, J.V. Moloney, S.W. Koch, W.W. Chow, IEEE J. Sel. Top. Quantum Electron. 9 (2003) 688.
[20] X. Lu, D.A. Beaton, R.B. Lewis, T. Tiedje, Y. Zhang, Appl. Phys. Lett. 95 (2009) 041903.

5.6 Investigation of the microstructure of metallic droplets on Ga(AsBi)/GaAs[1]

E. Sterzer, N. Knaub, P. Ludewig, R. Straubinger, A. Beyer, K. Volz, *Investigation of the microstructure of metallic droplets on Ga(AsBi)/GaAs*, Journal of Crystal Growth **408**, 71 (2014). DOI: 10.1016/j.jcrysgro.2014.09.006

Abstract

Low Bi content GaAs is a promising material for new optical devices with less heat production. The growth of such devices by metal organic vapor phase epitaxy faces several challenges. This paper summarizes results of the formation of metallic droplets during the epitaxial growth of Ga(AsBi) using all-liquid group III and V precursors. The samples that are grown, investigated by atomic force microscopy and scanning electron microscopy, show a different metal droplet distribution over the surface depending on the growth temperature and the V/III ratio of the precursors. Investigations with energy dispersive X-ray analysis and selective etching prove the appearance of phase separated Ga-Bi and pure Bi droplets at growth temperatures between 375 °C and 425 °C, which is explainable by the phase diagram of Ga-Bi. Since the pure Bi droplets show a preferred orientation on the surface after cool-down, transmission electron microscopy measurements were done by using the dark field imaging mode in addition to electron diffraction and high resolution imaging. These experiments show the single crystalline structure of the Bi droplets. The comparison of experimental diffraction patterns with image simulation shows a preferred alignment of Bi {10-1} lattice planes parallel to GaAs {202} lattice planes with the formation of a coincidence lattice. Thus it is possible to derive a model of how the Bi droplets evolve on the GaAs surface.

The Authors contribution

My contribution to this work was the growth of all samples and their characterization using HR-XRD. Furthermore I supervised Eduard Sterzer who did the SEM and AFM measurements and, as all other co-authors, helped to interpret the data and to correlate the observations with the applied growth condition.

1 Reprinted from *Journal of Crystal Growth **408** (2014) 71-77*, Copyright 2014, with permission from Elsevier.

Journal of Crystal Growth 408 (2014) 71–77

Contents lists available at ScienceDirect

Journal of Crystal Growth

journal homepage: www.elsevier.com/locate/jcrysgro

Investigation of the microstructure of metallic droplets on Ga(AsBi)/GaAs

E. Sterzer [1], N. Knaub [1], P. Ludewig, R. Straubinger, A. Beyer, K. Volz *

Materials Science Center and Faculty of Physics, Philipps-Universität Marburg, Marburg 35032, Germany

ARTICLE INFO

Article history:
Received 3 April 2014
Received in revised form
1 September 2014
Accepted 4 September 2014
Communicated by C. Caneau
Available online 19 September 2014

Keywords:
A1. Atomic force microscopy
A1. Electron microscopy
A1. Recrystallization
A3. Metal organic vapor phase epitaxy
B1. Bismuth compounds
B2. Semiconducting III–V materials

ABSTRACT

Low Bi content GaAs is a promising material for new optical devices with less heat production. The growth of such devices by metal organic vapor phase epitaxy faces several challenges. This paper summarizes results of the formation of metallic droplets during the epitaxial growth of Ga(AsBi) using all-liquid group III and V precursors. The samples that are grown, investigated by atomic force microscopy and scanning electron microscopy, show a different metal droplet distribution over the surface depending on the growth temperature and the V/III ratio of the precursors. Investigations with energy dispersive X-ray analysis and selective etching prove the appearance of phase separated Ga–Bi and pure Bi droplets at growth temperatures between 375 °C and 425 °C, which is explainable by the phase diagram of Ga–Bi. Since the pure Bi droplets show a preferred orientation on the surface after cool-down, transmission electron microscopy measurements were done by using the dark field imaging mode in addition to electron diffraction and high resolution imaging. These experiments show the single crystalline structure of the Bi droplets. The comparison of experimental diffraction patterns with image simulation shows a preferred alignment of Bi {10−1} lattice planes parallel to GaAs {202} lattice planes with the formation of a coincidence lattice. Thus it is possible to derive a model of how the Bi droplets evolve on the GaAs surface.

1. Introduction

The development of low bismuth (Bi) content gallium arsenide (GaAs) promises new devices with less heat generation [1] and a less temperature sensitive band gap [2,3]. First optically pumped [4], then electrically pumped lasing at room temperature [5] has been already demonstrated for dilute Bi containing devices grown by metal organic vapor phase epitaxy (MOVPE). Ga(AsBi) alloys with high Bi fractions above 10% have been grown; however, only by molecular beam epitaxy (MBE) and at growth temperatures around 200 °C [6]. In the case of MOVPE growth it is more challenging to achieve such high Bi fractions, since growth temperatures above 350 °C are required for the decomposition of the precursor chemicals. Because of the large covalent radius of the Bi atoms in comparison to the arsenic (As) atoms, the incorporation of Bi in GaAs causes local strain which makes this ternary material system highly metastable. Therefore, the crystal rejects the offered Bi, which segregates towards the surface and causes the formation of metallic droplets [7,8]. The understanding of the droplet formation is an important point for the growth improvement of Ga(AsBi)/GaAs alloys with high Bi concentration. A first theoretical description of Ga/GaAs core–shell structure formation during Ga-liquid droplet epitaxy on GaAs based on kinetic Monte Carlo simulations has been discussed in [9]. The mechanisms described in that paper can also take place in the growth of Ga(AsBi), where liquid Ga as well as liquid Bi droplets might be present at the surface due to the highly non-equilibrium growth conditions used.

There is already a first experimental description of droplet formation in MBE grown Ga(AsBi) thin films by atomic force microscopy (AFM), scanning electron microscopy (SEM), energy dispersive X-ray analysis (EDX) and reflection high energy electron diffraction (RHEED) [10], which shows Ga–Bi droplet formation for the Ga-rich Ga(AsBi) growth regime.

Since there are no crystallographic descriptions of Bi droplets on the Ga(AsBi) surface and no studies for MOVPE-grown samples yet, we will show the results of MOVPE-grown droplet containing Ga(AsBi) samples. This is interesting, as a decisive difference between MBE and MOVPE growth is the growth temperature compared to critical temperatures in the Ga–Bi phase diagram: Bi from Ga–Bi liquid mixtures solidifies at temperatures of 221.7 °C [11]. This temperature is above the MBE growth temperature of Ga(AsBi) in most cases, but below the MOVPE growth temperature of Ga(AsBi). We used SEM

* Corresponding author.
E-mail address: kerstin.volz@physik.uni-marburg.de (K. Volz).
[1] Both authors contributed equally.

http://dx.doi.org/10.1016/j.jcrysgro.2014.09.006
0022-0248/

combined with EDX as well as cross-section transmission electron microscopy (TEM). This allowed us not only to characterize the droplets and to get the structural information but also to gain crystallographic information, e.g. the crystallographic relationship between droplet and Ga(AsBi) layer surface normal, by evaluating the TEM diffraction pattern.

2. Experimental procedure

The investigated Ga(AsBi) samples were grown by MOVPE on GaAs (001) substrates in a commercially available AIX 200-GFR reactor with Pd-purified H_2 as carrier gas using a low reactor pressure of 50 mbar. The Ga precursor used was triethylgallium (TEGa), while tertiarybutylarsine (TBAs) and trimethylbismuth (TMBi) were used as group V precursors for As and Bi respectively. The growth temperature of the Ga(AsBi) alloys was chosen between 375 °C and 450 °C; we also varied TBAs/TEGa from 3.2 to 5 and TMBi/TBAs from 0.1 to 0.3 resulting in a V/III ratio from 6 to 7.35. A table with growth parameters and layer thicknesses of the investigated samples shown here is depicted in the Appendix. Our growth of droplet free Ga(AsBi) layers has been described in detail in [7, 12]. Sample surface characterization has been carried out in a Hitachi S-4100 SEM equipped with an Oxford Instruments EDX detector for composition determination. Further investigations of the surface were performed by using a Nanoscope IIIa AFM under atmospheric pressure to get a better understanding of the topology of the droplets on the surface. The droplets at the surface very often contain Ga as well as Bi. To further determine whether the droplets contain Bi or Ga a peculiar chemically selective etching process was also carried out. The samples were etched with hydrochloric acid (HCl, 30%) which only etches Ga and does not attack Bi, while sulfuric acid (H_2SO_4, 96%) was used to selectively etch Bi and not to attack Ga. After etching, either using both etchants or only one, the samples were again examined by AFM. Besides the topology we also investigated the crystallographic relation of the droplets with the GaAs substrate by using TEM. TEM samples were prepared in [010] cross-section conventionally by mechanical grinding, followed by Ar-ion milling with a Gatan PIPS. The microscopic investigations have been carried out in a JEOL JEM 3010 conventional TEM operating at 300 kV, as well as in a double C_s-corrected JEOL 2200FS scanning TEM, operating at 200 kV. The TEM methods used to investigate the Bi droplets in cross-section were dark field imaging and high resolution TEM as well as electron diffraction, which allowed to judge whether the metallic Bi droplets have a single crystalline or a polycrystalline structure.

3. Results and discussion

In this paper we will show the appearance of metallic droplets on the surface of Ga(AsBi) layers grown on GaAs under non-optimized conditions. Under optimized growth conditions [7,12], droplet formation can be avoided and thus will not be discussed here. It must be mentioned that under the growth conditions used here, we do not see metallic droplets when growing GaAs only. This shows that the metal droplet formation is a property of the Ga–As–Bi material system.

The SEM/EDX investigations show different arrangements of metallic droplets on the surface. We not only find droplets which form groups on the surface (clustering) but also detect droplets uniformly distributed across the surface. The droplet arrangement depends on the growth conditions. The temperature has a significant influence on the formation of metal droplet clusters as it is shown in Fig. 1a and b. The lower the growth temperature, the more clustering of metal droplets on the surface is observed. At low temperatures the decomposition of the metal organic precursors as well as the diffusivity of the atoms is lower compared to higher growth temperatures. We assume that a catalytic decomposition of the precursors takes place wherever a metal droplet is formed already. At these positions on the surface further metal droplets can hence form. As the diffusivity is low, the metal droplets are not evenly distributed on the surface, but cluster in groups (Fig. 1b). At higher growth temperatures a larger amount of metal organic precursor is decomposed and hence more evenly distributed metal droplets form (Fig. 1a).

Moreover we can correlate the size of the droplets and their density with the amount of group III precursor available in the reactor. The more group III precursor is available the bigger the droplets are, but the density of the droplets on the surface shrinks. The same results are obtained by reducing the As precursors partial pressure, which can be seen in the SEM images in Fig. 2a. Here, large Ga–Bi droplets form due to less As being available and the resulting Ga rich surface. Fig. 2b depicts smaller Bi droplets, containing much less Ga, but a surface more densely covered with droplets, because a higher As precursor partial pressure compared to the sample depicted in Fig. 2a was used here.

We will first determine the droplet composition for these two samples, before we look into their formation process during growth and cool-down.

Detailed SEM and EDX investigations of the droplets shown in Fig. 2a and b yield the chemical compositions of the different droplets. We found droplets containing Ga and Bi (Fig. 3a corresponding to Fig. 2a) or Bi mainly (Fig. 3b corresponding to Fig. 2b). The figures depict SEM images with an EDX spectrum for element analysis. Since the EDX measurements were performed at 20 keV the signal penetration depth for pure GaAs is up to 1.7 μm; therefore some signal is also detected from the underlying layer and substrate, in this case of GaAs. In Fig. 3a one can see that under these growth conditions the droplets are split, consisting in one part of Ga and in the other part of Bi. On top of the Bi-part, one can also find small Ga droplets (white arrows). A miscible liquid Ga–Bi mixture at growth temperature in the range 375–425 °C separates into a liquid Ga and a solid Bi phase at temperatures below 221.7 °C, i.e. during cool-down of the sample to room temperature. At 29.77 °C the liquid Ga solidifies. Therefore, the droplets develop into their final shape and compositional profile most likely during cool-down of the sample from growth temperature (above 300 °C) to room temperature, where the AFM and SEM/EDX measurements were made. Since we know the cool-down process of our reactor, one can indirectly say how long a wafer needs to cool down to the temperature at which Bi solidifies. In the case of the samples grown at 425 °C, the wafer takes about 14 min to cool down to the solid Bi phase (below 221.7 °C). The Bi metal solidifies first and all Ga is repelled from its lattice, as there is no solubility of Ga in solid Bi. This can also be seen in the droplets' morphology, as they often show faceted crystal regions where Bi is found and round Ga droplets aside or on top of the Bi (Fig. 3a). The droplet movement and their coalescence, which will be discussed in the following, take place at higher temperatures. In contrast to Fig. 3a, we see mainly pure Bi droplets if we use a higher As precursor partial pressure (Fig. 3b).

As the droplets' size increases and their density decreases when the layers are grown thicker (SEM images not shown here), the effect of droplet coalescence can be explained by Ostwald-ripening [13]. At the beginning, Bi only acts as a surfactant on the GaAs surface. By offering more and more Bi, a certain Bi fraction is incorporated into the growing Ga(AsBi) layer, while a planar metal film is on the growth surface. When a certain critical metal film thickness exceeds on the surface, metal droplets form as described before [7,12]. This happens possibly due to the increasing surface

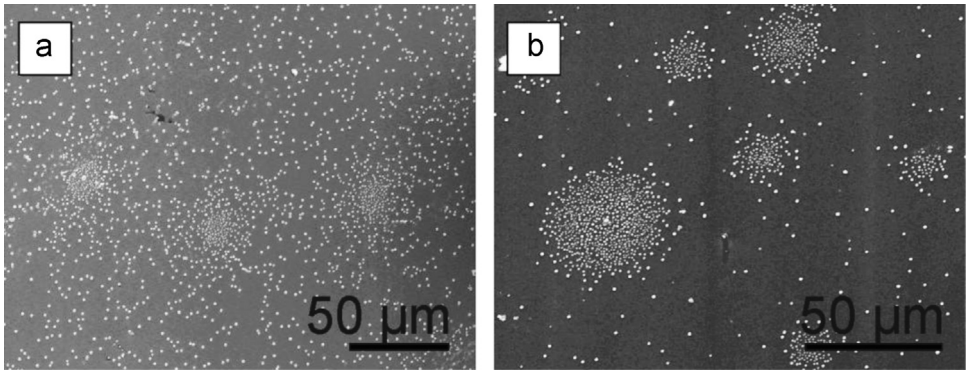

Fig. 1. (a) SEM image of a Ga(AsBi) sample grown at 400 °C. Three metal droplet clusters with pure Bi droplets are visible. There are additional droplets distributed uniformly between the clusters. (b) SEM image of a Ga(AsBi) sample grown at 375 °C. All other growth conditions were the same as for the sample shown in (a). In comparison to (a) the droplets evolve mainly in clusters; few droplets distributed between the clusters can be seen.

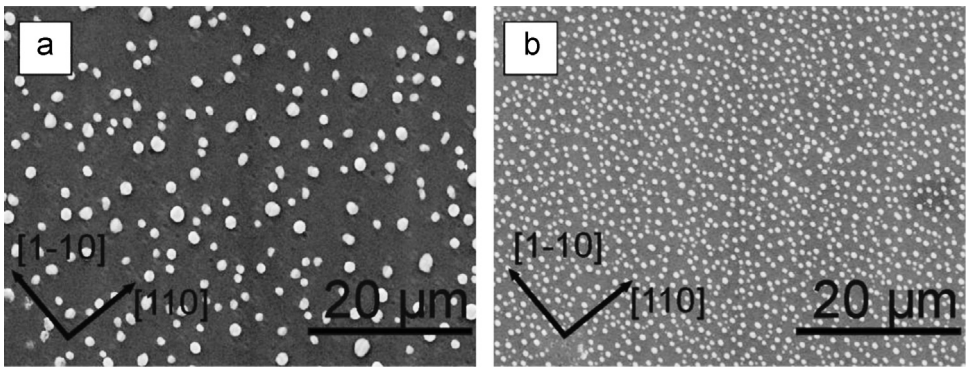

Fig. 2. (a) SEM image of a Ga(AsBi) sample surface covered with Ga–Bi droplets grown at 425 °C. The droplets are spatially separated and randomly distributed (TBAs partial pressure: 0.045 mbar). Compared to lower growth temperatures, larger droplets can be observed, but their density is lower. (b) SEM image of a sample grown using higher TBAs partial pressure compared to the one used for the sample shown in (a) (0.07 mbar). The surface is covered with droplets containing mainly Bi which are oriented along the [1–10] Ga-polar direction. In comparison to (a) the density of the droplets is higher.

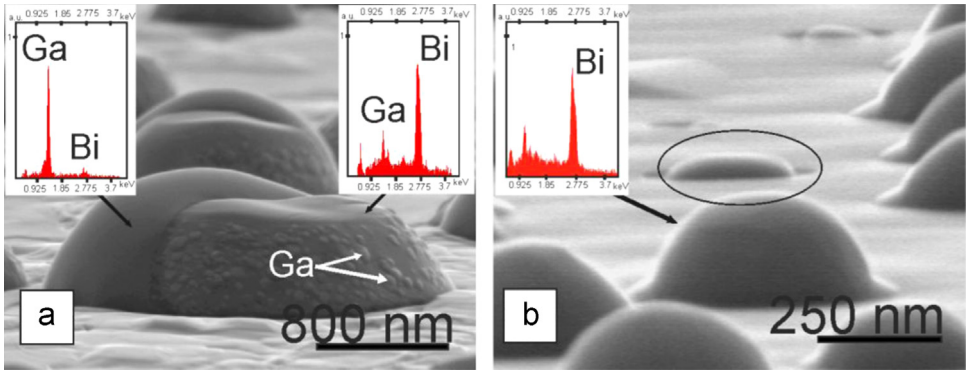

Fig. 3. (a) SEM image of the surface of a bulk Ga(AsBi)/GaAs sample grown at 425 °C (same sample as shown in Fig. 2a). The EDX spectra, shown as inset, show the composition of the droplet, which is separated in a Ga and a Bi part. The surface of the Bi part is covered by small Ga droplets. Due to the moving of droplets the surface is rough. (b) SEM image of a Ga(AsBi) surface containing droplets, made of mainly Bi (same sample depicted in Fig. 2b). The encircled droplet seems to extend into the layer which also indicates that the droplets are forming during the growth. The foot of the droplet is also mainly Bi.

tension of the planar film. However, the finding of an Ostwald ripening process also poses questions on the movement and formation of droplets on the surface during growth. Therefore, we investigated the sample surface (of the sample shown in Figs. 2a and 3a) before and after an etching process with sulfuric acid and hydrochloric acid. The results are shown in the SEM image in Fig. 4a (before etching) andb (AFM micrograph after the etching process with sulfuric acid). Both observations were performed on the same sample, but in slightly different positions. The SEM image in Fig. 4a shows clearly the appearance of Ga–Bi droplets. Moreover one can see holes (some are encircled) close to the droplets. The growth mechanism of the ring-like, elevated structure, consisting of GaAs and surrounding the area where the droplets were, is most probably similar to the one described in [9]. The appearance of holes in unetched samples leads to the assumption that smaller droplets were formed during growth and might form bigger ones by coalescence afterwards on the surface. A possible proof for this assumption is shown in Fig. 4c. This AFM micrograph is an enlarged image of the area which is marked by the black box in Fig. 4b. Here, one can see three holes (encircled positions) where probably three smaller droplets were before. A possible scenario could be the following: at temperatures where Bi is liquid, the three droplets moved towards the center of the image (moving direction is marked with black arrows) where

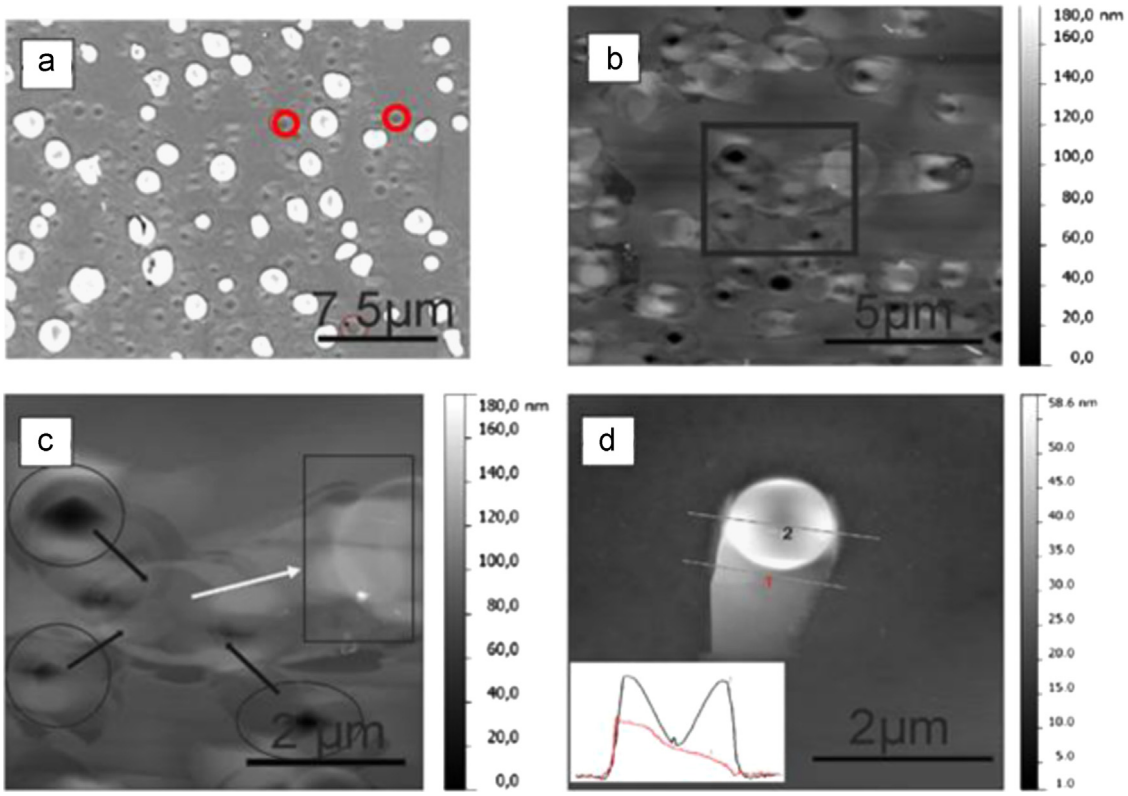

Fig. 4. (a) SEM image of a surface belonging to the same sample as shown in Fig. 3a. One can see Ga–Bi droplets distributed over the surface as well as some holes (two are encircled in red) close to them. The holes occur probably during growth and indicate positions where droplets were before they moved and coalesced, since the image was taken before an etching process. The image was intentionally overexposed to show the surface morphology better. (b) AFM micrograph of the same sample surface as shown in (a) but after etching with sulfuric acid. (c) Enlarged image of the squared area depicted in (b). The circles mark the holes where it is assumed that smaller droplets were before they moved towards the middle of the image (as marked with black arrows) and coalesce into a bigger droplet. Afterwards the bigger droplet probably moved (white arrow) to the area which is marked with the box. This droplet was then etched away before the AFM image was taken. (d) AFM micrograph of the same sample as shown in (a) and (b) after etching with sulfuric acid and hydrochloric acid. The position of a droplet as well as a trail behind it can be seen. The lines marked 1 and 2 represent the positions of the line profiles which are depicted as an inset in this figure. (For interpretation of the references to color in this figure legend, the reader is referred to the web version of this article.)

they formed a bigger droplet. The bigger droplet then moved on the surface (moving direction is marked with white arrow) until it finally stopped at the position which is marked (box). This droplet was etched away prior to taking the AFM image. Our assumption that the bigger droplet moved on the surface is based on the fact that a movement trace is still visible on the sample surface. Another hint for droplet moving is depicted in Fig. 4d. This AFM micrograph of the same sample as described in Fig. 4a and b was recorded after the etching process with sulfuric acid and hydrochloric acid. The micrograph depicts the former droplet position on the surface, but more important is the clearly visible trace left behind during the droplet movement. The inset in Fig. 4d depicts the line profiles across the trail of the droplet, marked in the figure with 1 and 2. The line marked as 1 shows the profile of the area of the droplet trail, while the second line represents the GaAs height profile at the position where the Ga–Bi droplet was etched away. The profile points out that the depth of the hole does not reach the underlying substrate and that the hole is surrounded by a mound on either side. Since the etches we used were to only attack either Ga or Bi and there is still a mound left around the hole after etching, one can assume a mound containing GaAs; as will be seen later this GaAs mound contains a small Bi fraction. A possible explanation for this could be a recrystallization process which took place as was simulated in [9]. The property where droplets move and coalesce on the surface has for our growth conditions only been found for droplets containing a large amount of Ga, which is liquid down to room temperature. Droplet movement could not be found for samples having Bi droplets only, as will be shown in the following. It should be noted that movement of metallic droplets on semiconductor surfaces (e.g. GaAs) has been observed before [14] and its driving force has been explained by different surface chemical potentials, which for our samples can easily occur due to surface composition fluctuations.

Fig. 5a shows an AFM micrograph of a sample surface (sample shown in Figs. 2b and 3b, having mainly Bi metal droplets), etched with sulfuric acid to remove Bi only and leaving Ga unetched. We observe holes in the Ga(AsBi) surface where the Bi droplets were before. This indicates that the metal droplets extend into the semiconductor layer under these growth conditions and hence also that mainly Bi-containing droplets are formed during the growth. The very peculiar morphology of the holes, especially their raised edges (Fig. 5b), also leads to the conclusion that liquid phase epitaxy (LPE) is taking place at growth temperature in the Bi–GaAs system studied here. Again, similar phenomena have been described using kinetic Monte Carlo simulations in [9] looking at the Ga–GaAs system. In addition to the holes left by the etched Bi, one can see small Ga droplets all over the surface, which could be removed by etching with HCl (depicted in Fig. 5c).

It is already known that Bi as a surfactant enhances the lateral growth rate of GaAs growth as well as for Ga(AsBi) growth [10,15] whereas the formation of pure Bi droplets on the surface is undesirable and hinders the growth of homogeneous Ga(AsBi) layers. The SEM image of the intact structure in Fig. 2b as well as the AFM image of the etched sample depicted in Fig. 5a shows a preferred alignment of the droplets on the surface. By investigating the droplets with respect to the known crystallographic

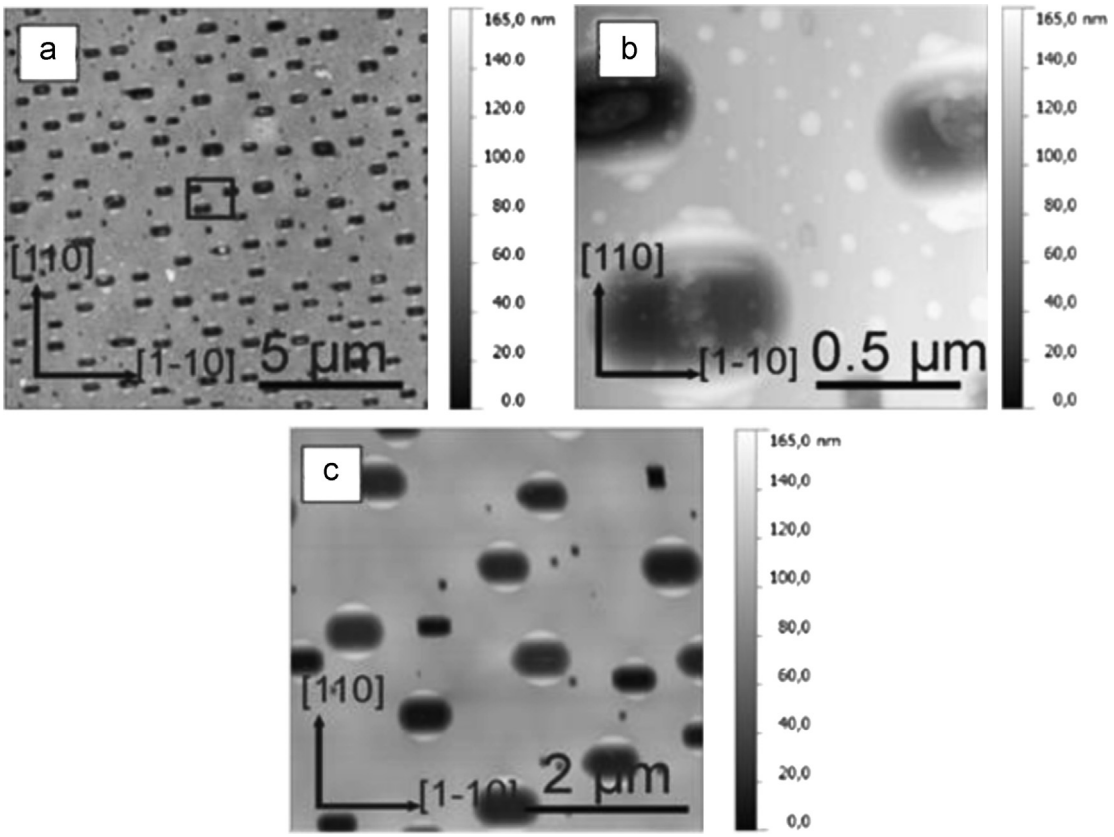

Fig. 5. (a) This AFM image confirms the preferred orientation of droplets, shown in Figs. 2b and 3b already, with their long axis along the Ga-polar [1–10] direction. The sample has been etched with sulfuric acid which is selective against Bi. Therefore holes remain where Bi droplets had been before. (b) The enlarged image of (a) reveals small droplets on the surface which are probably Ga. (c) AFM micrograph of the same sample depicted in (a) and (b) after a further etching process with hydrochloric acid which is selective against Ga. After this process the small droplets disappear.

direction of the substrate, we find that the long axis of the droplets is along the [1–10] Ga-polar direction of the GaAs substrate. The Bi droplets hence have a preferred orientation with respect to the surface. Therefore, we assume a crystallographic relationship between the metal Bi and the semiconductor crystal structure. To get a better understanding of why the Bi droplets form like that, we have performed cross-section investigation of the droplets in TEM.

Fig. 6a shows the bright field image of a 400–500 nm large Bi droplet on a Ga(AsBi) layer grown on GaAs. One can see the shape of the droplet and also some facets due to its crystalline structure. Since bright field imaging does not allow to derive crystallographic information on the sample, we also performed dark field imaging of the same droplet. The 002-diffraction spot of the cubic zinc-blende GaAs has been used for the dark field imaging. This reflection is chemically sensitive for the cubic zinc-blende lattice, and the measured intensity is proportional to the square of the absolute value of the structure factor of the investigated material. In this kind of imaging Ga(AsBi) appears brighter than GaAs. The higher the Bi content of the material, the brighter the Ga(AsBi) layer with respect to GaAs. One can see clearly the inhomogeneous Bi composition in the Ga(AsBi) layer in Fig. 6b. The composition depth profile is again very peculiar, pointing towards a LPE process taking place during growth, as has also been theoretically described in [9] and is now shown here experimentally with the example of a ternary material. We observe a Bi-poor region directly underneath the Bi droplet, which is sandwiched between two Ga(AsBi) layers on the sides. During LPE Bi can act as a catalyst for GaAs growth, as it is described in [16]. This leads to the conclusion that once a small droplet is formed during growth, the droplet is fed with the Bi from the underlying Ga(AsBi) layer until only GaAs remains, which can be recognized in the dark field images by nearly the same intensity as pure GaAs.

To get a better understanding of the Bi droplet's crystal structure and the possibility of pure Bi droplet formation in general we simulated the diffraction pattern of the Bi droplet depicted in Fig. 6c (using the electron diffraction simulation software JEMS [17]). The results are overlaid to the experimental pattern. The spots surrounded by circles belong to the typical GaAs [010] diffraction pattern, and the additional diffraction spots, which are surrounded by squares, belong to the Bi droplet. Judging from the spotty appearance of the diffraction pattern, as well as from the bright field image discussed before, one can say that the Bi droplet has a single crystalline structure assuming the pure Bi crystal structure, which is rhombohedral (space group R-3m). Due to the threefold symmetry of the Bi crystal structure we got the solution $\langle -1-13\rangle$ for the droplet orientation. In this case the diffraction spots of the Bi lattice planes parallel to GaAs {202} planes are Bi {10–1}. By simulating a rhombohedral Bi diffraction pattern with JEMS one can derive the lattice plane distance of Bi $\{10-1\}=0.2273$ nm, which is close to the known lattice plane distance of GaAs $\{202\}=0.2$ nm. This corresponds to a lattice mismatch of 12%. To accommodate this mismatch, a coincidence lattice of GaAs and Bi could form when the condition $7\times$ Bi $\{10-1\}\approx 8\times$ GaAs {202} is fulfilled, as it is shown in the ball and stick model of the Bi droplet on the GaAs surface in Fig. 6d, which was created with the free available software VESTA [18]. The model displays the crystallographic relationship between the lattice planes of Bi and GaAs which we experimentally found, and also shows which planes constitute the droplet's facets. To confirm

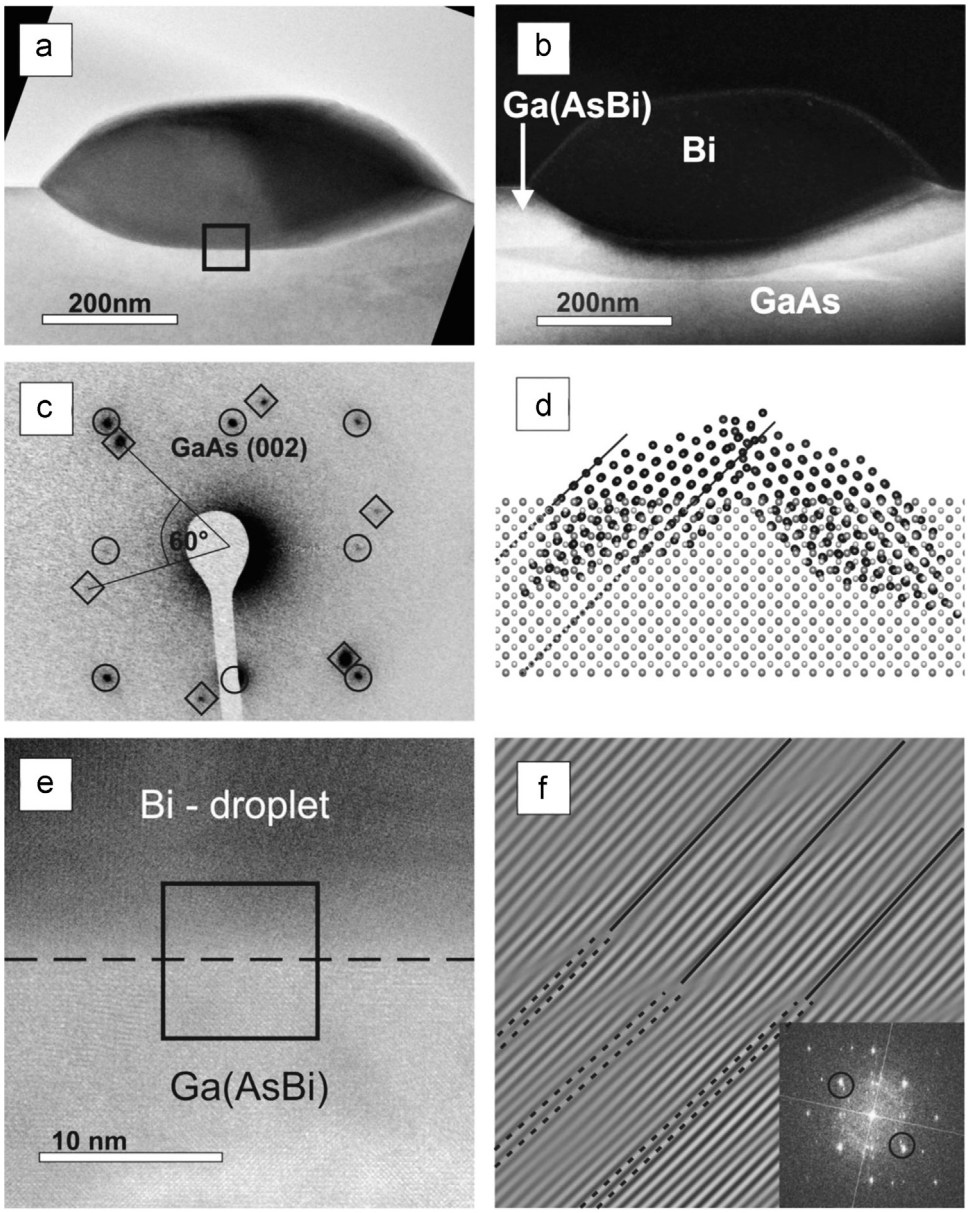

Fig. 6. (a) Cross-sectional [010] TEM bright field image of a 400–500 nm large Bi-droplet (dark) on Ga(AsBi) surface. The squared area represents the region where high resolution measurements were carried out. (b) TEM (002) dark field image of the same droplet as in (a). Under these imaging conditions the Ga(AsBi) layer appears brighter than pure GaAs. The Ga(AsBi) layer underneath and surrounding the droplet has inhomogeneous chemical composition. (c) Diffraction pattern of the Bi droplet on GaAs from (a). The encircled diffraction spots highlight the GaAs diffraction, while the squared ones highlight the Bi droplet diffraction. One can see the Bi (10–1) diffraction spots parallel to GaAs (202). The Bi crystal structure assumed for the simulation of this diffraction pattern is rhombohedral. (d) Ball and stick model of the investigated Bi droplet (black atoms) on GaAs (gray atoms). The dashed lines represent the {202} lattice planes of GaAs, while the black ones belong to the {10 − 1} planes of Bi. Every 7th Bi {10 − 1} lattice plane fits to every 8th GaAs {202} lattice plane. By the formation of this coincidence lattice the crystal accommodates its lattice mismatch from 12% to 0.6%. (e) High resolution TEM measurement of the region depicted in (a). The dashed line represents the interface of the Bi-droplet and the Ga(AsBi) layer. (f) Bragg-filtered region of the squared area in (e). The encircled spots in the Fourier transform mark the spots which were taken for the Bragg-filtering process. The filtered image highlights the additional zinc-blende {202} lattice planes (dashed lines) at each 7th Bi {10 − 1} lattice plane (straight lines).

Table 1
Growth parameters of the four investigated samples.

Sample	Sample shown in Fig.	T_{growth} [C°]	TEGa partial pressure [mbar]	TBAs/TEGa	TMBi/TBAs	Thickness [nm]	Growth scheme (pulsed gowth mode) #pulses
A	1a	400	0.014	3.6	0.2	32	300
B	1b	375	0.014	3.6	0.2	13	300
C	2a, 3a, 4a, 4b, 4c, 4d	425	0.014	3.2	0.194	91	250
D	2b, 3b, 5a, 5b, 5c, 6a, 6b, 6e	425	0.014	5	0.1	160	250

this model we carried out high resolution TEM measurement of the Bi-droplet/Ga(AsBi) interface depicted in Fig. 6e. Afterwards, we performed a fast Fourier transformation (FFT) of the image (inset in Fig. 6f) and a Bragg-filtering process of the GaAs {202} lattice planes. The result of the inverse FFT is shown in Fig. 6f, which is the filtered image of the squared region in Fig. 6e. Here

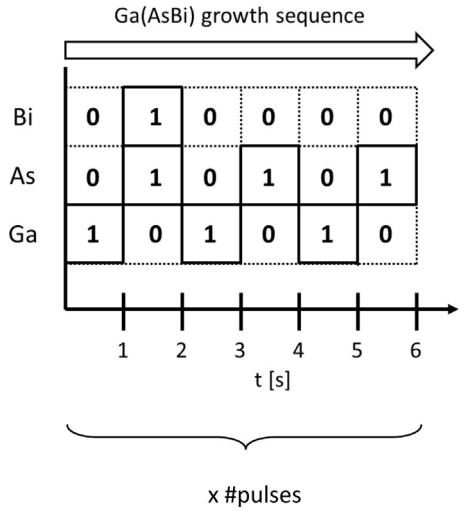

Fig. A1. Growth scheme.

one can see for every 7th Bi-droplet {10−1} lattice plane (straight line) an additional GaAs {202} lattice plane (dashed line). Hence, a coincidence lattice is formed, which significantly reduces the strain from 12% to 0.6%. With these results it is possible to explain the preferred orientation of the pure Bi droplets, which can form under certain growth conditions during the growth of Ga(AsBi) layers on GaAs by the accommodation of the droplets' lattice mismatch.

4. Summary

We have shown how metallic droplets (Bi and Ga–Bi) can evolve and behave on the Ga(AsBi) surface by using several investigation techniques like AFM, SEM/EDX and TEM. The SEM investigation combined with EDX measurements revealed the tendency that droplets can arrange on the surface uniformly or in clusters and be droplets of pure Bi or a mixture of Ga and Bi (Ga–Bi), depending on the As precursor as well as on the Bi precursor partial pressure. The arrangement of the droplets depends on the temperature due to the diffusivity of the Ga and Bi atoms and catalytic decomposition of the group III and group V precursors. After etching selectively (HCl 30% for Ga- and H_2SO_4 for Bi-etching) we could show that the droplets move on the surface during growth and that their morphology as well as the morphology and the composition of the surrounding semiconductor layers is determined by an LPE process taking place during growth. A preferred orientation of Bi droplets with respect to the GaAs lattice has been discovered in AFM/SEM images and further investigated in TEM by using dark and bright field imaging, as well as electron diffraction. The evaluation of a Bi droplet on GaAs diffraction pattern yields to the following arrangement of Bi {10−1} planes: Bi {10−1}||GaAs {202}. A ball and stick model of the recorded dark field image allows to visualize how a metallic Bi droplet can crystallize on the cubic zinc-blende structure of GaAs and additional high resolution TEM measurements confirm this model experimentally. Finally the results of this paper contribute to the understanding of why metallic (especially Bi) droplets with single crystal structure are formed on a semiconductor material under specific growth conditions.

Acknowledgments

This work was founded by the German Science Foundation (GRK 1782) and the European Union Project no. BIANCHO (FP7-257974).

Appendix A

See Table 1 and Fig. A1.

References

[1] K. Alberi, O.D. Dubon, W. Walukiewicz, K.M. Yu, K. Bertulis, A. Krotkus, Appl. Phys. Lett. 91 (5) (2007) 051909. http://dx.doi.org/10.1063/1.2768312.
[2] S.Sweeney, in: Proceedings of the 22nd IEEE International, Semiconductor Laser Conference (ISLC), 2010, pp. 111–112.
[3] M. Usman, C.A. Broderick, A. Lindsay, E.P. O'Reilly, Phys. Rev. B 84 (2011) 245202. http://dx.doi.org/10.1103/PhysRevB.84.245202.
[4] Y. Tominaga, K. Oe, M. Yoshimoto, Appl Phy Express 3 (6) (2010) 062201. http://dx.doi.org/10.1143/APEX.3.062201.
[5] P. Ludewig, N. Knaub, N. Hossein, S. Reinhard, L. Nattermann, I.P. Marko, S.R. Jin, K. Hild, S. Chatterjee, W. Stolz, S.J. Sweeney, K. Volz, Appl. Phys. Lett. 102 (24) (2013) 242115. http://dx.doi.org/10.1063/1.4811736.
[6] K. Oe, H. Okamoto, Jpn. J. Appl. Phys. 37 (Part 2, No. 11A) (1998) L1283–L1285. http://dx.doi.org/10.1143/JJAP.37.L1283.
[7] P. Ludewig, N. Knaub, W. Stolz, K. Volz, J. Cryst. Growth 370 (2013) 186–190. http://dx.doi.org/10.1016/j.jcrysgro.2012.07.002.
[8] X. Lu, D.A. Beaton, R.B. Lewis, T. Tiedje, M.B. Whitwick, Appl. Phys. Lett. 92 (2008) 192110. http://dx.doi.org/10.1063/1.2918844.
[9] K. Reyes, P. Smereka, D. Nothern, J. Mirecki Millunchick, S. Bietti, C. Somaschini, S. Sanguinetti, C. Frigeri, Phys. Rev. B 87 (2013) 165406. http://dx.doi.org/10.1103/PhysRevB.87.165406.
[10] G. Vardar, S.W. Paleg, M.V. Warren, M. Kang, S. Jeon, R.S. Goldman, Appl. Phys. Lett. 102 (4) (2013) 042106. http://dx.doi.org/10.1063/1.4789369.
[11] D. Manasijevic, D. Minić, D. Živković, I. Katayama, J. Vřešťál, D. Petković, J. Phys. Chem. Solids 70 (9) (2009) 1267–1273. http://dx.doi.org/10.1016/j.jpcs.2009.07.010.
[12] P. Ludewig, Z. Bushell, L. Nattermann, N. Knaub, W. Stolz, K. Volz, J. Cryst. Growth 396 (2014) 95–99. http://dx.doi.org/10.1016/j.jcrysgro.2014.03.041.
[13] C. Wagner, Z. Elektrochem. 65 (718) (1961) 581–591.
[14] W.-X. Tang, C.-X. Zheng, Z.-Y. Zhou, D.E. Jesson, J. Tersoff, IBM J. Res. Dev. 55 (4) (2011) 10:1–10:7. http://dx.doi.org/10.1147/JRD.2011.2158762.
[15] R.R. Wixom, L.W. Rieth, G.B. Stringfellow, J. Cryst. Growth 265 (3–4) (2004) 367–374. http://dx.doi.org/10.1016/j.jcrysgro.2004.02.019.
[16] M. Panek, M. Ratuszek, M. Tłaczała, J. Cryst. Growth 74 (3) (1986) 568–574. http://dx.doi.org/10.1016/0022-0248(86)90203-4.
[17] P. Stadelmann, Ultramicroscopy 21 (2) (1987) 131–145. http://dx.doi.org/10.1016/0304-3991(87)90080-5.
[18] K. Momma, F. Izumi, J. Appl. Crystallogr. 44 (6) (2011) 1272–1276. http://dx.doi.org/10.1107/S0021889811038970.

5.7 Physical properties and optimization of GaBiAs/(Al)GaAs based near-infrared laser diodes grown by MOVPE with up to 4.4% Bi[1]

I. P. Marko, P. Ludewig, Z. L. Bushell, S. R. Jin, K. Hild, Z. Batool, S. Reinhard, L. Nattermann, W. Stolz, K. Volz and S. J. Sweeney, Journal of Physics D: Applied Physics **47**, 345103 (2014). DOI: 10.1088/0022-3727/47/34/345103

Abstract

This paper reports on progress in the development of GaAsBi/(Al)GaAs based lasers grown using metal-organic vapour phase epitaxy and focuses on the underlying processes governing their efficiency and temperature dependence. Room temperature lasing has been achieved in devices with 2.2% Bi and lasing in devices with 4.4% Bi was observed up to 180 K.We show that the device performance can be improved by optimizing both electrical and optical confinement in the laser structures. Analysis of the temperature dependence of the threshold current together with pure spontaneous emission and high hydrostatic pressure measurements indicate that device performance is currently dominated by non-radiative recombination through defects (>80% of the threshold current at room temperature in 2.2% Bi samples) and that to further improve the device performance and move towards longer wavelengths for optical telecommunications (1.3-1.5 µm) further effort is required to improve and optimize material quality.

The Authors contribution

My contribution to this work was the MOVPE growth, characterization and optimization of test structures and finally the discussed laser devices. This includes the structural characterization concerning the composition and layer thicknesses as well as room temperature PL and electrical injection investigations.

1 Reprinted from *Journal of Physics D: Applied Physics* ***47*** *(2014) 345103.*

IOP Publishing Journal of Physics D: Applied Physics
J. Phys. D: Appl. Phys. **47** (2014) 345103 (8pp) doi:10.1088/0022-3727/47/34/345103

Physical properties and optimization of GaBiAs/(Al)GaAs based near-infrared laser diodes grown by MOVPE with up to 4.4% Bi

I P Marko[1], P Ludewig[2], Z L Bushell[1,2], S R Jin[1], K Hild[1], Z Batool[1], S Reinhard[2], L Nattermann[2], W Stolz[2], K Volz[2] and S J Sweeney[1]

[1] Advanced Technology Institute and Department of Physics, University of Surrey, Guildford, GU2 7XH, UK
[2] Material Science Center and Faculty of Physics, Philipps-Universität Marburg, 35032 Marburg, Germany

E-mail: i.marko@surrey.ac.uk

Received 16 May 2014, revised 1 July 2014
Accepted for publication 7 July 2014
Published 1 August 2014

Abstract

This paper reports on progress in the development of GaAsBi/(Al)GaAs based lasers grown using metal-organic vapour phase epitaxy and focuses on the underlying processes governing their efficiency and temperature dependence. Room temperature lasing has been achieved in devices with 2.2% Bi and lasing in devices with 4.4% Bi was observed up to 180 K. We show that the device performance can be improved by optimizing both electrical and optical confinement in the laser structures. Analysis of the temperature dependence of the threshold current together with pure spontaneous emission and high hydrostatic pressure measurements indicate that device performance is currently dominated by non-radiative recombination through defects (>80% of the threshold current at room temperature in 2.2% Bi samples) and that to further improve the device performance and move towards longer wavelengths for optical telecommunications (1.3–1.5 μm) further effort is required to improve and optimize material quality.

Keywords: GaAsBi, laser diode, efficiency, temperature performance, recombination mechanisms

(Some figures may appear in colour only in the online journal)

1. Introduction

Current near-infrared lasers, particularly those operating at the optical telecommunications wavelengths of 1.3–1.6 μm suffer from intrinsic losses due to non-radiative Auger recombination and inter-valence band absorption (IVBA) [1]. As a result, around 80% of the electrical power is wasted as heat in a 1.55 μm laser chip at laser threshold [2]. From previous work using high hydrostatic pressure it was found that Auger recombination process leading to the excitation of a hot hole into spin-orbit split off sub-band is responsible for the majority of the injected current (50% and 80% of threshold in 1.3 μm and 1.55 μm lasers, respectively [1, 3]). This loss increases exponentially as the lasing photon energy (or band gap) approaches the spin-orbit splitting energy [4]. Due to the strong temperature dependence of such processes, most systems require thermo-electric coolers and an air-conditioned environment, further increasing the system energy budget by over an order of magnitude. In the commonly used near-infrared laser material systems such as InGaAsP and AlInGaAs, the fact that the bandgap is greater than spin-orbit splitting energy causes the device performance to be strongly affected by non-radiative Auger recombination, in spite of the almost perfect material quality and optimized laser design [1, 2, 5]. Incremental approaches to solve these problems including development of quantum dot lasers [6–8] have not overcome these intrinsic loss mechanisms. Recently, a radical change to manipulate the electronic band structure of novel bismide alloys GaAsBi [4, 9] was proposed to eliminate Auger recombination and dramatically reduce the energy

consumption and temperature dependence of GaAsBi based lasers. The incorporation of only a small amount of Bi into GaAs causes a large reduction in the band gap, E_g, as much as ~80 meV/Bi%, due to valence band anti-crossing [9–12]. What is most promising is the fact that for Bi fractions above approximately 10% in GaAsBi, the spin-orbit splitting (Δ_{SO}) becomes larger than the band gap [9, 10, 12]. Under such conditions it is expected that the troublesome hot-hole generating Auger recombination and IVBA processes will be suppressed leading to higher efficiencies and more temperature stable output power for lasers operating at optical communications wavelengths.

There has been very little research to date on GaAsBi based devices, and in particular, the underlying carrier recombination processes occurring in the material. Using high hydrostatic pressure and low temperature techniques, the processes limiting device performance were probed in GaAsBi/GaAs light emitting diodes containing 1.8% Bi [13]. The results showed some evidence of a carrier leakage due to poor carrier confinement in these devices with low Bi composition and GaAs barriers. The development of GaAsBi based lasers have recently experienced a breakthrough due to improvements in growth technology and the first electrically pumped lasers operating above room temperature have been demonstrated [14]. In this paper we extend this study on the optical and electrical characterization of GaAsBi based lasers with an increased Bi fraction of up to 4.4% and discuss the main factors limiting the device performance.

2. Samples and methods

Electrically pumped GaAsBi/(Al)GaAs lasers with different Bi compositions in the active region have been grown by MOVPE. Single quantum well (SQW) as well as triple quantum well (TQW) laser devices were grown within $Al_{0.4}Ga_{0.6}As$ cladding layers on n-doped GaAs (0 0 1) substrates. A commercially available AIX 200-GFR reactor system with Pd-purified H_2 as carrier gas at a reduced reactor pressure of 50 mbar was used for the laser growth. The GaAsBi QW of the devices with 2.2% Bi was grown at 400 °C under pulsed precursor flow as reported in [14]. However, in order to increase the Bi fraction a continuous precursor flow was applied that enables higher growth rates and, after additionally optimizing the V/III and trimethyl bismuth/V ratios, the incorporation of 4.4% Bi at 400 °C growth temperature [15]. To form broad area laser structures, 50 and 100 μm wide Au/Cr metal stripes were deposited on the top contact and an Au/AuGe/Cr-based contact was deposited on the substrate backside. The sample was alloyed at 400 °C for ohmic contact formation. To avoid current spreading the GaAs : Zn-contact layer was etched-off using the metal stripes as a mask. Since the devices were grown on GaAs-substrates the laser facets were cleaved using standard techniques with a cavity length of 1 mm. The devices were all measured *as-cleaved*. Prior to the growth of the laser structures, the composition of the material, the growth rates and the material uniformity were assessed using high resolution x-ray diffraction, photoluminescence and transmission electron microscopy. The physical properties of the laser diodes were characterized using electrical and optical measurements as a function of temperature using a closed cycle cryostat (20–300 K). An optical spectrum analyser and optical power meters were used for the facet emission and pure spontaneous emission measurements where spontaneous emission was collected from a small 100 μm diameter window milled in the substrate contact [16]. In addition, high hydrostatic pressure measurements using a He-gas pressure system were used to investigate recombination and loss processes in the lasers [16, 17]. Pulsed measurements with pulse widths of 200–500 ns and frequencies of 1–10 kHz were used to avoid self-heating effects. Continuous wave mode was also used for voltage-current characteristics for currents below 50 mA.

For device modelling, the calculations of E_g and Δ_{SO} were based on recent experimental and theoretical data of GaAsBi on GaAs using the valence band anti-crossing model (VBAC) including the effects of strain [18]. Other material parameters of GaAsBi ternary alloys were calculated using the virtual-crystal approximation [19] from the related binary alloys [10]. Using these parameters as input, the band alignment and the energy states of electrons, heavy and light holes of GaAsBi/(Al)GaAs quantum well structures were determined using Nextnano software. In GaAsBi quantum well calculations the effective masses of GaAsBi were determined using 12-band $\boldsymbol{k}\cdot\boldsymbol{p}$ Hamiltonians, including strain effects [18].

Adding Bi to GaAs mainly affects the valence band. Hence, to improve electron confinement AlGaAs barriers were used in samples with lower Bi composition. Higher Al fraction in the barriers improves the electron confinement. However, the addition of Al in the GaAs waveguide layers reduces the optical confinement factor. Based on preliminary calculations of the optical confinement factor of AlGaAs barriers with 12% and 20% Al were chosen. The quantum well width was selected to minimize the effects of inhomogeneity while maintaining suitable sub-band splitting. The typical laser structure and calculated band alignment diagram is shown in figure 1. The structural details of the active region of the investigated laser diodes, calculated band offsets in the conduction (ΔE_c) and valence (ΔE_v) bands, transition energy ($E_{e1\text{-}hh1}$) at room temperature (RT) are summarized in table 1. The experimentally measured lasing wavelength (λ) and threshold current density (J_{th}) for these devices are also given in the table.

3. Results and discussion

The samples A, B, C and D have the same 6.4 nm quantum well(s) containing 2.2% Bi. The only difference between them is the composition of Al in the waveguide/barrier layers. The rest of the structure is the same as shown on the structural diagram in figure1. It can be seen from table 1 that there is a significant difference in the performance of these device with the lowest J_{th} of ~1 kA cm^{-2} being measured in the SQW laser with 12% Al in the waveguide (sample C). Figure 2 demonstrates a comparison of light-current characteristics of these devices at RT and the temperature dependencies of

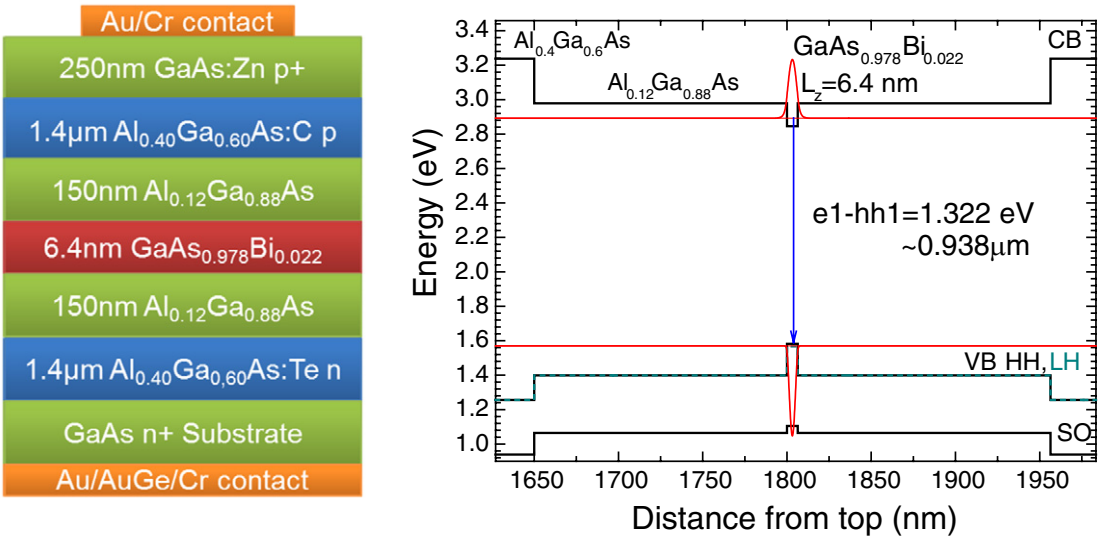

Figure 1. Layer sequence diagram and calculated band alignment (CB—conduction band, VB—valence band, SO—spin–orbit split off subband) of the active region of the SQW laser structure with 2.2% Bi in a 6.4 nm QW with AlGaAs barriers containing 12% Al (sample C).

Table 1. Active region details of the different structures investigated with calculated band offsets in the conduction (ΔE_c) and valence (ΔE_v) bands, transition energy ($E_{e1\text{-}hh1}$) at RT as well as experimentally measured lasing wavelength (λ) and threshold current density (J_{th}) for these devices.

Sample	N_{QW}	QW width (nm)	Bi%	Al% in AlGaAs barriers	$E_{e1\text{-}hh1}$, eV (λ, nm)	ΔE_c, (meV)	ΔE_v, (meV)	Measured λ, (nm)	RT J_{th}, (kA cm^{-2})
A	1	6.4	2.2	20	1.330 (932)	202	225	947	1.5–1.6
B	3	6.4	2.2	20	1.330 (932)	202	225	958	2.4–2.7
C	1	6.4	2.2	12	1.322 (938)	133	184	947	1.0–1.1
D	1	6.4	2.2	0	1.298 (955)	37	123	938	7.5
E	1	8	4.4	0	1.181 (1050)	73	206	1039 at 180 K	4.5 at 180 K

the lasing photon energy. RT lasing was observed in all of the devices containing 2.2% Bi with a range of threshold currents as we discuss below. The RT light versus current characteristics of these devices is shown in figure 2(*a*). The insert in figure 2(*b*) shows lasing spectra at RT measured at 10% above the threshold. The conduction band offset (from e_1-barrier) in sample D with GaAs barriers (see table 1) is relatively small (~37 meV) and close to the thermal energy of carriers at RT. This results in a high threshold current density of 7.5 kA cm^{-2}. Furthermore, in addition to the lasing peak from the quantum well at ~938 nm, for temperatures >250 K as evident in the inset of figure 2(*b*), we observe emission from the barrier layers around 897 nm consistent with carrier leakage due to the low conduction band offset. The relatively broad lasing spectrum in this device at RT consists of a multitude of Fabry–Pérot modes, which indicates a significantly broadened gain spectrum.

To reduce carrier escape into the barrier layers, Al was introduced into the barrier/waveguide layers to increase the band offset. However, a consequence of increasing the Al content of the waveguide has the negative effect of reducing the refractive index contrast between the waveguide region and the AlGaAs cladding layers leading to a reduced optical confinement factor and corresponding decrease in modal gain. To optimize the device performance, one should therefore take into account two opposite effects related to the composition of Al in the waveguide and barrier layers. Table 1 quantifies the influence of barrier Al fraction on the confining energy for electrons while figure 3 shows the effect of the waveguide Al fraction (for $Al_{0.4}Ga_{0.6}As$ cladding layers) on the optical confinement factor. Laser structures A and C are nominally identical but have an Al fraction in the barrier/waveguide layers of 20% and 12%, respectively. From table 1, it can be seen that the incorporation of Al in the barrier increases the electron confining potential from 37 meV for GaAs to 133 meV for 12% Al and 202 meV for 20% Al. For GaAs barriers, the confining potential is ~k_bT at room temperature (where k_b is the Boltzmann constant) whereas for both the 12% and 20% Al-containing barriers, the confining energy is >$5k_bT$ at room temperature, providing strong electrical confinement of the carriers. Figure 3 shows that the optical confinement factor changes from 1.21% to 0.89% for 12% and 20% Al-containing barrier/waveguide, respectively. Thus, in a simple approximation, one would expect the 12% Al barrier/waveguide structure to provide >35% improvement in modal gain compared with the 20% Al barrier/waveguide structure. The effect of this on device performance is clearly evident from figure 2(*a*) and table 1 where we find that the 12% Al-containing barrier/waveguide devices (sample C) have a RT J_{th} of 1.0–1.1 kA cm^{-2} compared with the 20% Al-containing barrier/waveguide devices (sample A) which have a substantially higher RT J_{th} of 1.5–1.6 kA cm^{-2}. Thus, it is clear that the in spite of the better electrical

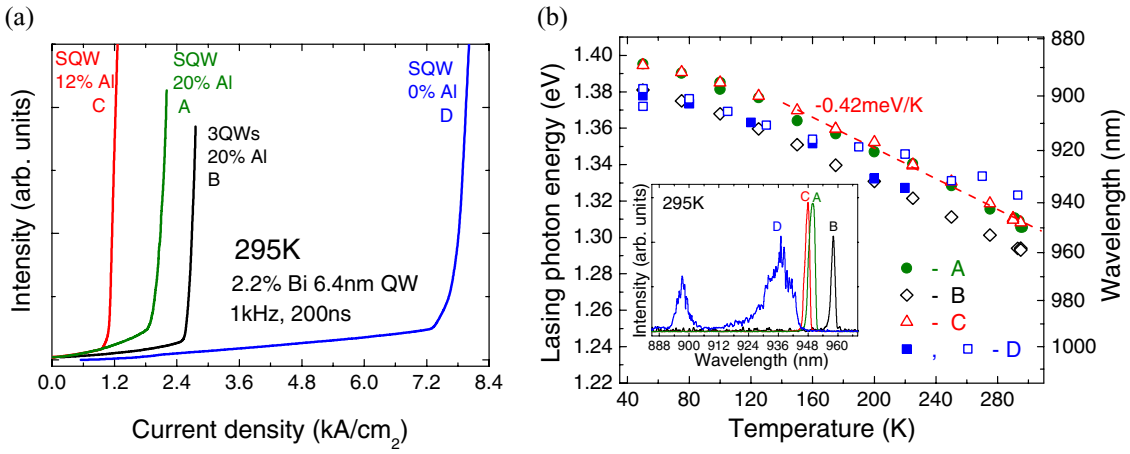

Figure 2. (*a*) Light-current characteristics at $T = 295$ K and (*b*) temperature dependence of the lasing photon energy of 2.2% Bi 6.4 nm SQW and 3QWs lasers with different Al composition in the waveguide/barrier layers (see details in table 1 for the samples A, B, C, D). Solid and open squares in (*b*) correspond to D devices with 100 μm and 50 μm stripes, respectively.

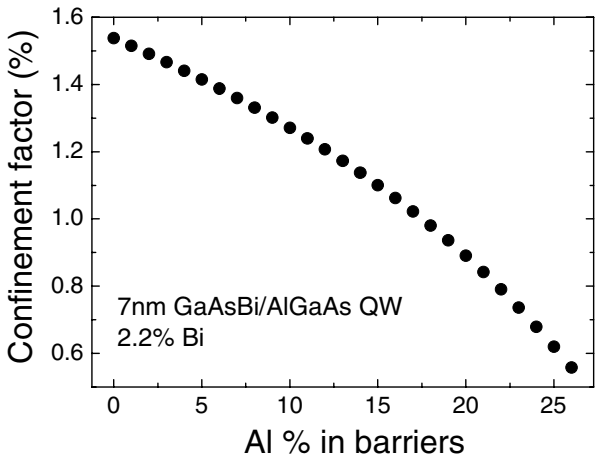

Figure 3. Dependence of the optical confinement factor of a GaAsBi/AlGaAs quantum well on composition of Al in the barriers.

confinement of carriers in the SQW device with 20% Al in the waveguide (sample A) compared to the corresponding 12% Al sample (sample C), the better optical confinement in the latter device resulted in an approximately 50% decrease in the RT J_{th}. However, as evidenced from sample D with a GaAs barrier/waveguide, the higher optical confinement factor cannot compensate for the very low electron confinement. These results clearly demonstrate the need to carefully design the barrier/waveguide structure in QW lasers with low Bi content.

The structures discussed thus far all consist of SQW active regions, however, optimized devices typically utilize a MQW active region. As an initial test of the influence of QW number, a 3QW structure (sample B) was grown based on the QW and barrier/waveguide compositions of structure A, the details of which are given in figure 2(*a*) and table 1. It was found that the 3QW devices exhibit a J_{th}/QW of $\sim$800 A cm^{-2}. This can be understood in terms of the increased optical confinement factor and the lower carrier density per QW required to achieve lasing threshold assuming negligible change in optical losses and material uniformity.

From table 1, we also note that the measured lasing wavelength of the devices agrees well with our band-anti-crossing modelling calculations [10]. The small deviation may be caused by many-body effects (band filling and band gap renormalization) under high carrier injection and non-idealities in the sample growth. The different devices also exhibited a broadly similar temperature dependence of the lasing photon energy with a gradient of -0.42 meV K^{-1} which is close to that for standard GaAs-based devices.

For all of the devices, whilst these results are promising, it is important to understand the origin of the relatively high J_{th} values and the extent to which J_{th} is temperature sensitive. To analyse the temperature-dependent performance and to identify the fundamental processes responsible for the relatively high J_{th} values, two techniques were used. Using direct measurements of pure spontaneous emission through a small circular window in the substrate contact (100 μm in diameter) [1, 16], the temperature dependence of the radiative component (J_{rad}) of the threshold current was analysed. In this method, J_{rad} is determined as the integrated spontaneous emission at the threshold current, which is proportional to the radiative recombination rate. Details of this approach are given in [1, 16]. Figure 4(*a*) shows that even in the best laser structure (sample C) the main contribution to the threshold current is due to a non-radiative recombination process. Both structures A and C showed a very similar temperature dependence of J_{th} with a characteristic temperature ($T_0 = (\mathrm{d}\ln J_{th}/\mathrm{d}T)^{-1}$) of $\sim$130 below 300 K and $T_0 \sim 100$ K at 300–350 K. In figure 4(*a*) J_{rad} was normalized to J_{th} at the lowest temperature where non-radiative/loss processes are expected to be minimized. For $T > 200$ K, an anomalous decrease of J_{rad} at threshold is observed because of the increasing absorption of the spontaneous emission by the GaAs substrate as shown in figure 4(*b*). At RT the shape of the high energy side of the spontaneous emission spectrum reflects the GaAs-substrate absorption edge, an effect previously seen in 960 nm InAs/GaAs quantum dot lasers [20]. Since $J_{rad} \propto T$ in an ideal QW laser [1], in figure 4 we used a linear interpolation of J_{rad} at low temperatures to estimate J_{rad} at RT. This assumption allows

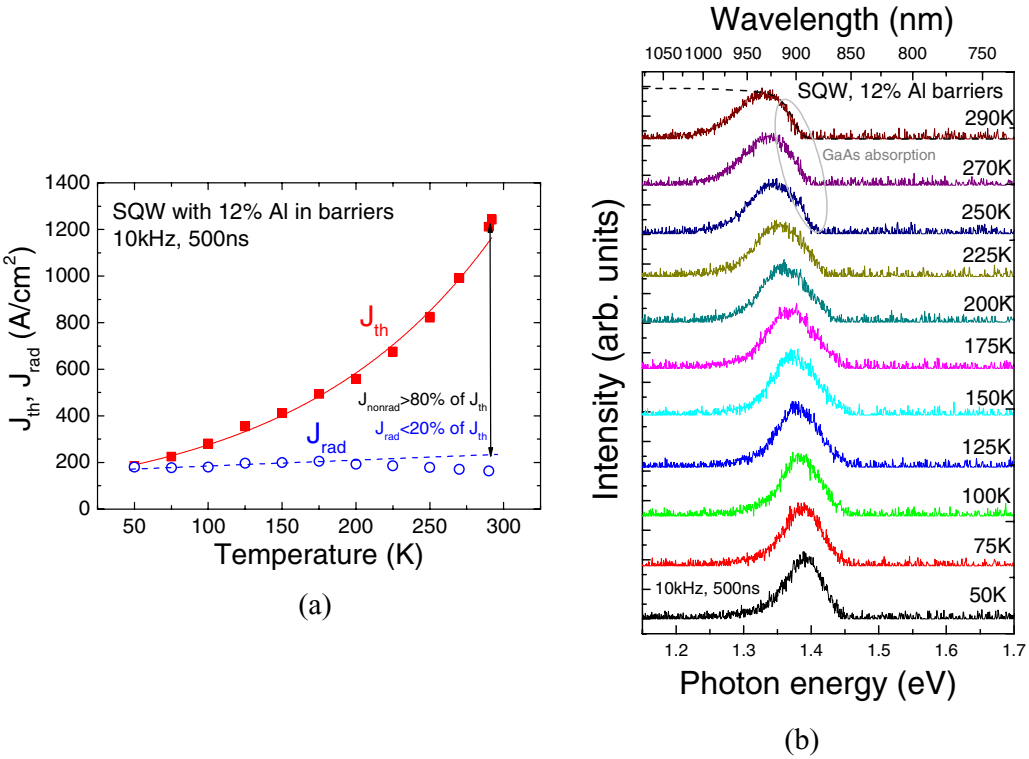

Figure 4. (*a*) Temperature dependence of J_{th} and J_{rad} in sample C with the lowest threshold current density at RT. J_{rad} was normalized to J_{th} at 50 K to estimate maximum value of ratio J_{rad}/J_{th} at RT. (*b*) Spontaneous emission spectra at the threshold. The dashed line presents a transmission spectrum of the GaAs substrate.

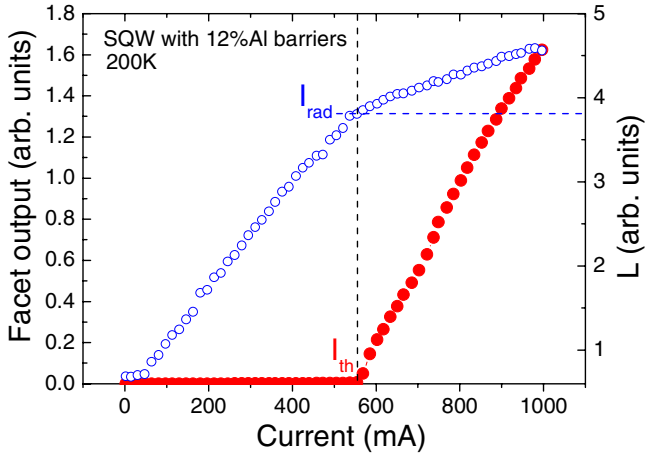

Figure 5. Light output from the laser facet (solid circles) and integrated spontaneous emission intensity (open circles) versus current density for device C at $T = 200$ K where influence of GaAs substrate absorption is not significant. Dashed lines show how J_{th} and J_{rad} were determined.

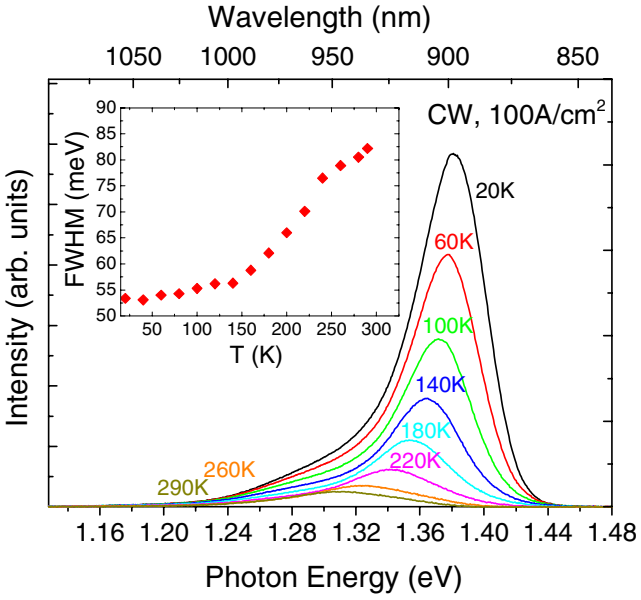

Figure 6. Spontaneous emission spectra of device A at low current (continuous wave mode, 100 A cm^{-2}) at different temperatures. The inset shows the temperature dependence of the FWHM of the spectra.

an estimation of the maximum value of J_{rad} and minimum value of the corresponding non-radiative current ($J_{non\text{-}rad}$) at lasing threshold. From figure 4 one can see that $J_{non\text{-}rad}$ accounts for up to 80% of the threshold current at RT. Very similar results were also observed in the sample A with 20% Al in the barriers.

The integrated spontaneous emission from the window and light output from the laser facet versus current density in the SQW device with 12% Al in barriers (sample C) at 200 K are presented in figure 5. In an ideal laser, the carrier density (and hence spontaneous emission) pins above threshold due to the onset of the fast stimulated emission process and the pinning of the quasi-Fermi levels [1]. In figure 5 we observe a degree of non-pinning in these devices above threshold. A non-pinned carrier density above threshold in the presence of non-radiative losses can further degrade the laser performance by reducing the laser light output and

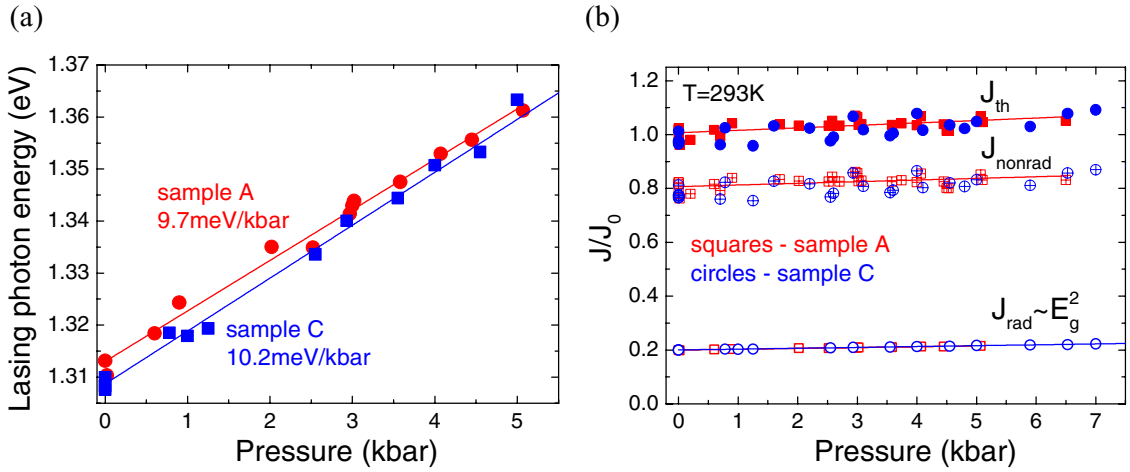

Figure 7. (*a*) Pressure dependence of the lasing photon energy (giving pressure dependence of E_g) in samples A and C. (*b*) Normalized threshold current density variation with pressure and its radiative and non-radiative components in A and C lasers. J_0 is a corresponding current density at atmospheric pressure.

the slope efficiency [21]. A possible explanation of this can be found at very low temperature (20–50 K) and low injected current density (100–150 A cm^{-2}) where we find that the full width at half maximum (FWHM) of the spontaneous emission spectra (55–65 meV) is $>10k_bT$ indicating a significant inhomogeneous broadening of the carrier distribution. As an example, the spontaneous emission spectra from sample A measured in CW mode at 100 A cm^{-2} and the corresponding FWHM are shown in figure 6.

To investigate the recombination and loss processes in these devices in more detail we applied high hydrostatic pressure to the devices. The application of pressure to a III–V semiconductor laser provides a useful means of (reversibly) varying the band gap in a fully-functioning device. The radiative and non-radiative recombination processes have characteristic dependencies on band gap, and hence high pressure can be used to identify the dominant recombination mechanisms [3, 16, 22]. From figure 4(*a*) it is apparent that even in the best 2.2% Bi containing QW devices reported here, more than 80% of J_{th} is wasted due to non-radiative recombination. Considering the different possible non-radiative recombination mechanisms, the emission wavelength of these devices is too short ($<1\,\mu$m) to expect a significant contribution from Auger recombination which typically becomes important in lasers emitting above 1.3 μm [1]. Auger recombination decreases strongly with increasing band gap (pressure) and hence in Auger dominated lasers, the threshold decreases with increasing pressure [3, 16, 22]. Carrier leakage into indirect satellite valleys, as often observed in visible lasers and quantum cascade lasers [17, 23] occurs when the Γ–X or Γ–L energy separations are small. Such a process typically gives rise to an exponential increase in J_{th} with pressure due to the fact that pressure causes a decrease in the Γ–X and Γ–L separation [16, 17, 23]. However, in these devices, the low Al composition in the barriers causes a large separation between Γ and X (L) indirect minima of the conduction band, and hence indirect carrier leakage is also not expected to be important in these devices. Non-radiative Shockley–Read–Hall (SRH) recombination due to defects occurs due to carriers recombining via localized states, releasing their energy in the form of phonons. This process is usually independent of pressure owing to the fact that shallow defect levels stay closely tied to the conduction band edge as pressure is applied [24]. In an ideal QW laser, the radiative part of threshold current increases approximately $\propto E_g^2$ [3, 16, 22] and for such devices, a weak increase in J_{th} with pressure would be expected.

To investigate the pressure dependence of J_{th}, we utilized a He-gas compressor connected to a pressure cell as described in [17]. The output emission from the laser facet was analysed using a broad area silicon detector with a power meter and an optical fibre coupled to an optical spectrum analyser. figure 7(*a*) shows the pressure dependence of the lasing peak energy for two of the 2.2% Bi laser structures (samples A and C). With the application of pressure the band gap increases causing an increase of the lasing photon energy at a rate of 9.7($\pm$0.3) meV kbar^{-1} and 10.2($\pm$0.2) meV kbar^{-1} in samples A and C, respectively, which is close to the pressure dependence of E_g in GaAs (9.8 meV kbar^{-1}) [25] and consistent with that previously observed for GaAsBi LEDs [13]. The pressure dependence of J_{th} for these structures is shown in figure 7(*b*). Also shown in the figure is the expected variation of J_{rad} with pressure. This has been calculated using the estimated J_{rad}/J_{th} ratio at room temperature (example shown in figure 4(*a*)) and under the assumption that $J_{rad} \propto E_g^2$ [3, 16, 22]. From this data, we can determine the pressure dependence of $J_{non\text{-}rad} = J_{th} - J_{rad}$ as shown in the diagram. In each case $J_{non\text{-}rad}$ has an almost constant pressure dependence, consistent with defect-related recombination dominating the non-radiative path. From the temperature and pressure dependence data, we therefore conclude that defect-related recombination dominates the devices and that further optimization of the growth of the GaAsBi/AlGaAs active regions is necessary.

Achieving the ultimate goal of Auger recombination suppression requires substantially higher ($>$12%) Bi fractions in the QW, which therefore needs the development of improved growth at higher Bi fractions. In this study samples with an increased Bi composition of 4.4% were grown (sample E),

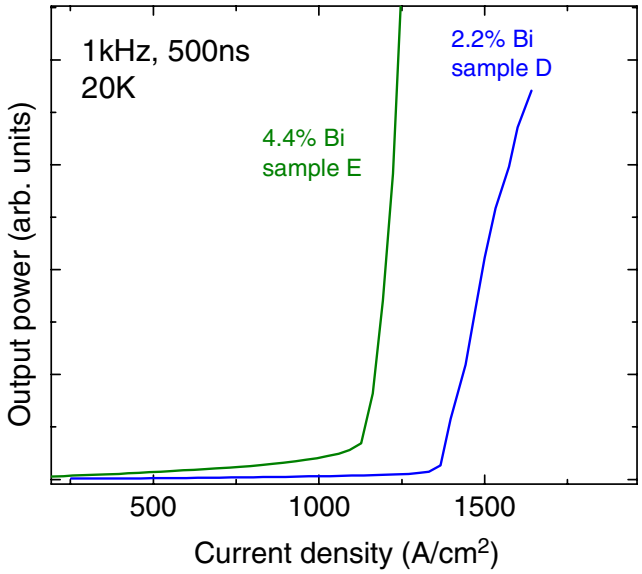

Figure 8. Output light intensity versus current density characteristics for SQW devices and GaAs barriers with 4.4% Bi (sample E) and 2.2% Bi (sample D) at $T = 20$ K.

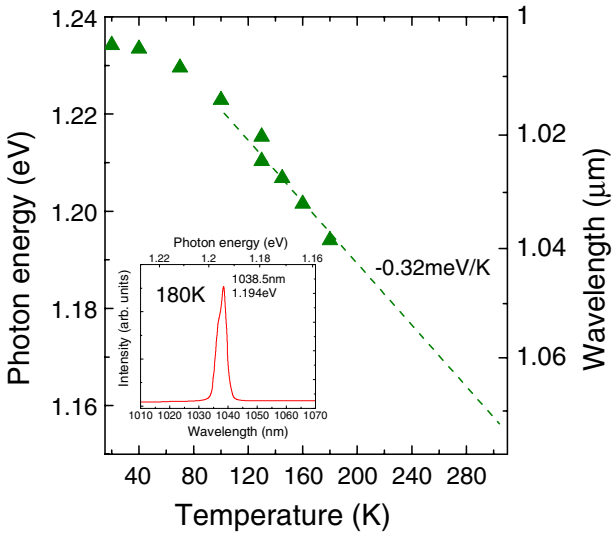

Figure 9. Lasing peak photon energy dependence on temperature of a laser with $GaAs_{0.956}Bi_{0.044}$ single quantum well (sample E). Insert shows a lasing spectrum at 180 K.

the details of which are provided in table 1. The threshold current density of these devices was substantially higher than the best 2.2% Bi-containing devices resulting in a reduced maximum operating temperature. In this device GaAs barriers were used leading to a relatively small electrical confinement in the conduction band (∼73 meV) which can partly explain the high threshold current density of 4.5 kA cm^{-2} at 180 K. For comparison, figure 8 shows the light versus current density characteristics for these devices (sample E) compared to the 2.2% Bi containing devices with GaAs barriers (sample D) at a low temperature of 20 K. The threshold current density for the sample E (4.4% Bi) at 20 K was 1.1 kA cm^{-2} compared with 1.4 kA cm^{-2} for the sample D (2.2% Bi) devices. Thus, in spite of the higher Bi content, at low temperature the 4.4% Bi devices E have a lower threshold current density than the 2.2% Bi D devices. The higher Bi fraction leads to larger band offsets and improved carrier confinement, which at low temperature, offsets the material quality issues associated with the higher Bi fraction. However, the fact that the higher Bi fraction devices have poorer high temperature characteristics suggests that the defect-related recombination may be more important at higher temperatures. This remains the subject of on-going investigations.

Figure 9 presents the temperature dependence of the lasing photon energy which decreased at a rate of 0.32 meV K^{-1} with increasing temperature. The inserts shows the lasing spectrum at 180 K where the lasing occurred at 1038 nm (1.195 eV) which is the longest emission wavelength currently in MOVPE-grown GaAsBi based laser diodes.

4. Conclusion

In summary, substantial progress in the development of GaAsBi/(Al)GaAs based lasers has been achieved with room temperature lasing in devices with 2.2% Bi and low temperature lasing in devices with 4.4% Bi. We have shown that the device performance can be improved by optimizing both electrical and optical confinement in the laser structures. However, these results also indicate that current device performance is dominated by non-radiative recombination through defects and that to further improve the device performance and move towards longer wavelength for optical telecommunications (1.3–1.5 μm) further effort is required to improve and optimize the material growth and device manufacturing.

Acknowledgments

We gratefully acknowledge financial support from the Engineering and Physical Sciences Research Council (EPSRC-grants EP/H005587/1 and EP/G064725/1), UK, the European Union Framework programme EU-FP7 'BIANCHO' project (FP7-257974) and the German Science Foundation (DFG: VO805/4 and DFG: GRK1782).

References

[1] Phillips A F, Sweeney S J, Adams A R and Thijs P J A 1999 The temperature dependence of 1.3 μm and 1.5 μm compressively strained InGaAs(P) MQW semiconductor lasers *IEEE J. Sel. Top. Quantum Electron.* **5** 401

[2] Sweeney S J *et al* 1998 The effect of temperature dependent processes on the performance of 1.5-μm compressively strained InGaAs (P) MQW semiconductor diode lasers *IEEE Photon. Technol. Lett.* **10** 1076–8

[3] Sweeney S J, Adams A R, Silver M, O'Reilly E P, Watling J R, Walker A B and Thijs P J A 1999 Dependence of threshold current on QW position and on pressure in 1.5 μm InGaAs(P) lasers *Phys. Status Solidi* b **211** 525

[4] Sweeney S J 2010 Bismide-alloys for higher efficiency infrared semiconductor lasers *Semiconductor Laser Conf. (ISLC) 22nd IEEE Int. (Kyoto, Japan)* pp 111–12

[5] Sweeney S J, McConville D, Masse N F, Bouyssou R-X, Adams A R, Ahmad C N and Hanke C 2004 Temperature

and pressure dependence of recombination processes in 1.5 μm InGaAlAs/InP-based quantum well lasers *Phys. Status Solidi* b **241** 3391

[6] Crowley M T, Marko I P, Masse N F, Andreev A D, Tomic S, Sweeney S J, O'Reilly E P and Adams A R 2009 The importance of recombination via excited states in InAs/GaAs 1.3 μm quantum-dot lasers *IEEE J. Sel. Top. Quantum Electron.* **15** 799–807

[7] Ishida M, Matsuda M, Tanaka Y, Takada K, Ekawa M, Yamamoto T, Kageyama T, Yamaguchi M, Nishi K, Sugawara M and Arakawa Y 2012 Temperature-stable 25-Gbps direct-modulation in 1.3-μm InAs/GaAs quantum dot lasers *Laser and Electro-Optics (CLEO) (San Jose, CA)* pp 1–2

[8] Marko I P, Massé N F, Sweeney S J, Andreev A D, Adams A R, Hatori N and Sugawara M 2005 Carrier transport and recombination in p-doped and intrinsic 1.3 μm InAs/GaAs quantum-dot lasers *Appl. Phys. Lett.* **87** 211114

[9] Usman M, Broderick C A, Batool Z, Hild K, Hosea T J C, Sweeney S J and O'Reilly E P 2013 Impact of alloy disorder on the band structure of compressively strained $GaBi_xAs_{1-x}$ *Phys. Rev.* B **87** 115104

[10] Sweeney S J and Jin S R 2013 Bismide-nitride alloys: promising for efficient light emitting devices in the near- and mid-infrared *J. Appl. Phys.* **113** 043110

[11] Alberi K, Wu J, Walukiewicz W, Yu K M, Dubon O D, Watkins S P, Wang C X, Liu X, Cho Y-J and Furdyna J 2007 Valence-band anticrossing in mismatched III–V semiconductor alloys *Phys. Rev.* B **75** 045203

[12] Batool Z, Hild K, Hosea T J C, Lu X F, Tiedje T and Sweeney S J 2012 The electronic band structure of GaBiAs/GaAs layers: influence of strain and band anti-crossing *J. Appl. Phys.* **111** 113108

[13] Hossain N, Marko I P, Jin S R, Hild K, Sweeney S J, Lewis R B, Beaton D A and Tiedje T 2012 Recombination mechanisms and band alignment of GaBiAs/GaAs LEDs *Appl. Phys. Lett.* **100** 051105

[14] Ludewig P *et al* 2013 Electrical injection Ga(AsBi)/(AlGa)As single quantum well laser *Appl. Phys. Lett.* **102** 242115

[15] Ludewig P *et al* 2014 Growth of Ga(AsBi) on GaAs by continuous flow MOVPE *J. Cryst. Growth* **396** 95

[16] Sweeney S J 2004 Novel experimental techniques for semiconductor laser characterisation and optimisation *Phys. Scr.* **2004** 152

[17] Marko I P, Adams A R, Sweeney S J, Teissier R, Baranov A N and Tomić S 2009 Evidence of carrier leakage into the L-valley in InAs-based quantum cascade lasers under high hydrostatic pressure *Phys. Status Solidi* b **246** 512–15

[18] Broderick C A, Usman M and O'Reilly E P 2013 12-band $k \cdot p$ models for dilute bismide alloys of (In)GaAs derived from supercell calculations *Phys. Status Solidi* b **250** 773

[19] Vurgaftman I, Meyer J and Ram-Mohan L R 2001 Band parameters for III–V compound semiconductors and their alloys *J. Appl. Phys.* **89** 5815

[20] Marko I P, Andreev A D, Adams A R, Krebs R, Reithmaier J P and Forchel A 2003 The role of Auger recombination in InAs 1.3 μm quantum dot lasers investigated using high hydrostatic pressure *IEEE J. Sel. Top. Quantum Electron.* **9** 1300–7

[21] Marko I P *et al* 2014 Effect of non-pinned carrier density above threshold in InAs quantum dot and quantum dash lasers *IET Optoelectron.* **8** 88–93

[22] Adams A R, Silver M and Allam J 1998 High pressure in semiconductor physics II: semiconductors and semimetals *Semiconductor Optoelectric Devices* ed T Suski and W Paul, vol 55 (London: Academic)

[23] Sweeney S J, Knowles G and Sale T E 2001 Evaluating the continuous-wave performance of AlGaInP-based red (667 nm) vertical-cavity surface-emitting lasers using low-temperature and high pressure techniques *Appl. Phys. Lett.* **78** 865

[24] Jin S R, Sweeney S J, Tomic S, Adams A R and Riechert H 2003 High-pressure studies of recombination mechanisms in 1.3-μm GaInNAs quantum-well lasers *IEEE J. Sel. Top. Quantum Electron.* **9** 1196

[25] Wei S H and Zunger Z 1999 Predicted band-gap pressure coefficients of all diamond and zinc-blende semiconductors: chemical trends *Phys. Rev.* B **60** 5404

5.8 Thermal quenching of photoluminescence in Ga(AsBi)[1]

M. K. Shakfa, M. Wiemer, P. Ludewig, K. Jandieri, K. Volz, W. Stolz, S. D. Baranovskii, M. Koch, Journal of Applied Physics **117**, 025709 (2015). DOI: 10.1063/1.4905687

Abstract

We report on a comparative experimental and theoretical study of the thermal quenching of the photoluminescence (PL) intensity in GaAsBi/GaAs heterostructures. An anomalous plateau in the PL thermal quenching is observed at intermediate temperatures under relatively low excitation intensities. Theoretical analysis based on the well-approved approach shows that this peculiar behavior points at a non-monotonous density of states (DOS) in the disorder-induced band tails with at least two-energy-scales. While in previous studies carried out at relatively high excitation intensities a single-energy-scale was sufficient to fit the thermal quenching of the PL in GaAsBi, our study at lower excitation intensities proves that both energy scales of disorder contribute to the thermal quenching of the PL. Possible energy shapes of the DOS, which can fit experimental data, are revealed.

The Authors contribution

My contribution to this work was the selection of the investigated sample and its growth by MOVPE and characterization concerning the composition and layer thickness. I was furthermore involved in the interpretation of the data and added an experimental part to the manuscript.

1 Reprinted with permission from *Journal of Applied Physics **117** (2015) 025709.*

JOURNAL OF APPLIED PHYSICS **117**, 025709 (2015)

Thermal quenching of photoluminescence in Ga(AsBi)

M. K. Shakfa,[a] M. Wiemer, P. Ludewig, K. Jandieri, K. Volz, W. Stolz, S. D. Baranovskii, and M. Koch
Department of Physics and Material Sciences Center, Philipps-University of Marburg, Renthof 5, 35032 Marburg, Germany

(Received 14 April 2014; accepted 24 December 2014; published online 12 January 2015)

We report on a comparative experimental and theoretical study of the thermal quenching of the photoluminescence (PL) intensity in Ga(AsBi)/GaAs heterostructures. An anomalous plateau in the PL thermal quenching is observed at intermediate temperatures under relatively low excitation intensities. Theoretical analysis based on a well-approved approach shows that this peculiar behavior points at a non-monotonous density of states (DOS) in the disorder-induced band tails with at least two-energy-scales. While in previous studies carried out at relatively high excitation intensities a single-energy-scale was sufficient to fit the thermal quenching of the PL in Ga(AsBi), our study at lower excitation intensities proves that two-energy-scales of disorder contribute to the thermal quenching of the PL. Possible energy shapes of the DOS, which can fit experimental data, are revealed. © *2015 AIP Publishing LLC*. [http://dx.doi.org/10.1063/1.4905687]

I. INTRODUCTION

Recently, much attention has been paid to the study of III-V-bismide ternary alloys such as Ga(NBi),[1] Ga(SbBi),[2] Ga(AsBi),[3] and In(PBi),[4] driven by not only their great potential for optoelectronic devices but also their interesting physical properties. In particular, Ga(AsBi) semiconductor alloys have been employed for a variety of applications including photoconductive terahertz antennas,[5] light-emitting diodes (LEDs),[6] and optically pumped[7] as well as electrically injected[8] laser diodes. The incorporation of Bi into GaAs is responsible for a strong shrinking in the bandgap energy as high as ∼62–84 meV/%Bi.[3,9,10] This is typically explained by a valence-band anti-crossing model, based on the interaction between the valence band of GaAs and resonant localized Bi states.[11] On the other hand, disorder effects, i.e., potential fluctuations associated with the Bi content together with the existence of Bi clusters within the alloy structure,[12] lead to an increasing density of localized states. This affects drastically carrier recombination processes, resulting in unusual characteristics which appear in photoluminescence (PL) spectra of Ga(AsBi): beside an asymmetric and obvious broad PL spectrum, a blue-shift of the excitation-dependent PL peak energy is observed at low temperature.[3,13] Moreover, the temperature dependence of the PL peak energy exhibits a non-monotonous behavior, the so-called S-shape.[14] Simultaneously, one observes a peak in the temperature-dependent PL linewidth around within a narrow temperature range.[12] A strong temperature dependence of the PL intensity is also observed in Ga(AsBi).[3,12,15] The PL intensity in disordered semiconductors, as in our case of Ga(AsBi), decreases dramatically with increasing temperature due to the increased nonradiative recombination of thermally delocalized carriers.[16]

The anomalous temperature-dependent PL peak energy as well as PL linewidth for Ga(AsBi) has been interpreted in the framework of a model with two spatial and energy scales for the disorder potential.[12] Within this two-scale model, the density of localized states below the mobility edge (DOS) is described by two different energy distributions:[12] (i) a Gaussian energy distribution corresponding to a long-range disorder, conditioned by the fluctuations of the Bi content in the alloy and (ii) an exponential energy distribution corresponding to a short-range disorder, which was ascribed to Bi clusters. The spatially much more localized states of the exponential energy scale form an exponential tail for each of the spatially more extended states of the Gaussian energy scale. Hence, the overall DOS is a convolution of the Gaussian and exponential distributions of states. On the other hand, the thermal quenching of the integrated PL intensity within this two-scale model has been treated using only the exponential DOS corresponding to the short-range disorder. Such approach was motivated by the assumption that Gaussian states are so much extended in space that an exciton being thermally excited from the exponential DOS tail to the corresponding Gaussian state can encounter centers of nonradiative recombination from this state.

In this paper, we show that conventional theoretical models assuming an monotonous, e.g., exponential,[12] DOS for the short-range disorder cannot be considered as an universal approach for the correct description of the PL thermal quenching in Ga(AsBi) alloys. In our experimental studies, a peculiar feature is observed in Ga(AsBi)/GaAs heterostructures under relatively low excitation intensities, i.e., the temperature-induced PL quenching exhibits an anomalous plateau at intermediate temperatures. Our general arguments lead to the conclusion that a non-monotonic DOS with at least two different components is necessary to explain the observed PL quenching. These components have different energy—but comparable spatial—scales. The localization length of the states in both components of the DOS is assumed to be so small that excitons cannot encounter centers of nonradiative recombination from these states. Instead, the excitons must be excited above the mobility edge in

[a]Electronic mail: m.k.shakfa@gmx.de

order to recombine nonradiatively.[17–19] Therefore, in contrast to the two-scale model suggested in Ref. 12, both components of the DOS and, hence, both energy scales are relevant for the theoretical description of the PL thermal quenching in Ga(AsBi) alloys.

The paper is organized as follows. The details and the results of our experimental studies are given in Secs. II and III, respectively. Section IV presents the theoretical treatment of the observed PL thermal quenching in the framework of the suggested two-component model. A detailed comparison of our two-component and conventional two-scale models is given in Sec. V. Concluding remarks are gathered in Sec. VI.

II. EXPERIMENTAL DETAILS

The samples used in this study are a series of $Ga(As_{1-x}Bi_x)/GaAs$ heterostructures with Bi contents of $x = 2.9\%$, 3.2%, 4.2%, and 4.5%, which are grown by metal organic vapor phase epitaxy (MOVPE) on undoped exact (001) GaAs substrates.[20] The growth is taken place in a commercially available horizontal reactor system with gas flow rotation (AIX 200-GFR-reactor) at a reduced reactor pressure of 50 mbar using Pd purified H_2 as carrier gas and triethylgallium (TEGa), tertiarybutylarsine (TBAs), and trimethylbismuth (TMBi) as precursors. The growth temperature is set to 400 °C. High resolution x-ray diffraction $\omega - 2\theta$ scans around the (004) reflection peak of GaAs are performed to determine the Bi fraction and layer thickness. The thicknesses of $Ga(As_{1-x}Bi_x)$ layers are 60, 59, 34, and 25 nm for $x = 2.9\%$, 3.2%, 4.2%, and 4.5%, respectively. All studied samples are deposited on a 250 nm thick GaAs buffer layer and capped by a 20 nm thick GaAs layer, both are grown at 625 °C.

For temperature-dependent measurements, the samples are mounted at the end of a cold finger fixed inside a liquid-helium-flow microscopy-cryostat. A temperature-sensor is also integrated inside the cryostat and directly connected to a temperature controller. The latter is also united with a suction pump used to suck up the helium that flows through the cryostat. Subsequently, the samples' temperature is adjusted between 10 K and room temperature (RT), i.e., 292 K by controlling both the sample heating and the helium flow. Furthermore, the samples are kept under a very low dynamic vacuum using a vacuum pump in order to avoid condensation forming on the sample's surface.

PL measurements are performed using a mode-locked Ti:sapphire laser tuned to 780 nm with a repetition rate of 80 MHz and a pulse duration of 100 fs. The laser beam is focused on the sample down to a spot size of 30 μm in diameter. An average excitation density used for all measurements is set to 142 W/cm^2 for an average laser power of 1 mW. The PL signal is collected normal to the sample surface in a reflection geometry, then spectrally dispersed by an imaging spectrometer and ultimately detected by a streak camera.

III. EXPERIMENTAL RESULTS

Fig. 1(a) shows PL spectra of the Ga(AsBi)/GaAs heterostructure with Bi content of 4.2% measured at various

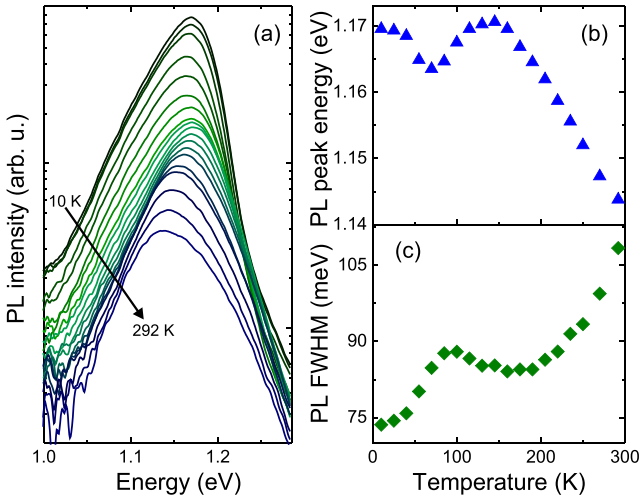

FIG. 1. Temperature-dependent PL spectra (a), PL peak energy (b) and PL FWHM (c) of the Ga(AsBi)/GaAs heterostructure with Bi content of 4.2%.

temperatures in a range from 10 K to RT. At low temperatures, PL emission peaks are significantly broad and show an asymmetric lineshape with a low energy tail. This reflects the fact that the dominant contribution to the PL arises from localized electron–hole pairs.[21] The temperature dependencies of the PL peak energy and the corresponding full width at half maximum (FWHM), shown in Figs. 1(b) and 1(c), respectively, follow the main trends common for disordered compound semiconductors. In particular, the PL peak energy exhibits a typical S-shape behavior with local minimum around 70 K, whereas the PL FWHM shows a local maximum of about 88 meV at a temperature of approximately 100 K. These specific features are generally attributed to the hopping dynamics of photo-excited excitons between disorder-induced localized states.[22]

In contrast to the temperature dependencies of the PL peak energy and the PL FWHM, the thermal quenching of the integrated PL intensity, shown in Fig. 2(a), exhibits an odd behavior as compared to common tendencies previously observed in disordered semiconductors[16,23,24] and also differs from the PL thermal quenching behavior in typical semiconductors like GaAs.[25] The latter is shown in Fig. 2(b). The prominent characteristic of the typical PL thermal quenching in disordered semiconductors is a relatively weak temperature dependence at low temperatures, followed by a dramatic decline in an intermediate range of temperature, and ultimately, by a saturation close to RT. As an example, the typical temperature-induced quenching of the PL intensity observed in Ga(NAsP)/GaP quantum wells[16] is shown in Fig. 2(c). Remarkably, a similar behavior has been reported in Ga(AsBi) under relatively high excitation intensities.[12] However, in our case of a relatively low excitation intensity, the situation is essentially different. The PL thermal quenching can be clearly distinguished in three regimes. A plateau area (shaded area between 115 K and 235 K in Fig. 2(a)) with rather weak temperature dependence separates two major regimes, where the quenching rate of the PL intensity is much faster. A similar peculiar behavior of the PL thermal quenching in Ga(AsBi) has been also observed elsewhere.[15]

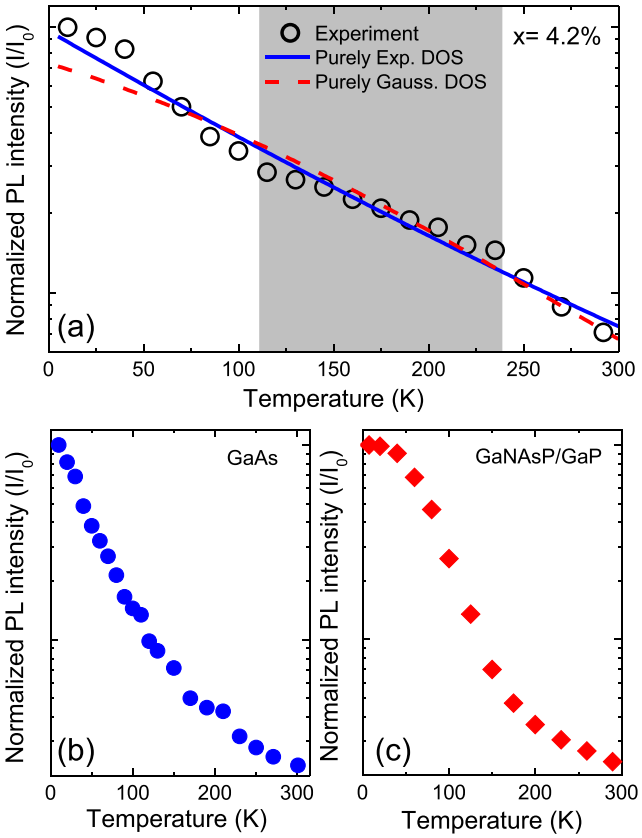

FIG. 2. (a) The temperature-dependent integrated PL intensity (I) of the sample with Bi content of 4.2%. Open circles indicate the experimental data, normalized to the PL intensity at 10 K (I_0). Theoretical results obtained from Eq. (3) are shown by solid and dashed lines for purely exponential DOS (Eq. (5) with $\varepsilon_M = 0$) and purely Gaussian DOS (Eq. (6) with $\varepsilon_M = 0$), respectively. The experimental data of the normalized PL intensity as a function of the temperature for GaAs layer and Ga($N_{0.04}As_{0.80}P_{0.16}$)/GaP quantum wells are presented in (b) and (c), adapted from Refs. 25 and 16, respectively.

Such specific temperature behavior motivates us to assume different sources for thermal activation of excitons from localized states into the extended states (with further recombination by nonradiative centers) and, hence, extend the conventional model with monotonous *single* shape DOS. Next, we demonstrate that a DOS with *two* different components is essential for a correct theoretical interpretation of our experimental observations.

IV. THEORETICAL ANALYSIS

In order to analyze our experimental data, we exploit a model of the PL thermal quenching suggested by Gee and Kastner[26] for semiconductors with extended band tails caused by the disorder potential. According to this model, the exponential temperature dependence of the PL intensity, $I(T) \propto \exp(-T/T_1)$ with some characteristic T_1, is due to the exponential distribution of energy barriers for nonradiative processes. Later, Orenstein and Kastner[17] as well as Street[27] ascribed the distribution of barriers to the density of localized states $g(\varepsilon)$ in the band tails of disordered semiconductors. Herewith, it was assumed that nonradiative recombination occurs via thermal activation of photoinduced excitons from radiative localized band tail states towards the mobility edge, since only mobile excitons are able to reach the spatially remote centers of nonradiative recombination. Assuming that the exciton thermally activated to the mobility edge does not necessarily recombine nonradiatively but can be recaptured into a radiative state, the nonradiative recombination rate can be expressed as

$$\nu_{nr} = \nu_0 \cdot \exp\left(-\frac{\varepsilon}{k_B T}\right) \cdot \frac{\sigma_{nr} N_{nr}}{\sigma_r N_r + \sigma_{nr} N_{nr}}, \tag{1}$$

where ν_0 is the attempt-to-escape frequency for the activation process, ε is the energy of the localized state measured from the mobility edge, k_B is the Boltzmann constant, T is the temperature and N_{nr}, σ_{nr} and N_r, σ_r are the density and capture cross sections of nonradiative and radiative centers, respectively. Equation (1) together with the radiative recombination rate $\nu_r = \tau_0^{-1}$, where τ_0 is the exciton lifetime, gives the following expression for the probability of radiative recombination

$$p(\varepsilon, T) = \left[1 + \frac{\nu_0 \tau_0 \sigma_{nr} N_{nr}}{\sigma_r N_r + \sigma_{nr} N_{nr}} \exp\left(-\frac{\varepsilon}{k_B T}\right)\right]^{-1}. \tag{2}$$

For the given density of localized states $g(\varepsilon)$ and for the probability of radiative recombination $p(\varepsilon, T)$ determined from Eq. (2), the temperature-dependent PL intensity can then be described as

$$I(T) = I_0 \int_0^\infty g(\varepsilon) \cdot p(\varepsilon, T)\, d\varepsilon, \tag{3}$$

where I_0 is the PL intensity at zero temperature.[26]

Trying to apply Eqs. (2) and (3) in combination with the commonly used exponential DOS, $g(\varepsilon) \propto \exp(-\varepsilon/\sigma)$ with some characteristic energy σ, we conclude that it is not possible to fit the experimentally observed $I(T)$. While the measured temperature dependence of the PL intensity shows a peculiar plateau at temperatures between 115 K and 235 K, no theoretical curves based on the exponential DOS can reproduce this behavior as illustrated by the blue solid curve in Fig. 2(a). Moreover, replacing the exponential DOS with a Gaussian DOS, $g(\varepsilon) \propto \exp(-\varepsilon^2/2\sigma^2)$, does not help to account for the plateau in the experimental dependence $I(T)$ as illustrated by the red dashed curve in Fig. 2(a).

Furthermore, let us show that it is generally impossible to obtain such a plateau in the dependence $I(T)$ with any monotonous distribution function $g(\varepsilon)$ in Eq. (3). The plateau of $I(T)$ is characterized by a certain temperature T_p at which the curvature vanishes, i.e., $d^2I/dT^2(T_p) = 0$. After using $p(\varepsilon, T) = p(\varepsilon/T)$ for transformation of the derivative d^2p/dT^2 and performing a partial integration, we are left with following expression:

$$\frac{d^2 I}{dT^2}(T_p) = -I_0 \int_0^\infty \frac{dg}{d\varepsilon'}(\varepsilon)\, \varepsilon^2\, \frac{dp}{d\varepsilon'}(\varepsilon, T_p)\, d\varepsilon = 0.$$

Since $\varepsilon^2\, dp/d\varepsilon$ is always positive, the quantity $dg/d\varepsilon$ must exhibit a change in sign in the interval $(0,\infty)$ in order to let

the integral vanish and fulfil the condition $d^2I/dT^2(T_p) = 0$. In other words, in order to obtain a plateau in the dependence $I(T)$ using Eq. (3), it is necessary that $g(\varepsilon)$ is a non-monotonous function.

Since a monotonous distribution of localized states below the mobility edge is incapable to reproduce the plateau in the dependence $I(T)$, we employed combinations of the two most prominent energy distributions in disordered systems,

$$g(\varepsilon;\varepsilon_M,\sigma_1,\sigma_2) = (1-y)\,g_1(\varepsilon;0,\sigma_1) + y\,g_2(\varepsilon;\varepsilon_M,\sigma_2), \quad (4)$$

where g_1 and g_2 are either of exponential (g_E) or Gaussian type (g_G) with

$$g_E(\varepsilon;\varepsilon_M,\sigma) = \Theta(\varepsilon-\varepsilon_M)\frac{1}{\sigma}\,\exp\left(-\frac{\varepsilon-\varepsilon_M}{\sigma}\right), \quad (5)$$

and

$$g_G(\varepsilon;\varepsilon_M,\sigma) = \frac{1}{\sqrt{2\pi}\,\sigma\,\Phi\left(\frac{\varepsilon_M}{\sigma}\right)}\,\exp\left[-\frac{1}{2}\left(\frac{\varepsilon-\varepsilon_M}{\sigma}\right)^2\right]. \quad (6)$$

Here, Θ and Φ denote the Heaviside step-function and the normal cumulative distribution function, respectively, and σ_1 and σ_2 are characteristic energies. Four different distribution functions arise from this definition of $g(\varepsilon)$, a double exponential DOS, a double Gaussian DOS, and two composite DOS's with exponential and Gaussian parts. In the two cases of $g_2 = g_E$, a mathematical unsteadiness appears at ε_M in the DOS due to the Heaviside step-function which may seem unphysical. Despite this artificial structure of the unsteady DOS, we will attempt all four distributions in order to account for our experimental data.

Considering ε_M, σ_1, and σ_2 as fitting parameters, we obtain excellent agreement between the measured temperature dependence of the PL intensity and the theoretical curves obtained from Eqs. (2) to (6) for all four possible combinations of the DOS. This is shown in Figs. 3(a), 3(c), 3(e), and 3(g) along with the corresponding shape of the DOS in Figs. 3(b), 3(d), 3(f), and 3(h) for "exponential plus exponential", "exponential plus Gaussian", "Gaussian plus exponential", and "Gaussian plus Gaussian" distributions, respectively. The respective contributions from the first $(1-y)\,g_1$ and second $y\,g_2$ parts of the DOS to the overall PL intensity are also depicted in Figs. 3(a), 3(c), 3(e), and 3(g) by dashed red and dashed-dotted green curves, respectively. The corresponding values of fitting parameters ε_M, σ_1, σ_2, and y are summarized in Table I. Around $y = 10\%$ of the states of the composite $g(\varepsilon)$ are provided by second parts $g_2(\varepsilon;\varepsilon_M,\sigma_2)$ whose maxima ε_M vary between 129 meV and 155 meV. The characteristic energies σ_1 and σ_2 of the two parts of the composite DOS lay between 17 meV and 33 meV. It should be noted that the given values of y, ε_M, σ_1, and σ_2 do also depend upon the parameter $\nu_0\tau_0(1+\sigma_r N_r/\sigma_{nr}N_{nr})^{-1}$, which is set to 10^{-3} after Ref. 12.

For further assessment of our above-motioned approach, the experimental results for each of other $Ga(As_{1-x}Bi_x)$/GaAs heterostructures are also theoretically discussed in a

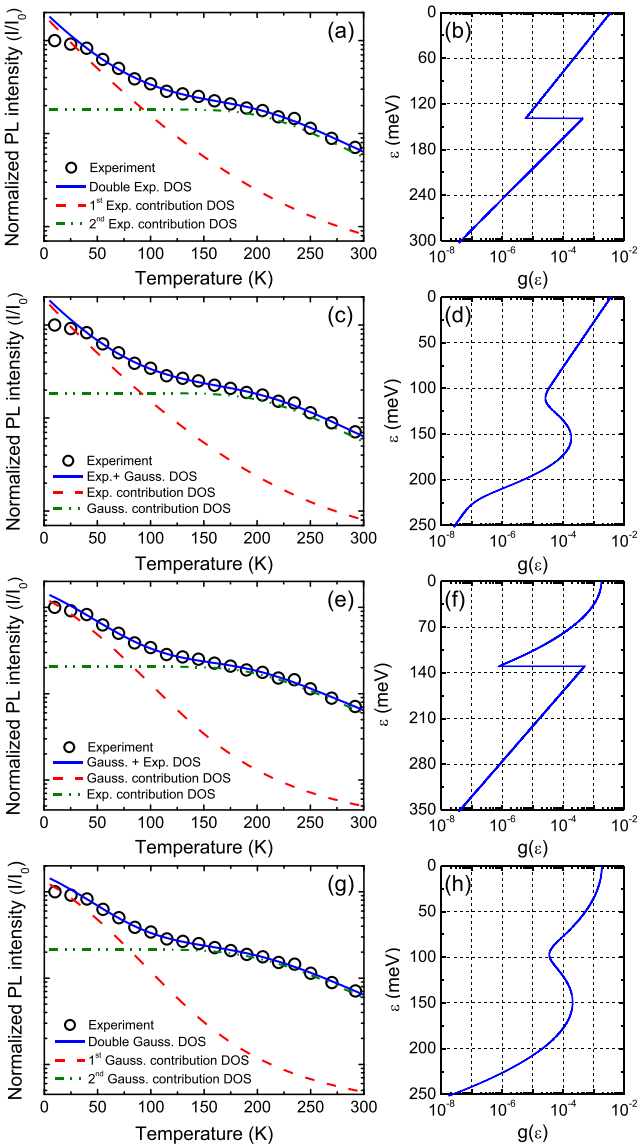

FIG. 3. Left-hand panels: temperature-dependent integrated PL intensities from experiment (open circles) and theory (lines). The blue solid lines are calculated from Eqs. (2) to (6) assuming either a double–exponential (a), an exponential–plus–Gaussian (c), a Gaussian–plus–exponential (e), or a double–Gaussian (g) distribution of localized states. Their respective contributions from each of the two parts of the composite DOS are depicted by the red dashed and green dashed-dotted curves. Right-hand panels: (b), (d), (f), and (h) show the densities of localized states $g(\varepsilon)$ as a function of the energy ε difference from the mobility edge for each of the blue lines in (a), (c), (e), and (g), respectively.

TABLE I. Fit parameters, obtained by minimizing the deviations of $I(T)$ calculated with Eq. (3) from the measured one, for various DOSs extracted from Eqs. (4)–(6).

g_1	g_2	y (%)	σ_1 (meV)	σ_2 (meV)	ε_M (meV)
g_E	g_E	9	22	17	139
g_E	g_G	9	21	17	155
g_G	g_E	14	33	23	129
g_G	g_G	14	32	24	149

similar way that used for the sample with $x = 4.2\%$. An excellent agreement is obtained between theoretical calculations and experimental results for all studied samples. Figs. 4(a)–4(c) show the theoretical and experimental results for the samples with $x = 2.9\%$, 3.2%, and 4.5% in the case of the DOS consists of exponential and Gaussian components, respectively. The corresponding fit parameters of energy-scales are summarized in Table II. The peak position ε_M of the second component of the DOS obviously decreases with increasing Bi content from around 190 meV for $x = 2.9\%$ to around 140 meV for $x = 4.5\%$. It may be explained with increasing repulsive interactions between neighboring localized centers, lattice distortions, or the shift of the valence band edge as x increases. The width σ_1 of the first part of the DOS does also decrease with increasing Bi content from 31 meV for $x = 2.9\%$ to 12 meV for $x = 4.5\%$. This behaviour can be related to the shrinkage of the distribution of localized states when the impurity band forms with increasing Bi content.[28] Only the width σ_2 of the second part of the DOS shows no straight tendency as a function of Bi content.

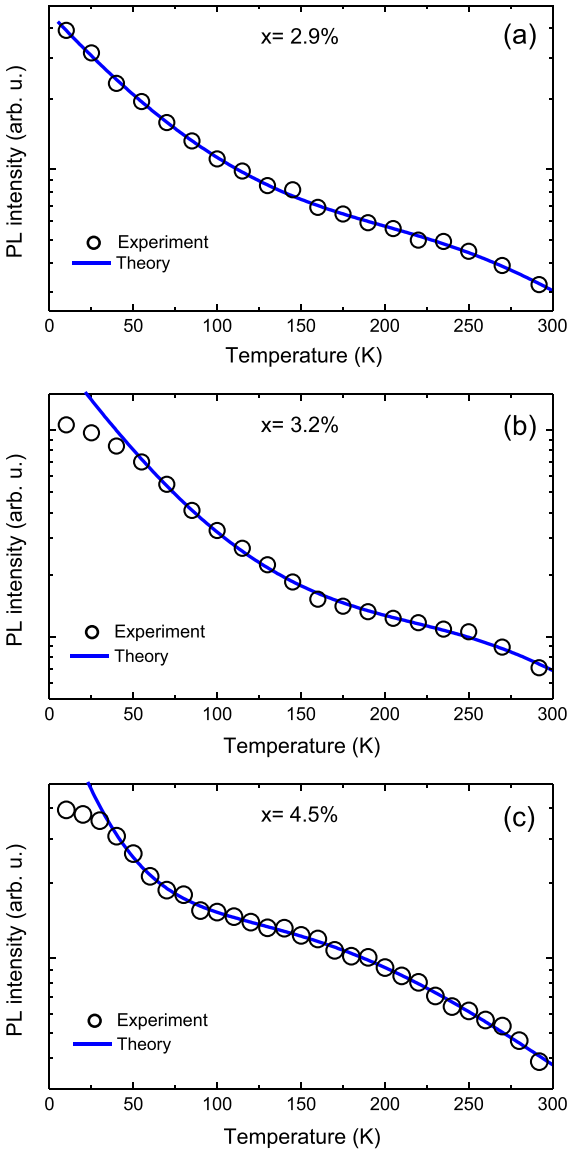

FIG. 4. Temperature-dependent integrated PL intensities of $Ga(As_{1-x}Bi_x)$/GaAs heterostructures from experiment (open circles) and theory (lines) for the DOS consists of exponential and Gaussian components, respectively.

TABLE II. Fit parameters in the case of the DOS consists of exponential and Gaussian components.

Bi–content (%)	σ_1 (meV)	σ_2 (meV)	ε_M (meV)
2.9	31	23	189
3.2	23	16	194
4.2	21	17	155
4.5	12	44	137

The plateau in the temperature-dependent PL intensity arises due to the following reason: at low temperatures, the PL intensity is dominated by excitons from the shallow part of the DOS (g_1). Due to their energetic proximity to the mobility edge, these excitons get rapidly quenched with rising temperature. On the other hand, the deeper laying excitons in the second part of the band tail are hardly affected by the thermal activation at low temperatures. Thus, they keep the PL intensity at a certain level until their rates for nonradiative recombination exceed the radiative recombination rate at high temperatures.

V. DISCUSSION

Our theoretical analysis shows that the PL thermal quenching in $Ga(As_{1-x}Bi_x)$/GaAs heterostructures is well reproduced on basis of Eq. (3) together with different two-component DOS's, extracted from Eqs. (4)–(6). From a computational point of view, none of the four tested composite DOS's is more favorable than others, even though, from a physical point of view, the two steady combinations with $g_2 = g_G$ are, of course, more reasonable. This clearly demonstrates, however, how important is to extend the monotonous DOS, i.e., adding further states to an exponential or Gaussian DOS tail, in order to fit the observed temperature-dependent PL intensity with its plateau at intermediate temperatures. On the other hand, the extension of the DOS is corresponded to the assumption of deep laying localized states. While the nonradiative recombination effectively occurs only above the mobility edge, trapped excitons in these deep states recombine radiatively, resulting in a very weak decrease of the PL intensity at intermediate temperatures. According to our results, deep localized states may be somewhere in the order of 100 meV away from the mobility (or band) edge. However, a reliable number for the bandgap energy is scarcely achievable for some currently unknown parameters in the equations like the density of nonradiative centers or their capture cross section.

From the existence of deep localized states, one would intuitively expect the PL spectrum to exhibit a distinct second, lower-in-energy peak appearing at intermediate temperatures. This is not the case as can be seen in Fig. 1(a) for the sample with Bi content of 4.2%. However, the existing PL peak is very broad and, hence, might easily cover two peaks. In most cases, the PL features caused by sometimes non-

monotonous DOS cannot be clearly distinguished due to, e.g., the short energetic distance between localized states (or bands).[3,12,13,24] Furthermore, the broadening of the PL emission from different localized states (bands) results in an overlap between their PL spectra. At the end, all contributed PL emissions are covered by an envelope curve, which is the detected PL spectrum. Therefore, the non-existence of a second peak in the PL spectrum alone cannot be seen as indicator for invalidity of the two-component DOS model proposed here.

Equation (3), which is the basis for our analysis, does not take into account hopping transitions of excitons between localized states. Such transitions are known to cause a plateau in the dependence $I(T)$ only at very low temperatures, at which the experimentally observed PL thermal quenching has not yet started.[16] However, hopping processes do not essentially affect the thermal quenching of the PL intensity at moderate temperatures under consideration in our case. Therefore, we think that our approach based on Eq. (1) is valid to study the plateau in the dependence $I(T)$ at intermediate temperatures.

Finally, let us consider the conventional two-scales model, which was proposed for the quantitative description of disorder-induced PL characteristics in Ga(AsBi),[12] and stress the differences to our two-components model. In both models, the DOS consists of two-energy-scales. However, in the two-scales model, the offset of the *second* exponential energy scale follows the long-range fluctuations of the *first* Gaussian energy scale resulting in a convolution of both energy distributions, whilst in our two-components model both energy distributions exist independently from each other resulting in a simple summation of both distributions. Moreover, in the two-scales model, excitons do not need to be lifted above the mobility edge to recombine nonradiatively but can be quenched already in the states of the Gaussian DOS with their large localization lengths. As a consequence of this assumption, the two-scale model reduces to an effective one-scale model with a *single* exponential energy distribution with respect to the PL thermal quenching since exciton quenching from localized states is driven only by the energetic difference to the states with a nonradiative recombination channel. Even without nonradiative recombination in Gaussian states, the DOS in the two-scale model would still be monotonous. Hence, the two-scale model would be incapable to reproduce a plateau in the dependence $I(T)$ at intermediate temperatures. An additional radiative channel, resulting from the extension of the DOS, is essential to produce the nearly temperature-independent PL intensity in the intermediate range of temperature.

VI. CONCLUSION

The temperature-dependent PL of a MOVPE-grown $Ga(As_{1-x}Bi_x)/GaAs$ heterostructures with different Bi contents of $x = 2.9\%$, 3.2%, 4.2%, and 4.5% is studied. The dependence of the PL peak energy as well as the PL FWHM on the temperature shows typical disorder-induced characteristics. However, we observed an unexpected thermal quenching behavior of the PL intensity under relatively low excitation intensities, e.g., the PL intensity is nearly temperature-independent in the range between 115 K and 235 K in the case of the sample with Bi content of 4.2%. Previously, a model with a monotonous *single-energy-scale* DOS[16] has been reported to be enough to fit the PL thermal quenching in disordered Ga(AsBi) under relatively high excitation intensities.[12] Our study, in contrast, demonstrates that an approach with a non-monotonous *two-component* DOS with two-energy-scales is indispensable to achieve a good agreement between experiment and theory for the anomalous plateau in the PL thermal quenching, observed in our case at lower excitation intensities. Several shapes of two-component DOS are used to fit the experimental data of the PL thermal quenching. By this means, we obtained almost perfect matching between experiment and theory. The non-monotonous DOS shapes imply the presence of deep-laying localized states in the bandgap. Consequently, we take the observed plateau in the thermal quenching of the PL intensity as a hint for the existence of such deep localized states in the bandgap of Ga(AsBi). However, further studies will be necessary in order to verify and characterize these states.

ACKNOWLEDGMENTS

Financial supports from the German Science Foundation (DFG) through the Research Training Group (GRK 1782): *Functionalization of Semiconductors* and the Collaborative Research Centre (SFB 1083): *Structure and Dynamics of Internal Interfaces* and from the European Union Framework 7 Project BIANCHO (FP7-257974) are gratefully acknowledged.

[1]A. X. Levander, K. M. Yu, S. V. Novikov, A. Tseng, C. T. Foxon, O. D. Dubon, J. Wu, and W. Walukiewicz, Appl. Phys. Lett. **97**, 141919 (2010).
[2]X. Chen, Y. Song, L. Zhu, S. M. Wang, W. Lu, S. Guo, and J. Shao, J. Appl. Phys. **113**, 153505 (2013).
[3]M. K. Shakfa, D. Kalincev, X. Lu, S. R. Johnson, D. A. Beaton, T. Tiedje, A. Chernikov, S. Chatterjee, and M. Koch, J. Appl. Phys. **114**, 164306 (2013).
[4]T. D. Das, J. Appl. Phys. **115**, 173107 (2014).
[5]K. Bertulis, A. Krotkus, G. Aleksejenko, V. Pačebutas, R. Adomavičius, G. Molis, and S. Marcinkevičius, Appl. Phys. Lett. **88**, 201112 (2006).
[6]R. Lewis, D. Beaton, X. Lu, and T. Tiedje, J. Cryst. Growth **311**, 1872 (2009).
[7]Y. Tominaga, K. Oe, and M. Yoshimoto, Appl. Phys. Express **3**, 062201 (2010).
[8]P. Ludewig, N. Knaub, N. Hossain, S. Reinhard, L. Nattermann, I. P. Marko, S. R. Jin, K. Hild, S. Chatterjee, W. Stolz, S. J. Sweeney, and K. Volz, Appl. Phys. Lett. **102**, 242115 (2013).
[9]S. Tixier, M. Adamcyk, T. Tiedje, S. Francoeur, A. Mascarenhas, P. Wei, and F. Schiettekatte, Appl. Phys. Lett. **82**, 2245 (2003).
[10]V. Pačebutas, K. Bertulis, G. Aleksejenko, and A. Krotkus, J. Mater. Sci.: Mater. Electron. **20**, S363 (2009).
[11]K. Alberi, O. D. Dubon, W. Walukiewicz, K. M. Yu, K. Bertulis, and A. Krotkus, Appl. Phys. Lett. **91**, 051909 (2007).
[12]S. Imhof, A. Thränhardt, A. Chernikov, M. Koch, N. S. Köster, K. Kolata, S. Chatterjee, S. W. Koch, X. Lu, S. R. Johnson, D. A. Beaton, T. Tiedje, and O. Rubel, Appl. Phys. Lett. **96**, 131115 (2010).
[13]Y. I. Mazur, V. G. Dorogan, M. Schmidbauer, G. G. Tarasov, S. R. Johnson, X. Lu, S.-Q. Yu, Zh. M. Wang, T. Tiedje, and G. J. Salamo, Nanotechnology **22**, 375703 (2011).
[14]Y.-H. Cho, G. H. Gainer, A. J. Fischer, J. J. Song, S. Keller, U. K. Mishra, and S. P. DenBaars, Appl. Phys. Lett. **73**, 1370 (1998).
[15]A. R. Mohmad, F. Bastiman, J. S. Ng, S. J. Sweeney, and J. P. R. David, Phys. Status Solidi C **9**, 259 (2012).

[16]O. Rubel, S. D. Baraovskii, K. Hantke, W. W. Ruhle, P. Thomas, K. Volz, and W. Stolz, Phys. Rev. B **73**, 233201 (2006).
[17]J. Orenstein and M. A. Kastner, Solid State Commun. **40**, 85 (1981).
[18]G. J. Adriaenssens, S. D. Baranovskii, W. Fuhs, J. Jansen, and Ö. Öktü, Phys. Rev. B **51**, 9661 (1995).
[19]H. Cordes, G. H. Bauer, and R. Brüggemann, Phys. Rev. B **58**, 16160 (1998).
[20]P. Ludewig, Z. L. Bushell, L. Nattermann, N. Knaub, W. Stolz, and K. Volz, J. Cryst. Growth **396**, 95 (2014).
[21]M. Y. Ryu, C. Q. Chen, E. Kuokstis, J. W. Yang, G. Simin, M. A. Khan, G. G. Sim, and P. W. Yu, Appl. Phys. Lett. **80**, 3943 (2002).
[22]S. D. Baranovskii, R. Eichmann, and P. Thomas, Phys. Rev. B **58**, 13081 (1998).
[23]K. Jandieri, C. Jurecka, J. Ohlmann, A. Beyer, B. Kunert, S. D. Baranovskii, K. Volz, W. Stolz, and F. Gebhard, Phys. Status Solidi C **8**, 163 (2011).
[24]H. D. Sun, M. Hetterich, M. D. Dawson, A. Yu. Egorov, D. Bernklau, and H. Riechert, J. Appl. Phys. **92**, 1380 (2002).
[25]T. Prutskij, C. Pelosi, and G. Attolini, Cryst. Res. Technol. **46**, 127 (2011).
[26]C. M. Gee and M. Kastner, Phys. Rev. Lett. **42**, 1765 (1979).
[27]R. A. Street, *Hydrogenated Amorphous Silicon* (Cambridge University Press, Cambridge, England, 1991).
[28]S. Mazzucato, H. Lehec, H. Carrère, H. Makhloufi, A. Arnoult, C. Fontaine, T. Amand, and X. Marie, Nanoscale Res Lett. **9**, 19 (2014).

Zusammenfassung (Summary in German)

Ein Großteil der Energie in der optischen Datenübertragung geht in Form von Wärme verloren, insbesondere auf Grund von ineffizienten optischen Bauelementen im Wellenlängenbereich von 1.55 µm. Der Einsatz des neuartigen Ga(AsBi) Verbindungshalbleiters könnte die Realisierung von hocheffizienten optischen Bauelementen wie Laserdioden im infraroten Bereich ermöglichen und damit zu einer deutlichen Reduzierung dieser Verluste beitragen. Bei Bi Konzentrationen oberhalb von 10% ist die spin-bahn Aufspaltung größer als die Bandlücke des Halbleiters, was auf das Bi induzierte *Band anti crossing* im Valenzband zurückzuführen ist. In diesem Fall wären Verlustmechanismen wie die Auger Rekombination und die Inter-Valenzband Absorption, die eine große Rolle bei konventionellen Bauelementen spielen, unterdrückt, was die Effizienz deutlich steigern würde. Das epitaktische Wachstum dieser hochgradig metastabilen Verbindung ist allerdings noch eine große Herausforderung da sich zum einen metallische Tropfen an der Oberfläche bilden können und zum anderen sehr niedrige Wachstumstemperaturen erforderlich sind um eine signifikante Menge Bi in GaAs einzubauen.

In dieser Arbeit wurde das Wachstum von Ga(AsBi) und Ga(NAsBi) auf GaAs Subtraten mittels metallorganischer Gasphasenepitaxie (MOVPE, *metal organic vapor phase epitaxy*) und den Precursoren Triethylgallium (TEGa), Tertiarbutylarsin (TBAs), Trimethylbismut (TMBi) und unsymetrisches Dimethylhydrazin (UDMHy) untersucht. Dabei wurden sowohl multi quantum well (MQW) als auch bulkartige Schichten abgeschieden. Sämtliche Wachstumsparameter wurden systematisch variiert, wobei die Precursoren entweder gepulst oder kontinuierlich angeboten wurden. Die abgeschiedenen Kristalle wurden strukturell mittels hochauflösender Röntgenbeugung (HR-XRD, *high resolution x-ray diffraction*), Rasterkraftmikroskopie (AFM, *atomic force microscopy*) (Raster-)Transmissionselektronenmikroskopie ((S)TEM, *(scanning) transmission electron microscopy*) und optisch mittels Photolumineszenz Spektroskopie (PL) charakterisiert. Darüber hinaus konnten die ersten auf Ga(AsBi) basierenden Laserdioden demonstriert werden.

Die Oberflächen der Ga(AsBi) Proben waren zunächst von metallischen Tropfen übersät, die entweder aus Ga oder Bi bestanden oder aus einer Phasenseparation der beiden entstanden waren. Eine deutliche Reduzierung des TMBi Angebots und eine Feinjustierung des TBAs/TEGa Verhältnisses ermöglichten die Abscheidung von tropfenfreien Schichten mit messbarem Bi Gehalt sowohl beim gepulsten als auch beim kontinuierlichen Precursoren

Fluss. Es wurde festgestellt, dass Bi während des Wachstums an der Oberflächen segregiert und der Bi Einbau im Wesentlichen von der Oberflächenbedeckung abhängt. Ist diese zu gering, schwimmt das Bi lediglich an der Oberfläche auf und wird nicht in den Kristall eingebaut. Erst mit steigender Oberflächenbelegung kann eine lineare Abhängigkeit des Bi Gehalts zum angebotenen Bi festgestellt werden, wobei der Bi Einbau auf Grund der Metastabilität des Ga(AsBi) bei einem bestimmten Wert sättigt, was dann zur Bildung der Tropfen an der Oberfläche führt. Der maximale Bi Gehalt kann erhöht werden wenn die Wachtsumstemperatur reduziert wird, wobei diese im Bereich von 350 °C bis 475 °C variiert wurde. Bei niedrigeren Temperaturen bilden sich allerdings vermehrt Kristalldefekte und die Zerlegung der Precursoren ist geringer, sodass sich Temperaturen von 375 °C und 400 °C als am geeignetsten für das Wachstum von Ga(AsBi) herausgestellt haben. Hier wurden bisher Bi Konzentrationen von bis zu 7% bzw. 5% erreicht. Die Einbaueffizienz steigt ebenfalls mit steigender Wachstumsrate und mit sinkendem TBAs Angebot im Bereich des TBAs/TEGa Verhältnisses, in dem tropfenfreies Ga(AsBi) Wachstum möglich ist. Die Schwierigkeit bei der Optimierung und Untersuchung der Wachstumsbedingungen liegt darin, dass die zuvor genannten Parameter nicht zwingend unabhängig voneinander sind. So sinkt beispielsweise die Wachstumsrate durch die Anwesenheit von Bi oder des nicht vollkommen zerlegten TMBi an der Oberfläche, was darauf hinweist, dass entweder die Zerlegung von TEGa reduziert wird oder dessen Anhaftung an die Oberfläche. Darüber hinaus ändert sich die Zerlegungsrate der Precursoren im betrachteten Temperaturbereich mit der Temperatur und damit auch die Wachstumsrate und die optimalen TMBi/V und TBAs/TEGa Verhältnisse.

Dennoch konnten chemisch homogene Ga(AsBi) Proben mit scharfen Hetero-Grenzflächen realisiert werden, sofern die auf das Ga(AsBi) folgende Schicht bei 625 °C abgeschieden wurde. Das aufschwimmende segregierte Bi agiert als Surfactant (Oberflächen aktive Spezies), was den unbeabsichtigten Einbau von C, der bei den tiefen Wachstumstemperaturen auftritt, unterdrückt und zusätzlich die Punktdefektdichte im Kristall reduziert. Daher konnte insbesondere bei den Proben, die in dem Wachstumsregime indem die Bi Sättigung einsetzt abgeschieden wurden, eine starke Bandlücken PL beobachtet werden. Die Emissionswellenlänge zeigt dabei eine nahezu perfekte Übereinstimmung mit der Vorhersage der Theorie. Die Linienbreiten (FWHM, *full width half maximum*) liegen bei 80 bis 90 meV, was auf die Unordnung in verdünnten Bismiden zurückzuführen ist.

Um die Eignung von Ga(AsBi) für optoelektronische Bauelemente zu untersuchen wurden Breitstreifen Ga(AsBi) QW Laser mit Bi Konzentrationen von 2.2% und 4.4% hergestellt. Elektrisch injizierte Verstärkung bei diesem Materialsystem konnte zum ersten Mal anhand eines $Ga(AsBi_{0.022})$ SQW Lasers mit (AlGa)As Barrieren gezeigt werden. Die Schwellstromdichte von I_{th}=1.0 kA/cm^2 bei Raumtemperatur unter gepulster Stromzuführung ist vielversprechend für ein derartiges neues Material. Allerdings gehen etwa 80% des Schwellstroms durch nichtstrahlende Rekombination aufgrund von Defekten im Ga(AsBi) verloren. Laserdioden mit 4.4% Bi funktionierten bislang nur bei Temperaturen unterhalb

von 180 K. Dies zeigt die Notwendigkeit die Wachtsumsbedingungen von Ga(AsBi) weiter zu verbessern, insbesondere im Hinblick auf die angestrebten Bi Konzentrationen von mehr als 10%.
Beim Wachstum von Ga(NAsBi) wurde festgestellt, dass bei konstanter Bi Konzentration der N Gehalt einfach über das UDMHy Angebot kontrolliert werden kann. Proben mit bis zu 4% Bi und N wurden hergestellt, allerdings war es nicht möglich an diesen Strukturen PL bei Raumtemperatur zu beobachten. Daher wurden Photo-Reflektionsmessungen durchgeführt, die zeigten, dass bei konstantem Bi Gehalt die Bandlücke um etwa 140 meV/%N verringert wird was die Annahme, dass Bi und N unabhängig auf die Bandlücke von GaAs wirken, bestätigt.
Insgesamt konnte in dieser Arbeit sowohl die erfolgreiche Abscheidung verdünnt Bi-haltiger Halbleiterschichten mittels MOVPE demostriert werden als auch deren Potential für den Einsatz in optoelektronischen Bauelemente im infraroten Wellenlängenbereich.

Bibliography

[1] M. Silver, E. P. O'Reilly and A. R. Adams, IEEE J. Quantum Electron. **33**, 1557 (1997).

[2] S. J. Sweeney, A. F. Phillips, A. R. Adams, E. P. O'Reilly and P. J. A. Thijs, IEEE Photonics Technol. Lett. **10**, 1076 (1998).

[3] T. Higashi, S. J. Sweeney, A. F. Phillips, A. R. Adams, E. P. O'Reilly, T. Uchida and T. Fujii, IEEE J. Sel. Top. Quantum Electron. **5**, 413 (1999).

[4] A. F. Phillips, S. J. Sweeney, A. R. Adams and P. J. A. Thijs, IEEE J. selcted Top. Quantum Electron. **5**, 401 (1999).

[5] S. J. Sweeney and S. R. Jin, J. Appl. Phys. **113**, 043110 (2013).

[6] C. A. Broderick, M. Usman, S. J. Sweeney and E. P. O'Reilly, Semicond. Sci. Technol. **27**, 094011 (2012).

[7] K. Oe and H. Okamoto, Jpn. J. Appl. Phys. **37**, L1283 (1998).

[8] K. Oe, Jpn. J. Appl. Phys. **41**, 2801 (2002).

[9] M. Yoshimoto, W. Huang, G. Feng and K. Oe, Phys. status solidi **243**, 1421 (2006).

[10] Y. Tominaga, K. Oe and M. Yoshimoto, Appl. Phys. Express **3**, 62201 (2010).

[11] M. Ferhat and A. Zaoui, Phys. Rev. B **73**, 115107 (2006).

[12] R. N. Kini, L. Bhusal, A. J. Ptak, R. France and A. Mascarenhas, J. Appl. Phys. **106**, 043705 (2009).

[13] K. Bertulis, A. Krotkus, G. Aleksejenko, V. Pačebutas, R. Adomavičius, G. Molis and S. Marcinkevičius, Appl. Phys. Lett. **88**, 201112 (2006).

[14] K. Oe, J. Cryst. Growth **239**, 1481 (2002).

[15] H. Fitouri, I. Moussa, A. Rebey, A. Fouzri and B. El Jani, J. Cryst. Growth **295**, 114 (2006).

[16] I. Moussa, H. Fitouri, A. Rebey and B. El Jani, Thin Solid Films **516**, 8372 (2008).

[17] Z. Chine, H. Fitouri, I. Zaied, A. Rebey and B. El Jani, J. Cryst. Growth **330**, 35 (2011).

[18] K. Forghani, A. Anand, L. J. Mawst and T. F. Kuech, J. Cryst. Growth **380**, 23 (2013).

[19] M. Yoshimoto, S. Murata, A. Chayahara, Y. Horino, J. Saraie and K. Oe, Jpn. J. Appl. Phys. **42**, L1235 (2003).

[20] S. Tixier, M. Adamcyk, T. Tiedje, S. Francoeur, A. Mascarenhas, P. Wei and F. Schiettekatte, Appl. Phys. Lett. **82**, 2245 (2003).

[21] X. Lu, D. A. Beaton, R. B. Lewis, T. Tiedje and M. B. Whitwick, Appl. Phys. Lett. **92**, 192110 (2008).

[22] Y. Tominaga, Y. Kinoshita, K. Oe and M. Yoshimoto, Appl. Phys. Lett. **93**, 131915 (2008).

[23] F. Bastiman, A. G. Cullis, J. P. R. David and S. J. Sweeney, J. Cryst. Growth **341**, 19 (2012).

[24] F. Bastiman, A. R. Mohmad, J. S. Ng, J. P. R. David and S. J. Sweeney, J. Cryst. Growth **338**, 57 (2012).

[25] A. J. Ptak, R. France, D. A. Beaton, K. Alberi, J. Simon, A. Mascarenhas and C.-S. Jiang, J. Cryst. Growth **338**, 107 (2012).

[26] D. Fan, P. C. Grant, S.-Q. Yu, V. G. Dorogan, X. Hu, Z. Zeng, C. Li, M. E. Hawkridge, M. Benamara, Y. I. Mazur, G. J. Salamo, S. R. Johnson and Z. M. Wang, J. Vac. Sci. Technol. B **31**, 03C105 (2013).

[27] P. Ludewig, N. Knaub, W. Stolz and K. Volz, J. Cryst. Growth **370**, 186 (2013).

[28] P. Ludewig, N. Knaub, N. Hossain, S. Reinhard, L. Nattermann, I. P. Marko, S. R. Jin, K. Hild, S. Chatterjee, W. Stolz, S. J. Sweeney and K. Volz, Appl. Phys. Lett. **102**, 242115 (2013).

[29] P. Ludewig, Z. Bushell, L. Nattermann, N. Knaub, W. Stolz and K. Volz, J. Cryst. Growth **396**, 95 (2014).

[30] Z. Bushell, P. Ludewig, N. Knaub, Z. Batool, K. Hild, W. Stolz, S. Sweeney and K. Volz, J. Cryst. Growth **396**, 79 (2014).

[31] B. Breddermann, A. Bäumner, S. W. Koch, P. Ludewig, W. Stolz, K. Volz, J. Hader, J. V. Moloney, C. A. Broderick and E. P. O'Reilly, J. Lumin. **154**, 95 (2014).

[32] E. Sterzer, N. Knaub, P. Ludewig, R. Straubinger, A. Beyer and K. Volz, J. Cryst. Growth **408**, 71 (2014).

[33] I. P. Marko, P. Ludewig, Z. L. Bushell, S. R. Jin, K. Hild, Z. Batool, S. Reinhard, L. Nattermann, W. Stolz, K. Volz and S. J. Sweeney, J. Phys. D. Appl. Phys. **47**, 345103 (2014).

[34] M. K. Shakfa, M. Wiemer, P. Ludewig, K. Jandieri, K. Volz, W. Stolz, S. D. Baranovskii and M. Koch, J. Appl. Phys. **117**, 025709 (2015).

[35] R. Hall, G. Fenner, J. Kingsley, T. Soltys and R. Carlson, Phys. Rev. Lett. **9**, 366 (1962).

[36] D. Manasijević, D. Minić, D. Živković, I. Katayama, J. Vřešťál and D. Petković, J. Phys. Chem. Solids **70**, 1267 (2009).

[37] S. Francoeur, M.-J. Seong, A. Mascarenhas, S. Tixier, M. Adamcyk and T. Tiedje, Appl. Phys. Lett. **82**, 3874 (2003).

[38] W. Huang, M. Yoshimoto, Y. Takehara, J. Saraie and K. Oe, Jpn. J. Appl. Phys. **43**, L1350 (2004).

[39] B. Fluegel, S. Francoeur, A. Mascarenhas, S. Tixier, E. Young and T. Tiedje, Phys. Rev. Lett. **97**, 067205 (2006).

[40] H. Li and Z. M. Wang, *Bismuth-Containing Compounds*, volume 186 of *Springer Series in Materials Science*, Springer New York, 2013.

[41] K. Alberi, O. D. Dubon, W. Walukiewicz, K. M. Yu, K. Bertulis and A. Krotkus, Appl. Phys. Lett. **91**, 051909 (2007).

[42] K. Alberi, J. Wu, W. Walukiewicz, K. M. Yu, O. D. Dubon, S. Watkins, C. Wang, X. Liu, Y.-J. Cho and J. Furdyna, Phys. Rev. B **75**, 045203 (2007).

[43] W. Shan, W. Walukiewicz, J. Ager, E. Haller, J. Geisz, D. Friedman, J. Olson and S. Kurtz, Phys. Rev. Lett. **82**, 1221 (1999).

[44] M. Usman, C. A. Broderick, A. Lindsay and E. P. O'Reilly, Phys. Rev. B **84**, 245202 (2011).

[45] C. A. Broderick, M. Usman and E. P. O'Reilly, Semicond. Sci. Technol. **28**, 125025 (2013).

[46] C. A. Broderick, P. E. Harnedy, P. Ludewig, R. J. Manning, Z. L. Bushell, R. J. Manning, K. Volz and E. P. O'Reilly, *"Determination of type-I band offsets in* $GaBi_xAs_{1-x}$ *quantum wells using polarisation-resolved photovoltage spectroscopy and 12-band* $\boldsymbol{k}\cdot\boldsymbol{p}$ *calculations"*, submitted to Semicond. Sci. Technol. (2015).

[47] P. Carrier and S.-H. Wei, Phys. Rev. B **70**, 035212 (2004).

[48] Z. Batool, K. Hild, T. J. C. Hosea, X. Lu, T. Tiedje and S. J. Sweeney, J. Appl. Phys. **111**, 113108 (2012).

[49] A. Janotti, S.-H. Wei and S. Zhang, Phys. Rev. B **65**, 115203 (2002).

[50] R. B. Lewis, D. A. Beaton, X. Lu and T. Tiedje, J. Cryst. Growth **311**, 1872 (2009).

[51] N. Hossain, I. P. Marko, S. R. Jin, K. Hild, S. J. Sweeney, R. B. Lewis, D. A. Beaton and T. Tiedje, Appl. Phys. Lett. **100**, 051105 (2012).

[52] T. Fuyuki, R. Yoshioka, K. Yoshida and M. Yoshimoto, Appl. Phys. Lett. **103**, 202105 (2013).

[53] I. Vurgaftman, J. R. Meyer and L. R. Ram-Mohan, J. Appl. Phys. **89**, 5815 (2001).

[54] Y. Zhang, A. Mascarenhas and L.-W. Wang, Phys. Rev. B **71**, 155201 (2005).

[55] S. Q. Wang and H. Q. Ye, Phys. status solidi **240**, 45 (2003).

[56] A. Allred, J. Inorg. Nucl. Chem. **17**, 215 (1961).

[57] P. J. Klar, H. Grüning, W. Heimbrodt, G. Weiser, J. Koch, K. Volz, W. Stolz, S. W. Koch, S. Tomi, S. A. Choulis, T. J. C. Hosea, E. P. O'Reilly, M. Hofmann, J. Hader and J. V. Moloney, Semicond. Sci. Technol. **17**, 830 (2002).

[58] J. Wu, W. Shan and W. Walukiewicz, Semicond. Sci. Technol. **17**, 860 (2002).

[59] I. Suemune, K. Uesugi and W. Walukiewicz, Appl. Phys. Lett. **77**, 3021 (2000).

[60] F. Höhnsdorf, J. Koch, C. Agert and W. Stolz, J. Cryst. Growth **195**, 391 (1998).

[61] A. Moto, S. Tanaka, N. Ikoma, T. Tanabe, S. Takagishi, M. Takahashi and T. Katsuyama, Jpn. J. Appl. Phys. **38**, 1015 (1999).

[62] T. Miyamoto, T. Kageyama, S. Makino, D. Schlenker, F. Koyama and K. Iga, J. Cryst. Growth **209**, 339 (2000).

[63] G. Feng, K. Oe and M. Yoshimoto, Jpn. J. Appl. Phys. **46**, L764 (2007).

[64] K. Volz, D. Lackner, I. Németh, B. Kunert, W. Stolz, C. Baur, F. Dimroth and A. Bett, J. Cryst. Growth **310**, 2222 (2008).

[65] W. Huang, K. Oe, G. Feng and M. Yoshimoto, J. Appl. Phys. **98**, 053505 (2005).

[66] M. Yoshimoto, W. Huang, Y. Takehara, J. Saraie, A. Chayahara, Y. Horino and K. Oe, Jpn. J. Appl. Phys. **43**, L845 (2004).

[67] G. B. Stringfellow, J. Cryst. Growth **128**, 503 (1993).

[68] G. B. Stringfellow, *Organometallic vapor-phase epitaxy: theory and practice*, Academic Press, 2 edition, 1998.

[69] E. Bourret-Courchesne, Q. Ye, D. W. Peters, J. Arnold, M. Ahmed, S. J. C. Irvine, R. Kanjolia, L. M. Smith and S. A. Rushworth, J. Cryst. Growth **217**, 47 (2000).

[70] T. F. Kuech, M. A. Tischler, P.-J. Wang, G. Scilla, R. Potemski and F. Cardone, Appl. Phys. Lett. **53**, 1317 (1988).

[71] A. R. Mohmad, F. Bastiman, J. S. Ng, S. J. Sweeney and J. P. R. David, Appl. Phys. Lett. **98**, 122107 (2011).

[72] A. R. Mohmad, F. Bastiman, C. J. Hunter, J. S. Ng, S. J. Sweeney and J. P. R. David, Appl. Phys. Lett. **99**, 42107 (2011).

[73] R. Kudrawiec, J. Kopaczek, P. Sitarek, J. Misiewicz, M. Henini and S. V. Novikov, J. Appl. Phys. **111**, 66103 (2012).

[74] M. Usman, C. A. Broderick, Z. Batool, K. Hild, T. J. C. Hosea, S. J. Sweeney and E. P. O'Reilly, Phys. Rev. B **87**, 115104 (2013).

[75] C. Gogineni, N. A. Riordan, S. R. Johnson, X. Lu and T. Tiedje, Appl. Phys. Lett. **103**, 041110 (2013).

[76] Y. I. Mazur, V. G. Dorogan, M. Schmidbauer, G. G. Tarasov, S. R. Johnson, X. Lu, M. E. Ware, S.-Q. Yu, T. Tiedje and G. J. Salamo, J. Appl. Phys. **113**, 144308 (2013).

[77] S. Tixier, M. Adamcyk, E. C. Young, J. H. Schmid and T. Tiedje, J. Cryst. Growth **251**, 449 (2003).

[78] R. R. Wixom, L. W. Rieth and G. B. Stringfellow, J. Cryst. Growth **265**, 367 (2004).

[79] S. Prucnal, K. Gao, W. Anwand, M. Helm, W. Skorupa and S. Zhou, Opt. Express **20**, 26075 (2012).

[80] K. Gao, S. Prucnal, W. Skorupa, M. Helm and S. Zhou, J. Appl. Phys. **114**, 093511 (2013).

Acknowledgments

At this point I would like to take the opportunity to thank a lot of people who helped finishing this thesis.

First, I would like to express my very great appreciation to my supervisor Prof. Dr. Kerstin Volz for providing the opportunity and encouraging me to write my thesis on this interesting and challenging topic. I'm very thankful for all the valuable and constructive discussions and for her deep interest in my research.
I gratitude PD Dr. Sangam Chatterjee not only for the kind acceptance of the second opinion, but also for the interesting discussions concerning our cooperation.
I would like to give particular thanks to Dr. Wolfgang Stolz for always being interested in the progress of my work and his capable advice.
For their contribution to this work and their great support in the lab, I want to thank the former Diploma, Master and Bachelor students Katharina Werner, Zoe Bushell, Lukas Nattermann and Eduard Sterzer.
Special thanks also to Celina Becker, Nikolai Knaub and Andreas Beyer for all TEM images and for the TEM sample preparation and to Stefan Reinhard for the fabrication of the laser devices.
Of course I would also like to thank all co-operation partners for the valuable discussions, the scientific exchange and their contributions to this work.
Stefan Reinhard and Thomas Ochs provided excellent technical support at all times.
I furthermore wish to acknowledge the help concerning all organizational issues provided by Elke Vaupel, Isabelle Kimmel and Marina Koch.
I would like to extend my thanks to the entire team of the STRL and NAsP for the great scientific and non-scientific exchange and the incredible time I have spent here.
Finally, I want to thank my family, friends and particularly my wife Anja for their support and encouragement throughout my study and for providing diversion from work-related thoughts.